International Journal of Biological Macromolecules 249 (2023) 126084

Contents lists available at ScienceDirect

International Journal of Biological Macromolecules

journal homepage: www.elsevier.com/locate/ijbiomac

In-vitro anticancer evaluation of newly designed and characterized tri/tetra-substituted imidazole congeners- maternal embryonic leucine zipper kinase inhibitors: Molecular docking and MD simulation approaches

Monalisa Mahapatra [a], Priyanka Mohapatra [b], Kakarla Pakeeraiah [a], Ravi Kumar Bandaru [c], Iqrar Ahmad [d,e], Suvadeep Mal [a], Rambabu Dandela [c], Sanjeeb Kumar Sahoo [b], Harun Patel [d], Sudhir Kumar Paidesetty [a,*]

[a] *Medicinal Chemistry Research Laboratory, School of Pharmaceutical Sciences, Siksha 'O' Anusandhan Deemed to be University, Bhubaneswar 751003, Odisha, India*
[b] *Institute of Life Sciences, Bhubaneswar, Orissa 751 023, India*
[c] *Institute of Chemical Technology-Indian Oil Campus, Bhubaneswar, Odisha 751024, India*
[d] *Department of Pharmaceutical Chemistry, Prof. Ravindra Nikam College of Pharmacy, Gondur, Dhule 424002, Maharashtra, India*
[e] *Division of Computer Aided Drug Design, Department of Pharmaceutical Chemistry, R. C. Patel Institute of Pharmaceutical Education and Research, Shirpur 425405, Maharashtra, India*

ARTICLE INFO

Keywords:
Tri-substituted/tetra-substituted imidazole
Sulfanilamide
Molecular docking
MD simulation
Anticancer activity

ABSTRACT

Our cascading attempt to develop new potent molecules now involves designing a series of imidazole derivatives and synthesizing two sets of 2,4,5- tri-substituted (**4a–4d**) and 1,2,4,5-tetra-substituted (**6a–6d**) imidazole by the principle of Debus-Radziszewski multicomponent synthesis reaction. The structures of the obtained compounds were confirmed by $^{1}H/^{13}C$ NMR, FT-IR, elemental analysis, purity and the retention time was analyzed by HPLC. Based upon the binding affinity in the molecular docking studies, we have synthesized different imidazole derivatives from which compound **6c** have been found to show more anti-proliferative activity by inducing apoptosis at a higher rate than the other compounds corroborating the *in-silico* prediction. The structure and crystallinity of compound **4d** have been confirmed by single XRD analysis. The synthesized molecules were screened for their *in vitro* anti-cancer properties in triple negative breast cancer cell line (MDA-MB-231), pancreatic cancer cell lines (MIA PaCa-2) and oral squamous cell carcinoma cell line (H357) and results indicated that all the compounds inhibited the cell proliferation in a concentration-dependent manner at different time points. The compounds **4b** and **6d** were found to be effective against the *S. aureus* bacterial strain whereas only compound **4d** fairly inhibited the fungal strain of *T. rubrum* with a MIC 12.5 μg/mL. Molecular docking study reveals good interaction of the synthesized compounds with known target MELK involved in oncogenesis having high binding profiles. The lead compound **6c** was further analyzed by the detailed molecular dynamics study to establish the stability of the ligand–enzyme complex.

1. Introduction

Cancer is a curse to society due to the unpredicted and unprecedented number of deaths. According to the reports of GLOBOCAN 2020, the prevalence rate of breast cancer among women represents the migration rate reporting a ratio of 4:1 indicating one in every four cancer cases is diagnosed with breast cancer worldwide. As per the predictions of two organizations; the WHO (World Health Organization) 2012 and UNDESA (United Nations Department of Economic and Social Affairs) cancer cases will rise two fold within the upcoming two decades, among which breast cancer will lead the mortality rate in females, unlike lung cancer in males [1,2]. The predictions have been proved as reported by GLOBOCAN 2018, cancer is a global burden by estimating 18.1 million new cancer cases every year which has increased to 19 million by the reports of GLOBOCAN 2020 [3,4]. This burgeoning number of cases has motivated researchers and pharmacists to unravel several pathways and therapies to decode cancer epidemiology as most of the cancer-related diseases occur due to alterations in the genetic

* Corresponding author.
E-mail address: sairampaidesetty@gmail.com (S.K. Paidesetty).

https://doi.org/10.1016/j.ijbiomac.2023.126084
Received 28 May 2023; Received in revised form 28 July 2023; Accepted 29 July 2023
Available online 1 August 2023

makeup. Hence, unlocking newer schemes for synthetic or natural compounds that could target the gene for modulation through receptor blocking or altering has remained the key challenge for researchers.

Heterocyclic ring are the leading moieties for the development of new anticancer drug candidates, being imidazole among one of them. The diazo ring being electron rich facilitates the drug binding affinity towards the receptor's active site [5]. Usually, the rings containing nitrogen, sulfur and oxygen are the most abundantly used potent heterocyclic scaffolds. Synthesizing small potent molecules with high or sufficient yield from a low-cost starting material is the need of the hour, which is well addressed by the five membered 1, 3-diazole ring, usually rests in tautomeric form with non-adjacent nitrogen atoms in the *meta* position. The high polar nature of the imidazolyl-nitrogen makes it a potent moiety for many types of reaction initiator and facilitates drug solubility. Some of FDA approved anticancer imidazole derived drugs are one/di-substituted imidazole (diazenylimidazole derived Dacarbazine, imidazole with bisphosphate - Zoledronic acid, Tipifarnib, and Nilotinib) [6–8] and also some tri-substituted (Fenflumizole) and tetra-substituted drugs were in the pipeline for anticancer approval *viz.*, imidazole bearing *N*-methylbenzamide "Apoptozole" reported in Fig. 1. The compounds bearing nitrogen atom have been a boon to the pharmaceutical sector for its broad spectrum of biological activities. Imidazole is a privileged scaffold and key structural pharmacophore ubiquitously available in synthetic compounds (important motif of metronidazole, ketoconazole, Losartan, etc.) as well in the natural compounds *viz.*, biotin (a protein), pilocarpine alkaloids, histamine (a chemical messenger), histidine (an amino acid). In the process of drug discovery, imidazole and its derivatives have been an efficient contributor by possessing anticancer, antifungal, antiviral, antitubercular, and antihistaminic had also been explored for combating neurodegenerative diseases [9–11]. The hybridization approach has been depicted in Fig. 2.

Recently, much efforts have been emphasized to develop new anticancer candidates bearing imidazole moiety against several disease targeting enzymes *viz.*, cytochrome P450 enzyme, microtubule, topoisomerases, transforming growth factor-β (TGF-β), rapidly accelerated fibrosarcoma (RAF) kinases, and TLR8 signaling [12,13]. In this context, Ali et al. have reported a series of triaryl-substituted imidazole congeners bearing sulfonamide by modifying the lead anticancer drug Dabrafenib (thiazolyl derived). The desired molecules were screened for their anticancer activity against melanoma cell lines and evaluated for BRAF inhibitory activity [14]. Also, Sharma et al. have successfully designed and synthesized 2,4,5-trisubstituted and 1,2,4,5-tetrasubstituted imidazole derivatives from vanillin and isovanilin compounds by multicomponent reaction as an efficient inhibitor of anchorage-independent growth and cell migration against 60 human cancer cell lines [5]. The 2,4,5 tri-substituted imidazole derivative bearing bromophenyl at the 4th and 5th-position and nitro phenyl at the 2nd position has displayed significant *in-vitro* anticancer activity than all other 24 compounds reported by Guda et al., suggesting the significant role of the electron withdrawing group at 2nd position of imidazole may enhance the cytotoxic potential [15]. Nikalje et al. have successfully synthesized tetra-substituted imidazole using an oxidant- CAN (ceric ammonium nitrate) and Hu et al. reported an interesting tetra-substituted imidazole while anticipating a [3 + 3] or a [3 + 2] cycloaddition of nitrones with 2-azido acrylates [16–18]. The sulfonamide-containing molecules gaining wide attention for most of the anticancer core substituents due to their specificity towards cancer causing targets *viz.*, carbonic anhydrase enzymes, aromatase, and topoisomerase. The anticancer drugs bearing sulfonamides currently marketed are Belinostat, Amascarine, Pazopanib *etc.*, whereas SLC-0111 is in Phase II clinical trial [19–22].

The strategic maneuver of the above studies has inspired our group to design and synthesize an array of imidazole derivatives by following the Debus-Radziszewski reaction but without using any catalyst *viz.*, CAN, acrylate or any specific base or acid. The rationale approach depicted in Fig. 2, has been kept simple and interesting by inserting benzene sulfonamide with an electron rich group at 1st position of imidazole making it a tetra-substituted; for which Apoptozole – an hsp70 inhibitor could serve as a structural reference. The designed imidazole derivatives have been screened against a selective receptor for triple-negative breast cancer (TNBC) *i.e.*, MELK bearing PDB ID: 4BKY for *in-silico* investigation, additionally other physiological parameters have also been studied along with the drug likeness and ADME profiles [23,24].

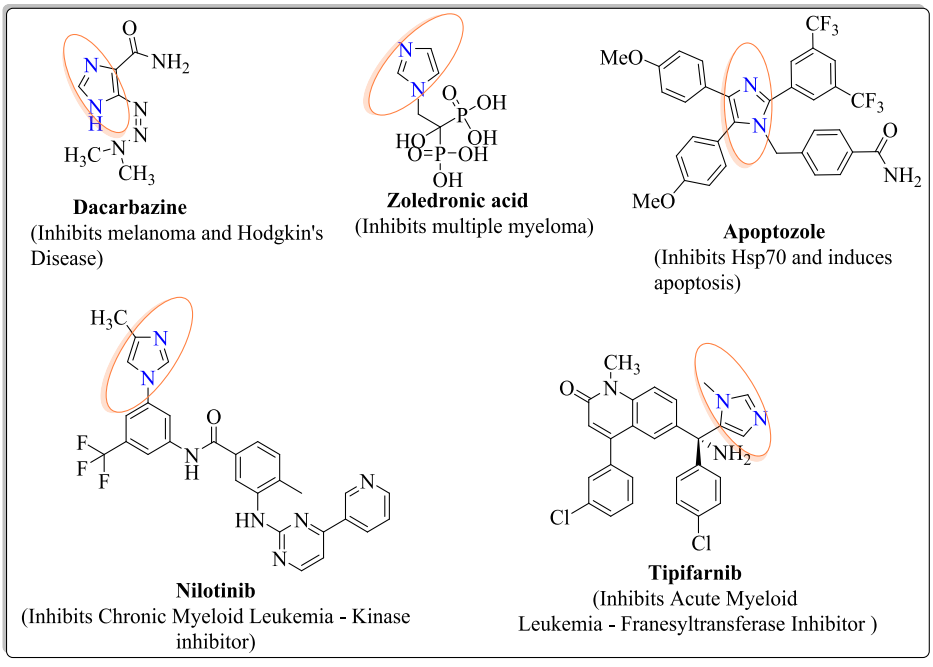

Fig. 1. Imidazole bearing commercial anticancer drugs based on the mechanism of action.

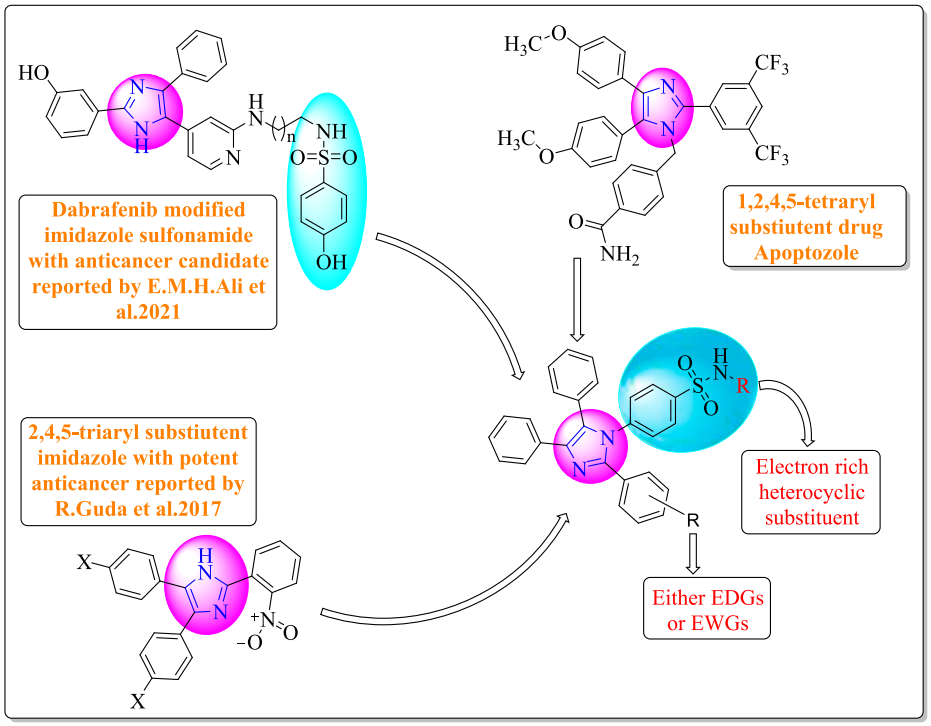

Fig. 2. Rationality behind designing the novel imidazole hybrids.

2. Experimental

2.1. Materials

All the necessary chemicals were used as AR grade and procured from Sigma-Aldrich and were used without purification. The functional group was analyzed by JASCO FT/IR 4600 spectrophotometer. The $^{1}H/^{13}C$ NMR spectral data on a Bruker analyzer spectrometer with (DMSO-d_6 or $CDCl_3$) as solvent and tetramethylsilane (TMS) as internal standard and chemical shift are reported in terms of ppm, δ values. Mass spectroscopy (MS) was recorded on Shimadzu GC–MS and the sample purity was confirmed by HPLC system, Schimadzu – LC-2030C 3D with Prominence-I pump, Autosampler: PDA detector maintains a flow rate of 1 mL/min and the acetonitrile: acetic acid in millipore water was chosen as mobile phase. The harvested crystals from the crystallization experiments were analyzed using Bruker's D8 QUEST Single Crystal X-ray Diffractometer, equipped with IμS 3.0 microfocus Mo source (λ = 0.71073 Å) and PHOTON II area detector. Diffraction data for all the crystals were collected by the 'φ and ω scans' method at room temperature. The data was solved using Bruker's APEX 4 software. Data reduction was performed using Bruker SAINT Software. Absorption correction was applied using SADABS. Structure solution was carried out by Direct Methods and structure refinement was performed by least-squares method using SHELXL. All non-hydrogen atoms were refined anisotropically and hydrogen atom positions were calculated by HFIX command and refined based on the riding model. Mercury (2022.3.0) was utilized to visualize crystal structures. Elemental analysis (C, H, N) was performed on PerkinElmer 240 analyzer. The reaction mixture was monitored by thin-layer chromatography (TLC) using appropriate solvents ethyl acetate and *n*-Hexane in 1:1.

2.2. Molecular docking study

To better comprehend the interaction between the novel series of synthesized derivatives, molecular docking studies were performed using the Schrödinger glide docking module within the Crystal Structure of *Maternal Embryonic Leucine Zipper Kinase (MELK)* (PDB: **4BKY**). Using Epik, the protein was prepared after confirming chemical correctness, assigning bond ordering, removing water molecules, and adding hydrogens for a pH of 7. Prime was used to fill up the gaps between side chains and loops, and termini were capped [25–27]. The receptor grid was created around the co-crystalized *pyrrolopyrazole inhibitor* and the binding site was delineated around it. The 3-dimensional structures of the synthesized compounds were created using Chemdraw and prepared with LigPrep. Using the SP (Standard precision) scoring algorithm, the lowest energy conformation of the ligand structures was chosen and docked into the active site [27–29].

2.3. Molecular dynamics (MD) simulation

The all-atom MD simulation was run for 100 ns to determine the structural stability and dynamic behavior of the 6c-MELK complex. The MD simulation was carried out using the Schrodinger's Desmonds tool, which was running on the Z2 G4 workstation with the configuration Ubuntu 22.04.2 LTS 64-bit, Intel Xeon W-2245 @ 3.90 GHz, 8-Cores, CUDA 12, and NVIDIA RTX A4000 graphics processing unit. [30]. The 6c-MELK complex was solvated in a constricted orthorhombic box using the SPC water model prior to simulation. To make the system electrically neutral, 12 and 15 Na+ (62.309 mM) and Cl− (49.847 mM) counter ions were added, respectively. The physiological pH was maintained by retaining the ionic strength at 0.15 M salt concentration. By using the steepest descent and the limited-memory Broyden-Fletcher-Goldfarb-Shanno (LBFGS) protocols with a maximum run of 2000 at a convergence threshold of 1 KJ/mol, the neutral system was well equilibrated and minimized. [31,32]. The simulation was ran for 100 ns under a 'isothermal-isobaric ensemble' (NPT) at a temperature of 300 K and a pressure of 1 bar after importing the built minimized system (.cms file) into the MD module. [33,34]. At 100 ps intervals, simulation snapshots were retrieved and the resulting trajectories were evaluated.

2.4. Synthesis of tri-substituted/tetra-substituted imidazole (*3a–3d*) and (*6a–6d*)

For preparation **4a–4d**, an individual substituted benzaldehyde

2a–2d (5-nitro vanillin, 5-bromo vanillin, 4-bromo benzaldehyde, and 5-bromosalicyladehyde) (1.0 mmol), benzil 1 (1.0 mmol) and ammonium acetate (1.0 mmol) was mixed and stirred well and poured in a round bottom flask fitted with a reflux condenser [15]. Then, the mixture was refluxed at 100 °C for 4–8 h. The reaction was monitored by TLC with solvent ethyl acetate: n-hexane. After, the completion of the reaction, the mixture was poured into ice-cold water and refrigerated overnight. The obtained crude precipitate colorless mass was filtered and dried in anhydrous calcium chloride and finally re-crystallized from a hot ethanol solution. Similarly, the synthesis procedure for tetra-substituted imidazole derivatives of **6a** and **6d**; had been initiated by the substitution of benzaldehyde such as 5-nitro vanillin (1.0 mmol), benzil 1 (0.1 mmol), and ammonium acetate (1.0 mmol) with sulfapyridine and sulfamethoxazole, individually. Also for compounds **6b** and **6c**, the reaction commences with substituted benzaldehyde such as 2-nitro benzaldehyde and 5-bromosalicyladehyde, benzil and ammonium acetate with sulfamethoxazole, respectively. Henceforth, the same procedure has been followed but without using any catalyst [17].

2.5. Cell line and culture condition

Different cancer cell lines such as pancreatic cancer cell line MIA Pa Ca-2 cells, breast cancer cell line MDA-MB-231 cells and oral cancer cell line H357 cells were purchased from American Type Culture Collection (ATCC) (Manassas, VA, USA). MIA PaCa-2 cells and MDA-MB-231 cells were cultured in DMEM media supplemented with 10 % FBS (PAN-Biotech GmbH, Germany) and 1 % penicillin-streptomycin (Sigma-Aldrich, St. Louis, USA) in a humidified incubator maintained at 37 °C with 5 % CO_2 [35]. H357 cells were cultured in DMEM/F12 media (PAN-Biotech GmbH, Germany) supplemented with 10 % FBS (Gibco, USA), hydrocortisone (Sigma-Aldrich, St. Louis, USA) and 1 % penicillin-streptomycin (Sigma-Aldrich, St. Louis, USA) in a humidified incubator maintained at 37 °C with 5 % CO_2 as per our previously published protocol [36].

2.6. MTT cell proliferation assay

The *in vitro* cytotoxic effect of imidazole compounds (**4a–4d)** and (**6a–6d**) was evaluated by MTT-based colorimetric assay. MIA PaCa-2, MDA-MB-231 and H357 cells were seeded at a density of 2×10^3 cells per well in a 96-well plate with the desired concentration (1, 10, 20, 30, 40 and 50 μM) of the above compounds for 48 h and 72 h respectively. Cell viability was estimated post treatment as per our previously published protocol [35]. The inhibitory concentration causing 50 % of cell death (IC_{50}) was calculated by nonlinear regression analysis through OriginPro 8.5 software [36].

2.7. Apoptosis assay

MDA-MB-231 cells were seeded at a density of 5×10^4 per well of 6 well plates overnight. Then cells were treated with 10 μM of imidazole compounds (**4d**, **6c** and **6d**) for 48 h. Further, control and treated cells were stained with PE Annexin-V and 7-AAD using PE-Annexin V Apoptosis Detection Kit (BD Biosciences, CA) as per the manufacturer's instructions. The stained cells were acquired by flow cytometer (LSR Fortessa, BD Biosciences, CA), collecting 10,000 event.

2.8. Western blotting

MDA-MB-231 cells were seeded at a density of 6×10^5 cells in 60 mm petri dish (Corning) for overnight at 37 °C. The cells were then treated with imidazole compounds (**4d**, **6c**, and **6d**) (10 μM) for 48 h. Further, cell lysate was isolated, protein concentration was estimated followed by SDS-polyacrylamide gel electrophoresis, transferred onto PVDF membrane and blocked using skimmed milk. The blot was then incubated with primary antibody (1:1000 dilutions) overnight at 4 °C. Next, incubated with horseradish peroxidase (HRP)-conjugated secondary antibody (1:5000 dilutions) (Novus Biologicals) at room temperature, and blots were developed using a chemiluminescence detection kit (ECL system; GE Healthcare). The band intensity of Western blots was determined using ImageJ software. The primary antibodies used are as follows: β-actin (sc-47778, Santa Cruz Biotechnology), Bax (2772S, Cell Signaling Technology), and Bcl-2 (2876S, Cell Signaling Technology). The detailed protocol is briefly explained in our previously published paper [35,36].

2.9. Antimicrobial assay

The synthesized tri/tetra-substituted imidazole compounds (**4a–4d**) and (**6a–6d**) were assayed for their antimicrobial sensitivity using the agar well diffusion method. The pathogenic strains against which the compounds were screened are the uropathogenic strains *S. aureus* (hswx88) and *E. coli* (MTCC 614) also screened against two fungal strains (dermatopathogenic) *C. albicans* (MTCC 3017), and *A. niger* (MTCC 9933). For the bacterial and fungal screening the strains were previously incubated for about 24-48 h at 37 °C in nutrient broth (NB) and Sabouraud dextrose broth (SDB). Further all the procedures and standards have been followed as in our previously published articles [37,38].

2.10. Determination of MIC (bacteria and fungus)

The imidazole substituted compounds have been screened for their minimum inhibitory concentration against different species of bacteria and fungi. The micro-dilution method have been followed using 96 microwell plates (Flat Bottom; Polystyrene, Eppendorf) as described in our previous research articles [39]. The eight selected compounds were screened against two bacterial strains *S. aureus* (hswx88) and *E. coli* (MTCC 614), and also two fungal strains *C. albicans* (MTCC 3017), and *A. niger* (MTCC 9933). The colour change was observed for the MIC determination for the tested samples which occurs due to the inhibition of bacterial growth [40].

2.11. Statistical analysis

The mean values of all experiments are given with a standard deviation (SD). The statistical significance of differences was calculated by one-way ANOVA using GraphPad Prism 9.0.0 software. *P*-values ≤ 0.05 is considered significant.

3. Result and discussion

3.1. Chemistry

The skeptical idea of the nineteen new tri and tetra-aryl substituted imidazoles was designed virtually using ChemDraw 19.0. The screening of the samples from **SPM-1** to **SPM-19** was performed based on the docking score in Table 3, and further, the compounds **SPM-12** to **SPM-19** have been re-coded for the ease of synthetic names as **4a–4d** (for SPM-12 to SPM-15; the tri-substituted) & **6a–6d** (for SPM-16 to SPM-19; the tetra-substituted) were validated basing upon different computational tools *viz.*, physicochemical parameters and ADMET profiles which are depicted in Tables 1 and 2. The compounds SPM-1 to SPM-11 has been excluded from the *in-vitro* studies due to their poor molecular docking score as well as their structural exploration described in the Fig. S33. All the compounds were in good agreement and passed Lipinski's rule which indicated that no such congeners had violated the RO5 rule parameters as depicted (Table 2.). The ADMET profiles include Blood-Brain Barrier (BBB), Caco-2 permeability (the Caco-2 cells for the prediction of oral drug absorption method), Human Intestinal Absorption (sum of bioavailability and absorption), skin permeability and LD_{50} toxicity of synthesized imidazole derivatives were determined by

Table 1
Pharmacokinetics (pre-ADMET) profiles of tri (**4a–4d**)/tetrasubstituted (**6a–6d**) imidazole derivatives.

Compound	Pre-ADMET profile scores of newly synthesized imidazole derivatives toxicity class					
	Blood-brain barrier (BBB)	Caco-2 permeability	Human intestinal absorption (HIA, %)	Skin_Permeability (logKp, cm/h)	LD50 mg/kg	
4a	1.1656	11.2656	90.8085	−3.1805	2000 mg/kg	4
4b	9.1861	42.96	93.64	−3.02	2000 mg/kg	4
4c	16.3576	55.9572	95.247	−2.0456	300 mg/kg	3
4d	10.9182	41.4286	93.7508	−2.9232	300 mg/kg	3
6a	0.0459	4.6014	96.5064	−2.3746	300 mg/kg	3
6b	0.0492	7.8170	97.4696	−2.2659	347 mg/kg	5
6c	0.0902	4.6104	97.3634	−2.2659	347 mg/kg	5
6d	0.0195	2.7807	96.9264	−2.3106	347 mg/kg	5

Table 2
Molecular properties parameters of newly synthesized (**4a–4d**) and (**6a–6d**) imidazole analogues (RO5).

Compound	Chemical name of the compound	Lipinski rule of five				
		MW	HA	HB	cLogP	tPSA
4a	4-(4,5-Diphenyl-1H-imidazol-2-yl)-2-methoxy-6-nitrophenol	387.39	21	2	5.56	103.96
4b	2-Bromo-4-(4,5-diphenyl-1H-imidazol-2-yl)-6-methoxyphenol	421.29	20	2	5.89	58.14
4c	2-(4-Bromophenyl)-4,5-diphenyl-1H-imidazole	375.26	16	1	6.17	28.68
4d	4-Bromo-2-(4,5-diphenyl-1H-imidazol-2-yl)phenol	391.26	17	2	5.88	48.91
6a	4-(2-(4-Hydroxy-3-methoxy-5-nitrophenyl)-4,5-diphenyl-1H-imidazol-1-yl)-N-(pyridin-2-yl) benzenesulfonamide	619.65	33	2	8.37	160.54
6b	N-(5-Methylisoxazol-3-yl)-4-(2-(2-nitrophenyl)-4,5-diphenyl-1H-imidazol-1-yl) benzenesulfonamide	577.61	29	1	8.56	144.22
6c	4-(2-(5-Bromo-2-hydroxyphenyl)-4,5-diphenyl-1H-imidazol-1-yl)-N-(5-methylisoxazol-3-yl) benzenesulfonamide	627.51	29	2	8.59	118.63
6d	4-(2-(4-Hydroxy-3-methoxy-5-nitrophenyl)-4,5-diphenyl-1H-imidazol-1-yl)-N-(5-methylisoxazol-3-yl) benzenesulfonamide	623.64	33	2	8.27	173.68

theoretical calculation and results of these calculated parameter congeners were expressed in Table 1; all these compounds appeared under toxicity classes 4 and 5 which signals for the desired imidazole-derived compounds as a lead molecule to carry out a further *in-vitro* analysis. Therefore, the eight potent candidates were synthesized by the principle of organic reactions. A two series of imidazole derivatives (**4a–4d**) triaryl-substituted and tetra-aryl substituted compounds with sulfonamide group (**6a–6d**) were synthesized by the principle of Debus-Radziszewski multicomponent synthesis reaction. Newly synthesized compounds were confirmed by their structure through UV–Visible, ^{1}HNMR, ^{13}CNMR, and FTIR, and elemental analysis and the percentage purity of compounds was analyzed by HPLC. In **Scheme-1** compounds have been prepared by the condensation reaction of benzil (**1**), corresponding aldehydes (**2a–2e**) and ammonium acetate in ethanolic solution afforded 2,4,5-tri-aryl substituted imidazole; similarly another series 1,2,4,5-tetra-substituted imidazole (**6a–6d**) compounds were synthesized by the mixing of equimolar multi-component of benzil, corresponding aryl aldehydes and respective sulfanilamide derivative (sulfapyridine and sulfamethoxazole) in single pot *in-situ* reaction and refluxed the content mixture solution atr 100 °C for 3 h. Then, the crystallized products were obtained from a hot ethanolic solution. The reaction was monitored by TLC with the solvent system (ethylacetate:*n*-hexane). The benzil (**1**) is an intermediate obtained by the oxidation of benzoin with the help of nitric acid and copper sulfate in the presence of pyridine [41]. All the obtained compounds were checked for their solubility in both polar and non-polar solvents.

FT-IR spectra were analyzed to provide more information about the functional group of synthesized desired chemical structure. In FT-IR analysis, the two frequencies of dicarbonyl stretching benzil disappeared in all the synthesized molecules and showed new stretching at a range of 1681–1645 cm^{-1} that assumed the presence of C═N str. of imidazole nucleus. Thus, the disappearance of dicarbonyl stretching of benzil proves that the compounds are cyclized. All the compound's FTIR spectral data were depicted in Figs. S1–S8. The absorption bands for the compounds had appeared between 3465 and 3185 cm^{-1} could be attributed to NH and OH groups, in addition the bands at nearly 2922 cm^{-1} are associated with the CH_2 stretching of methoxy group for compounds **4a**, **4b**, **6a** and **6d**. Furthermore, the wave number at a range between 1666 and 1647 cm^{-1} and 1622–1602 cm^{-1} contributed to the stretching vibration of -C═C- and -C═N of the imidazole ring, respectively [42]. The compounds (**6a–6d)** appeared with two strong absorption bands at 1374–1325 cm^{-1} and 1183–1163 cm^{-1} were assigned to sulfonyl asymmetrical and symmetrical stretching vibrations of

Table 3
Molecular docking results along with the docked sore of cocrystal ligand.

Compounds	Docking score	Glide model
1. SPM-1	−5.501	−53.947
2. SPM-2	−5.394	−55.003
3. SPM-3	−4.802	−49.313
4. SPM-4	−5.848	−59.261
5. SPM-5	−5.184	−55.118
6. SPM-6	−5.648	−54.437
7. SPM-7	−5.541	−54.46
8. SPM-8	−5.011	−58.14
9. SPM-9	−5.429	−54.46
10. SPM-10	−5.702	−54.981
11. SPM-11	−5.647	−54.976
12. SPM-12 **(4a)**	−6.184	−60.118
13. SPM-13 **(4b)**	−6.648	−65.746
14. SPM-14 **(4c)**	−6.429	−65.746
15. SMP-15 **(4d)**	−6.541	−64.978
16. SPM-16 **(6a)**	−6.447	−80.519
17. SPM-17 **(6b)**	**−7.182***	−78.371
18. SPM-18 **(6c)**	−6.803	−83.787
19. SPM-19 **(6d)**	−6.803	−83.787
20. Cocrystal ligand	−6.737	−85.125

* Compound SPM-17 (6b) exhibits the highest binding score (7.182) among all the compounds.

Table 4
Inhibitory concentration (IC_{50}) values of different compounds (**4a–4d**) and (**6a–6d**) in MIA Pa Ca-2, MDA MB 231, and H357 cell lines after 48 h and 72 h of treatment as observed by cell cytotoxicity assay. Data represented as mean ± SD, ($n = 3$).

IC_{50} (μM)						
Drug	MIA Pa Ca-2		MDA MB 231		H357	
	48 h	72 h	48 h	72 h	48 h	72 h
4a	25.40 ± 1.76	19.26 ± 0.97	28.32 ± 2.41	12.81 ± 1.01	21.81 ± 3.07	16.08 ± 2.76
4b	27.87 ± 3.75	19.82 ± 1.71	33.35 ± 2.49	16.75 ± 2.10	36.87 ± 2.54	21.23 ± 3.02
4c	31.32 ± 0.20	14.41 ± 0.93	24.55 ± 3.48	14.42 ± 0.61	32.29 ± 0.64	12.58 ± 3.72
4d	33.39 ± 1.02	18.26 ± 4.65	22.35 ± 3.95	10.92 ± 2.92	29.24 ± 4.01	16.82 ± 2.51
6a	41.40 ± 1.34	15.08 ± 1.32	36.87 ± 0.97	30.59 ± 1.38	58.25 ± 1.76	28.48 ± 1.45
6b	25.78 ± 1.36	16.15 ± 1.45	17.36 ± 0.96	10.89 ± 2.20	48.34 ± 1.78	22.16 ± 0.56
6c	27.86 ± 2.89	20.33 ± 1.46	12.13 ± 0.89	5.94 ± 1.78	51.51 ± 1.87	24.94 ± 0.78
6d	27.39 ± 2.43	12.28 ± 0.71	19.65 ± 1.43	13.90 ± 1.75	43.97 ± 1.32	24.42 ± 2.43

Table 5
Antimicrobial activity of Imidazole congeners in terms of zone of inhibition and MIC values (**4a–4d**) & (**6a–6d**).

Imidazole derivatives (**4a—4d**) & (**6a–6d**)	*S. aureus* (hswx88)		*E. coli* (MTCC 614)		*C. tropicalis* (MTCC 3017)	*T. rubrum* (MCC 1598)	
	ZOI (mm)	MIC (μg ml^{-1})	ZOI (mm)	MIC (μg ml^{-1})	ZOI (mm)	ZOI (mm)	MIC (μg ml^{-1})
4a	13	100	NA	100	13	19	25
4b	22	12.5	NA	50	13	18	25
4c	16	25	NA	100	13	16	25
4d	15	25	15	50	12	21	12.5
6a	18	NA	ND	NA	13	13	NA
6b	19	25	18	50	18	18	12.5
6c	20	25	NA	200	NA	14	NA
6d	24	12.5	NA	400	NA	12	200
GEN (Std.)	24		24		–	–	–
KT (Std.)	–	–	–	–		22	1.56

sulfonamide group respectively; another moderate peak appeared in the range of 972–916 cm^{-1} with respect to S—N stretching of sulfonamide group [37,43]. Compounds **4b** and **4d** appeared to moderate peaks at 1273 cm^{-1} nearly, which is associated with C—O stretching of the phenolic group. The strong absorption bands appeared at nearly equal to 1146 cm^{-1} that contributed to the symmetrical stretching of the nitro group in the structures of the compounds **6a**, **6b** and **6d**. The compounds except **4c** and **6b** containing vanilinyl residues showed a characteristic colour when treated with neutral ferric chloride indicating the presence of phenolic hydroxyl in the structure which is confirmed by the C—O str. appeared in the FTIR spectra [36].

Similarly, $^{1}H/^{13}C$ NMR spectral data are analyzed to get information about the proton and carbon structural environment of the candidate's skeleton. The compounds **4a**, **4b**, **6a,** and **6d** have been showing sharp singlet signals at nearly equal to δ 3.83 ppm assigning to methyl protons of methoxy which in C^{13}NMR, reflected at δ 57.22 ppm in all the above-noted structures. The compounds triaryl substituted imidazole (**4a–4d)** appeared at a broad singlet signal in the region ~δ 12.76 ppm which is indicated as imine hydrogen of imidazole nucleus whereas proton information for the compounds **4a** and **4b** has been specifying for singlet aromatic proton peak at δ 7.93 and δ 7.67 ppm respectively. Compounds **6b**, **6c**, and **6d** have also exhibited singlet protons at ~δ 2.25 ppm that

Table 6
Details of compound **4d** crystal structure.

Sl. No	Name of Comp	4b
1	Empirical Formulae	C_{21} H_{15} Br N_2 O
2	Formulae weight	391.25
3	Crystal system	Monoclinic
4	Space group	C 2/C
5	Temp (k)	295 ± K
6	A	26.110(3)
7	Alpha	90
8	B	12.8023(16)
9	Beta	94.086(4)
10	C	22.212(3)
11	Gamma	90
12	Volume	7405.8 (16)
13	Density Dx, g cm^{-3}	1.404
14	Z value	16
15	F(000)	3168
16	h min	31
17	h max	34
18	k min	−16
19	k max	−16
20	l min	−28
21	l max	28
22	N measured reflections	−8577
23	Independent reflections	8529
24	Observed reflections	4106
25	R1 Value	4.7
26	WR2	0.116
27	Goodness of fit	0.991
28	CCDC	2,247,503

contribute to methyl proton of isoxazole nuclei and the peak for C^{13}NMR appeared at ~δ 12.50 ppm whereas the compounds displaying another singlet peak at ~δ 6.09 ppm with respect to isoxazolyl H-4 proton whose parallel carbon peak appeared at ~δ 96.16 ppm. The triaryl subst. imidazole **4a**, and **4b** containing two unsubstituted phenyl of benzil and subst. vanillyl displayed their signals for the twelve aromatic protons in the region between δ 7.29–7.93 ppm, whereas the bromo-substituted derivatives **4c** exhibits signals for the fourteen aromatic protons in the region between δ7.21–7.67 ppm. The relevant spectra of all obtained synthesized compounds are depicted in Suppl. Figs. S1–S31. Moreover, all the synthesized molecules have not yet been reported earlier. All the compound's electronic spectra were scanned in dimethyl sulfoxide (DMSO) and displayed bands that are assigned for π- π* and n-π* transitions at 195–199 nm and 301–315 nm respectively. The molecular weight of all the synthesized compounds was determined by Mass spectroscopy (ESI-HRMS) in terms of *m/z* value. The ESI-HRMS spectra prepared compounds with **(4a–4d)** and **(6a–6d)** revealed the highest fragmented ion peaks strongly assigned to their prediction molecular formulae. The compound **4d** had shown a molecular ion peak at 390.20, which strongly indicated the predicted molecular formula for $C_{21}H_{15}BrN_2O_2$. From the HPLC chromatograms, it has been noticed that the compound **6c** is highly pure by a percentage area of 99.38 % with a retention time of 58.258 mins; and the Inertsil ODS-3 (C-18) analytical column was used with a 55:45 *v*/v ratio of HPLC grade water and acetonitrile. The chromatogram has been depicted in the supple figure Fig. 3. [44]. Details of the single XRD-crystallographic data collection, processing, and interpretation of the structure and refinement were depicted in the Table 6. along with the CCDC number, 2247503. These desired data can be obtained at Cambridge Crystallographic Data Centre http://www.ccdc.cam.ac.uk/deposit@ccdc.cam.ac.uk.

All the compounds appeared amorphous in nature after re-crystallization except compound **4d**. The crystal structure of **4d** was analyzed by single X-ray diffraction. The compound **4d** crystal structure was solved in the C2/c space group of monoclinic crystal system. The asymmetric unit contains two **4d** molecules (Z' = 2) Fig. 4 and the unit cell contains 16 molecules of 3B (Z = 16). The empirical formula of the compound from SCXRD data was found to be $C_{21}H_{15}ON_2Br$. **4d** molecule

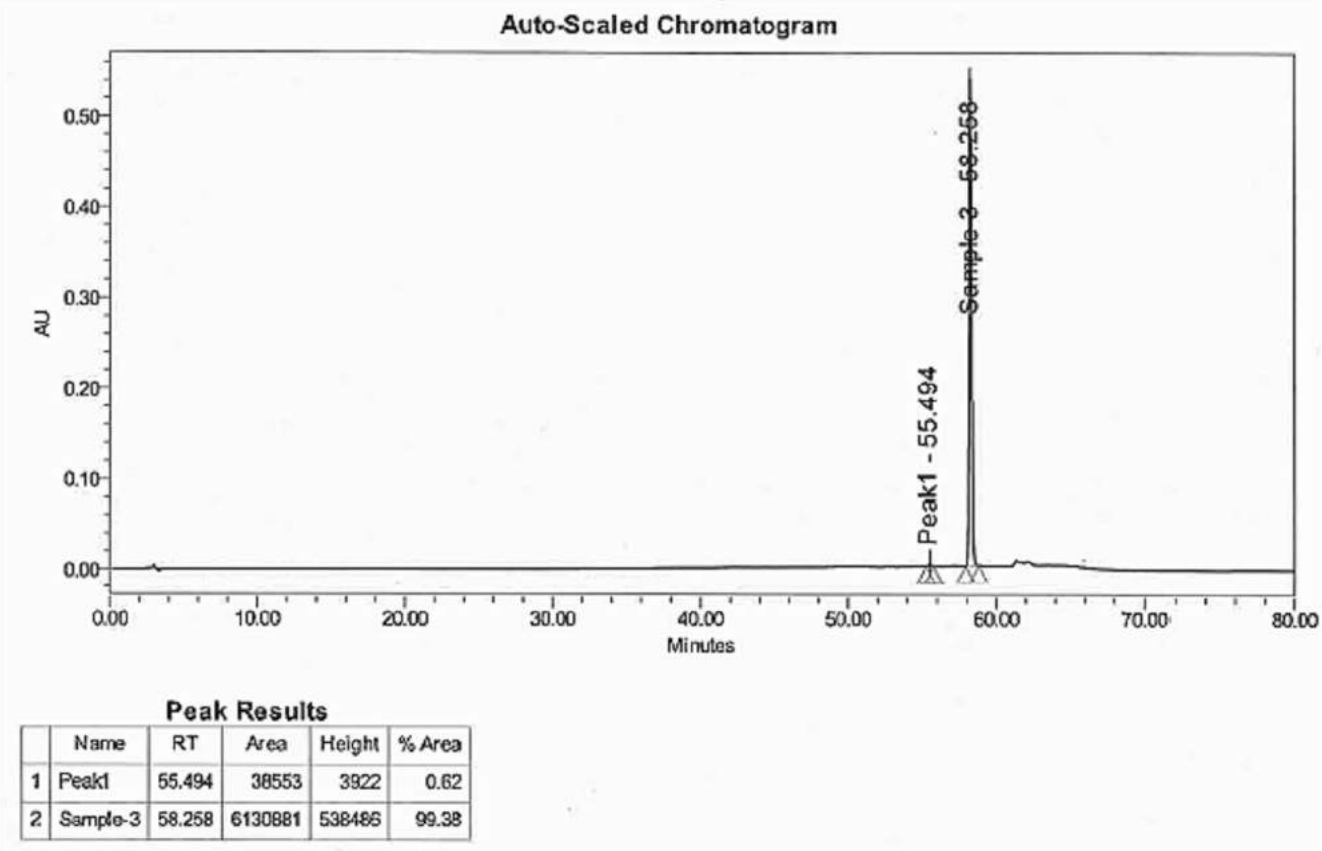

Peak Results

	Name	RT	Area	Height	% Area
1	Peak1	55.494	38553	3922	0.62
2	Sample-3	58.258	6130881	538486	99.38

Fig. 3. HPLC chromatogram of compound **6c**.

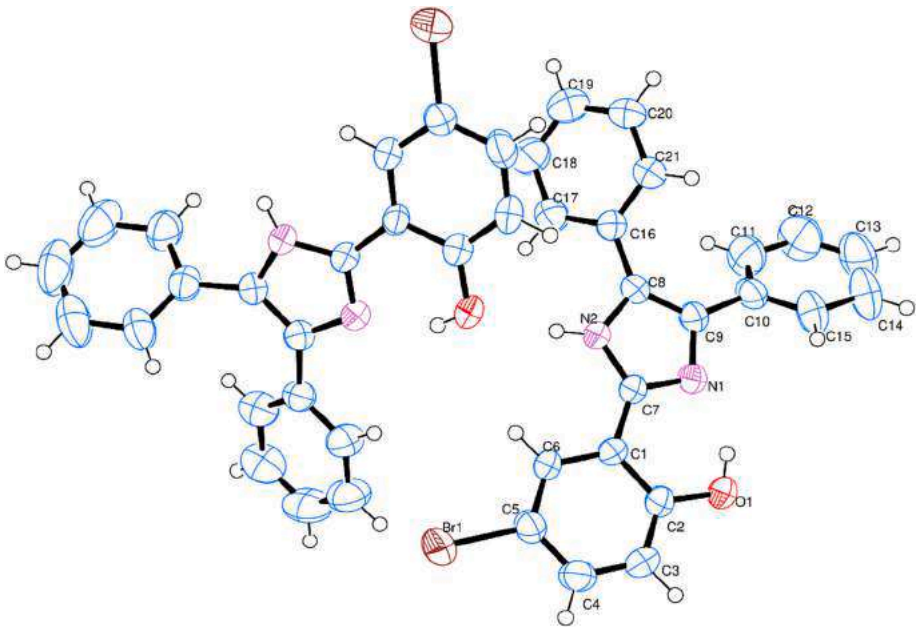

Fig. 4. Asymmetric unit of **4d** crystal structure.

is showing intra and intermolecular hydrogen bonding in the crystal structure and also Intramolecular hydrogen bond formed between N_1 and O_1 ($O_1 - H_1 \cdots N_1$; 0.863Å; 1.762Å; 149.16°) Fig. 5. The molecule **4d** molecule is forming a 1D chain structure by N – H···O intermolecular hydrogen bonding ($N_2 - H_{2A} \cdots O_2$; 0.860Å; 1.980Å; 168.22°) Fig. 6. These 1D chains are interacting with each other by C—H···π, $\pi \cdots \pi$ and Br···H long- range van der Waal interactions forming the 3D structure. The crystal packing diagram of compound **4d** along with their interaction were illustrated in Fig. 7.

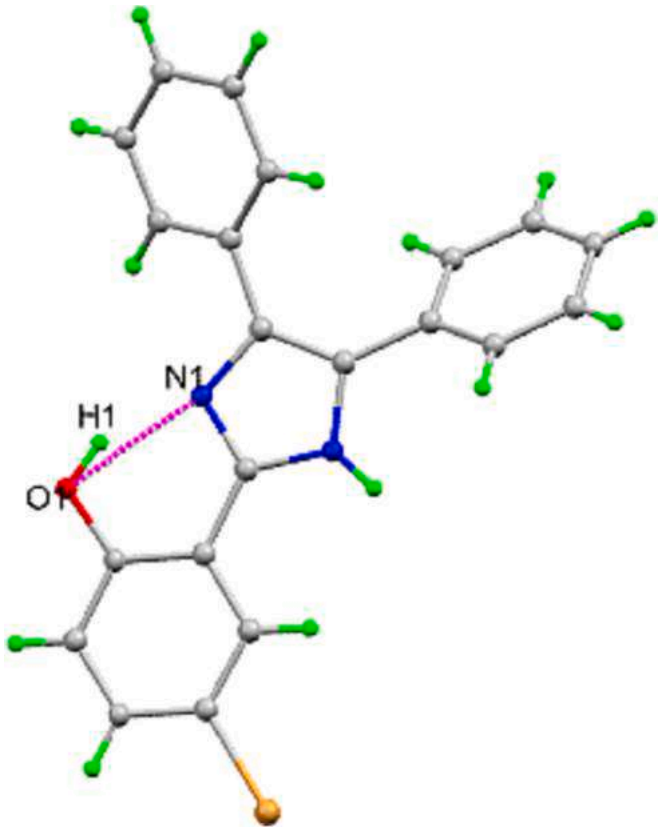

Fig. 5. Intramolecular hydrogen bonding in **4d**.

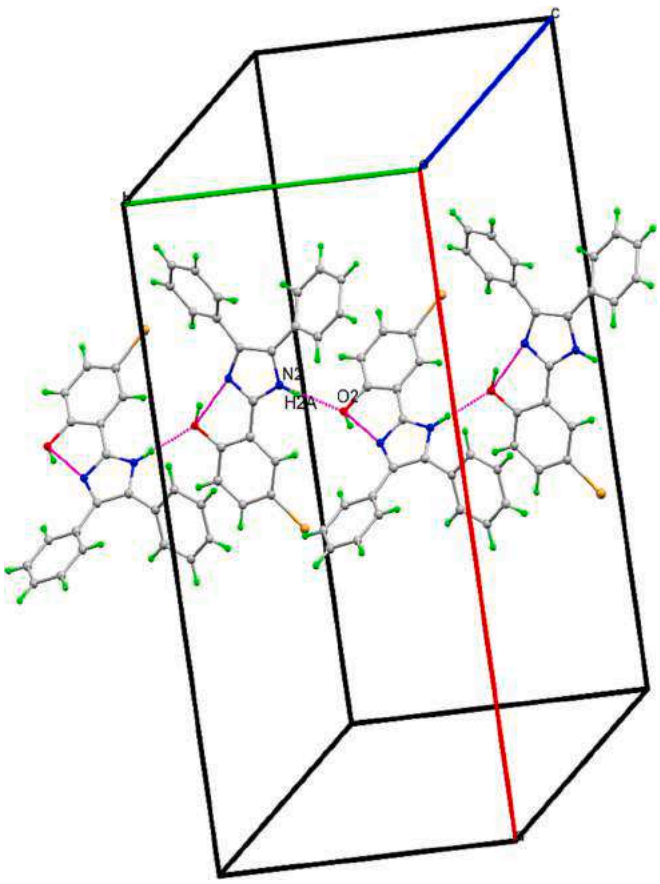

Fig. 6. Intermolecular hydrogen bonding between **4d** molecules and 1D chain structure.

*3.2. Spectral characterization of tri/tetra-aryl substituted imidazole hybrids (**4a**–**4d**) and (**6a**–**6d**)*

*3.2.1. 4-(4,5-diphenyl-1H-imidazol-2-yl)-2-methoxy-6-nitrophenol (**4a**)*

Yield: 75 %; white powder; UV–Visible (λ_{max}, DMSO): 301 nm; IR (ATR, γ, cm^{-1}): 3185 (NH/OHstr.); 2928(CH_2str.); 1649(CH_2str.); 1604 (C=Cstr.); 1446,1116(NO_2str.); 1240(C-Ostr.), 869(trisubst. ArCH bend); ^{1}HNMR (DMSO-d_6δppm, 400 MHz); 12.70 (br,1H, imidazole NH); 8.23 (s,1H, phenolH-4); 7.93 (s, 1H, phenolH-6); 7.29–7.55 (m, 10H, 2Phenyl); 3.98 (s, 3H, OCH_3); ^{13}CNMR: 150.34, 144.42, 143.45, 137.62, 136.02, 130.07, 129.98, 128.93, 128.16, 127.82, 121.26, 113.06, 112.05, 57.21, 40.45; ESI-HRMS (*m/z*): 387.33, 388.77 (M + 1); Analysis for $C_{22}H_{17}N_3O_4$; Calcd %: C, 63.24; H, 4.34; N, 10.89; Found %: C, 62.94; H, 4.22; N, 10.86.

*3.2.2. 2-Bromo-4-(4,5-diphenyl-1H-imidazol-2-yl)-6-methoxyphenol (**4b**)*

Yield: 78 %; white powder; UV–Visible (λ_{max}, DMSO): 315 nm; IR (ATR, γ,cm^{-1}): 3391 (NH/OHstr.); 2918(CH_2str.); 1654(C=Nstr.); 1602 (C=Cstr.); 1540(ArCH bend); 1272(C-Ostr.), 827(trisubst. ArCH bend); ^{1}HNMR (DMSO-d_6δppm, 400 MHz); 12.56 (br, 1H, imidazoleNH); 7.87 (s,1H, phenolH-4); 7.67 (s, 1H, phenolH-6); 7.21–7.56 (m,10H, 2Phenyl); 3.92 (s, 3H, OCH_3);^{13}CNMR: 149.11, 145.06, 144.52, 131.57, 130.07, 129.98, 128.79, 128.66, 127.56, 126.99, 123.15, 121.64, 110.07, 108.52, 56.79; ESI-HRMS (*m/z*): 421.29, 422.69 (M + 1); Analysis for $C_{22}H_{17}BrN_2O_2$; Calcd %: C, 62.74; H, 4.03; N, 6.65; Found %: C, 62.84; H, 3.92; N, 6.56.

*3.2.3. 2-(4-Bromophenyl)-4,5-diphenyl-1H-imidazole (**4c**)*

Yield: 78 %; white powder; UV–Visible (λ_{max}, DMSO): 301 nm; IR (ATR, γ,cm^{-1}): 3023 (NHstr.); 1647 (C=Nstr.); 1599 (C=Cstr.); 825 (1,4-disubt.Ar); ^{1}HNMR (DMSO-d_6δppm, 400 MHz); 12.79 (br, 1H, imidazoleNH); 7.68 (d,2H, BrphenylH-2&6); 7.57 (d, 2H, BrphenylH-3&5); 7.21–7.43 (m,10H, 2Phenyl); ^{13}CNMR: 144.95, 137.82, 135.47, 132.10, 131.38, 130.02, 129.15, 129.08, 128.89, 128.67, 128.36, 127.58, 127.54, 127.09, 121.86; ESI-HRMS (*m/z*): 374.64, 375.68 (M + 1); Analysis for $C_{21}H_{15}BrN_2$; Calcd %: C, 67.14; H, 4.02; N, 7.48; Found %: C, 67.84; H, 3.88; N, 7.56.S.

*3.2.4. 4-Bromo-2-(4, 5-diphenyl-1H-imidazol-2-yl) phenol (**4d**)*

Yield: 78 %; white powder; UV–Visible (λ_{max}, DMSO): 300 nm; IR (ATR, γ,cm^{-1}): 3396 (NH/OH str.); 2850 (CH_2 str.); 1666 (C=N str.), 1622 (C=C str.); 1279 (C—O str.); 831 (trisubt. Ar. CH bend); ^{1}HNMR (DMSO-d_6δppm, 400 MHz); 12.91 (br, 1H, imidazoleNH); 8.31 (s,1H, BrphenolH-3); 7.28 (d,1H,BrphenolH-5); 6.95 (d,1H,BrphenolH-6); 7.34–7.54 (m,10H, 2Phenyl); ^{13}CNMR: 173.45, 156.37, 144.59, 134.99, 132.62, 129.89, 129.02, 128.61, 127.81, 126.13, 119.33, 114.53, 110.52; ESI-HRMS (*m/z*): 390.20, 391.73 (M + 1); Analysis for $C_{21}H_{15}BrN_2O$; Calcd %: C, 64.47; H, 3.85; N, 7.17; Found %: C, 64.54; H, 3.80; N, 7.76.

*3.2.5. 4-(2-(4-Hydroxy-3-methoxy-5-nitrophenyl)-4,5-diphenyl-1H-imidazol-1-yl)-N-(pyridin-2-yl)benzenesulfonamide (**6a**)*

Yield: 75 %; white powder; UV–Visible (λ_{max}, DMSO): 303 nm; IR (ATR, γ,cm^{-1}): 3198 (NHstr.); 2921(CH_2str.); 1651(C=Nstr.); 1524 (C=Cstr.); 1484,1140(CHAr); 1361,1183 (SO_2str.); 1001 (S-Nstr.); 872 (trisubst. ArCH bend); ^{1}HNMR (DMSO-d_6δppm, 400 MHz); 12.75 (br, 1H, SO_2NH), 10.31 (br, 1H, OH), 9.38 (s, 1H, nitrophenolH-3), 8.18 (s, 1H, nitrophenolH-5), 7.32–7.69 (m, 14H, ArH), 7.15 (d, 1H, pyridineH-3), 7.43 (m, 1H, pyridineH-4), 7.12 (m, 1H, pyridineH-5), 7.97 (d, 1H, pyridineH-6), 3.81 (s, 3H, OCH_3); ^{13}CNMR: 172.66, 172.17, 153.55, 146.07, 136.25, 131.64, 130.74, 129.91, 128.93, 128.71, 128.34, 128.24, 127.52, 126.94, 118.96, 114.69, 110.86, 56.48; ESI-HRMS (*m/z*): 619.35, 620.06 (M + 1); Analysis for $C_{33}H_{25}N_5O_6S$; Calcd %: C,

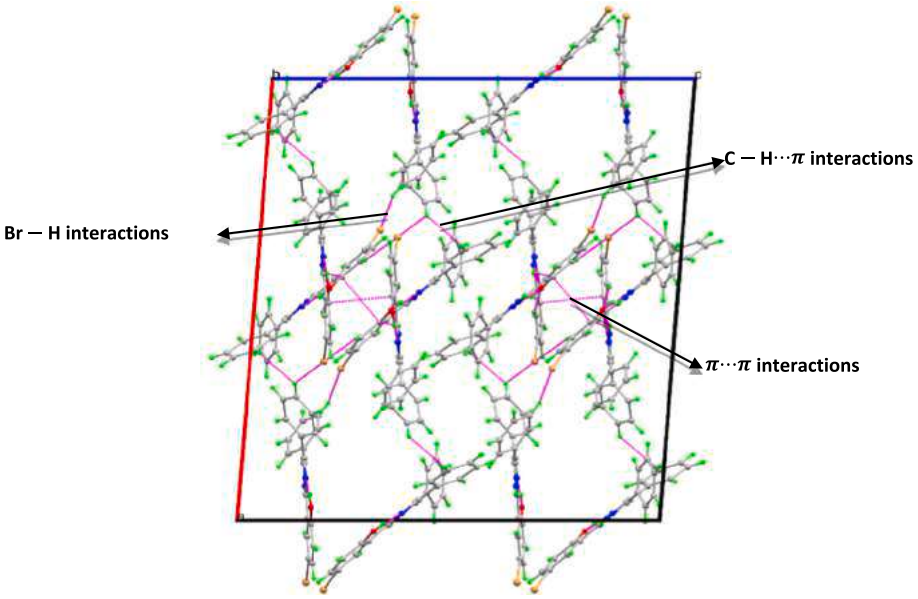

Fig. 7. Crystal packing diagram of **4d** (view along b axis).

63.92; H, 4.24; N, 11.13; S, 5.13; Found %: C, 62.84; H, 4.52; N, 11.56.S, 5.15.

*3.2.6. N-(5-Methylisoxazol-3-yl)-4-(2-(2-nitrophenyl)-4,5-diphenyl-1H-imidazol-1yl)benzenesulfonamide (**6b**)*

Yield: 79 %; white powder; UV–Visible (λ_{max}, DMSO): 307 nm; IR (ATR, γ,cm^{-1}): 3465, 3072 (ArCHstr.); 2854 (CH_2str.); 1681 (C=Nstr.); 1611(C=Cstr.); 1353,1163 (SO_2str.), 972(S-Nstr.); 1142, 1482(NO_2 str.); 852 (trisubst. Ar.CH bend); ^{1}HNMR (DMSO-d_6δppm, 400 MHz); 12.67 (br, 1H, SO_2NH), 7.97–7.90 (m, 4H, nitrophenylH), 7.43–7.88 (m, 14H, ArH), 6.09 (s, 1H, isoxazoleH-4), 2.25 (s, 3H, isoxazoleCH_3); ^{13}CNMR: 170.68, 169.67, 158.02, 148.88, 144.32, 141.52, 138.05, 135.25, 133.49, 132.67, 131.48, 130.32, 130.08, 129.27, 128.82, 127.54, 124.58, 123.95, 119.20, 95.92, 12.76; ESI-HRMS (*m/z*): 577.62, 578.88 (M + 1); Analysis for $C_{31}H_{23}N_5O_5S$; Calcd %: C, 64.51; H, 4.03; N, 12.12; S, 5.52; Found %: C, 64.51; H, 4.03; N, 12.56.S, 5.55.

*3.2.7. 4-(2-(5-Bromo-2-hydroxyphenyl)-4,5-diphenyl-1H-imidazol-1-yl)-N-(5-methylisoxazol-3-yl)benzenesulfonamide (**6c**)*

Yield: 79 %; white powder; UV–Visible (λ_{max}, DMSO): 305 nm; IR (ATR, γ,cm^{-1}): 3408 (NH/OH str.); 2850 (CH_2 str.); 1663 (C=Nstr.); 1533 (C=C str.); 1279 (C-Ostr.); 1325, 1166 (SO_2 str.); 917 (S—N str.); 879 (mono. subt. ArCH bend); 831 (trisubst. Ar.CH bend); ^{1}HNMR (DMSO-d_6δppm, 400 MHz); 12.86 (br, 1H, SO_2NH), 10.29 (br, 1H, OH), 7.42 (s, 1H, bromophenolH-3), 7.25 (d, 1H, bromophenolH-5), 6.55 (d, 1H, bromophenolH-6), 7.33–7.88 (m, 14H, ArH), 6.03 (s, 1H, isoxazoleH-4), 2.22 (s, 3H, isoxazoleCH_3); ^{13}CNMR: 172.03, 169.55, 156.30, 144.09, 143.54, 136.11, 132.92, 130.16, 130.07, 129.23, 128.33, 127.64, 119.64, 119.09, 113.31, 110.66, 96.16, 12.62; ESI-HRMS (*m/z*): 627.51, 628.71 (M + 1); Analysis for $C_{31}H_{23}BrN_4O_4S$; Calcd %: C, 59.33; H, 3.69; N, 8.93; S,5.11; Found %: C, 59.34; H, 3.69; N, 8.96.S, 5.17.

*3.2.8. 4-(2-(4-Hydroxy-3-methoxy-5-nitrophenyl)-4,5-diphenyl-1H-imidazol-1-yl)-N-(5-methylisoxazol-3-yl)benzenesulfonamide (**6d**)*

Yield: 70 %; white powder; UV–Visible (λmax, DMSO): 300 nm; IR (ATR, γ,cm^{-1}): 3201 (NHstr.); 2922 (CH_2str.); 1669 (C=Nstr.); 1528 (C=Cstr.); 1445,1112(NO_2str.); 1374,1163 (SO_2str.); 1244(C-Ostr.); 921(S-Nstr.); 862 (trisub. ArCH bend); ^{1}HNMR (DMSO-d_6δppm, 400 MHz); 12.76 (br, 1H, SO_2NH), 10.96 (br, 1H, OH), 8.23 (s, 1H, nitrophenolH-3), 7.93 (s, 1H, nitrophenolH-5), 7.32–7.92 (m, 14H, ArH), 7.32 (s, 1H, isoxazoleH-4), 3.98 (s, 3H, OCH_3), 2.29 (s, 3H, isoxazoleCH_3); ^{13}CNMR: 172.05, 169.57, 150.29, 144.40, 144.00, 143.27, 137.64, 136.02, 130.07, 132.72, 133.38, 129.88, 129.29, 129.22, 128.92, 128.49, 128.11, 121.48, 119.94, 115.31, 113.04, 112.99, 95.85, 57.22, 12.51; ESI-HRMS (m/z): 623.64, 624.88 (M + 1); Analysis for $C_{32}H_{25}N_5O_7S$; Calcd %: C, 61.63; H, 4.01; N, 11.36; S, 5.18; Found %: C, 61.75; H, 4.02; N, 11.36.S, 5.15.

3.3. Anticancer activity

We have evaluated the cytotoxic potential of the synthesized imidazoles (**4a–4d**) and (**6a–6d**) on MIA Pa Ca-2, MDA-MB-231 and H357 cells by MTT assay. Results suggested that all the above compounds have showed cytotoxic effects in different cancer cell lines in a concentration-dependent manner (1, 10, 20, 30, 40 and 50 μM) in MIA Pa Ca-2 cell line Fig. 8A–H, MDA-MB-231 cell line Fig. 9A–H and H357 cell line Fig. 10A–H. The IC50 concentration of compounds (**4a–4d**) and (**6a–6d**) evaluated for the above study are shown in Table 4. However, we found that compounds such as **4d**, **6c** and **6d** showed higher cytotoxic effects in MDA-MB-231 cells at 48 h and 72 h post-treatment compared to other compounds and other cell lines. Further, the apoptotic potential of **4d**, **6c** and **6d** compounds was evaluated by Annexin V-PE apoptosis assay in MDA-MB-231 cells and results indicated that the compound **6c** induced higher apoptosis compared to other compounds Fig. 11A–B. Western blotting results also corroborated with the above data, suggesting that upon treatment pro-apoptotic protein Bax up-regulated and anti-apoptotic protein Bcl2 down-regulated compared to control (without treatment) in MDA-MB-231 cells Fig. 11C. Thus, results demonstrated that imidazole derived compounds have potent anticancer activity by inducing apoptosis.

In this aspect, doxorubicin is a chemotherapy used as a standard drug for cancer treatment in clinics. Looking into the literature, it has been found that the IC50 value of doxorubicin is 0.69–3.16 μM in the MDA-MB-231 triple-negative breast cancer cell line [45,46] and 0.20–0.46 μM in pancreatic cancer cell line MIA PaCa-2 [47,48]. Similarly, cisplatin is a standard drug for oral cancer treatment. So going through the literature, it has been found that the IC_{50} value of cisplatin is 8.5 μM in H357 oral cancer cell line [49]. The *in vitro* cytotoxic effect of the standard anti-cancer drugs showing higher cytotoxicity effect at a lower concentration as compared to the above synthesized imidazole compounds. However, compound **6c** is showing better cytotoxic effect in

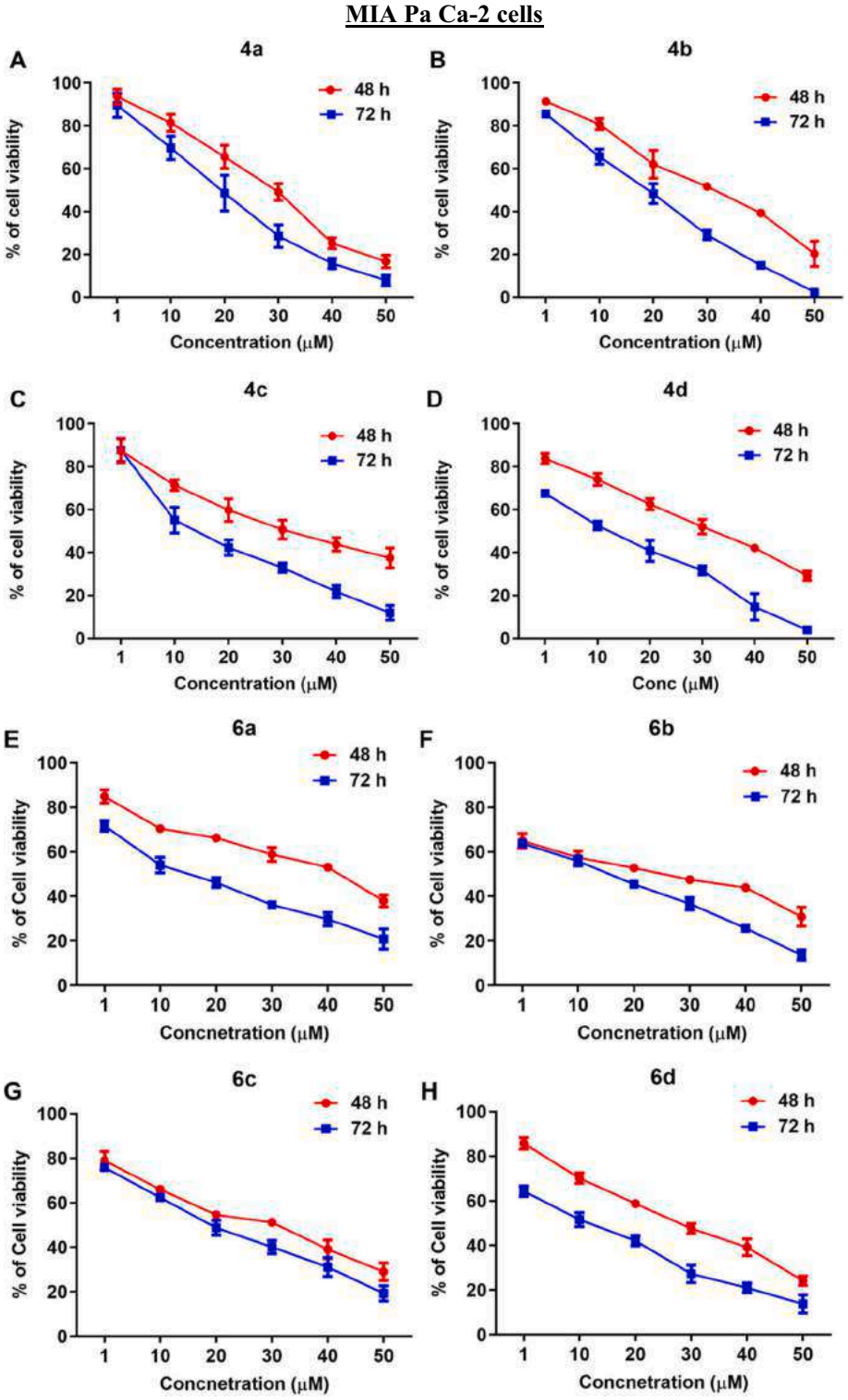

Fig. 8. *In vitro* cytotoxicity assay in MIA Pa Ca-2 cells. **A–H** Cells were treated with different concentrations (1–50 μM) of compounds (**4a–4d**) and (**6a–6d**) for 48 h and 72 h respectively; cell viability was assessed using the MTT assay ($n = 6$). Data represented as mean ± SD.

MDA-MB-231 human triple negative breast cancer cell line and its effect is comparable to the currently available anticancer chemotherapy.

The synthesized compound **6c** bearing a 5-methyl-isoxazolyl bearing benzene sulfonamide at the *N*1 position of the five membered imidazolyl moiety along with a substituted ortho bromo phenyl at C-2 position of the core nucleus could be the sole reason for the higher apoptosis. The compound **4d** though contains bromo group however the absence of sulfonamide could have been the main reason for the decrease in activity. In contrast, the compound **6d** inhibited the pro-apoptotic protein lesser than other two compounds, might be due to the presence of both electron withdrawing and donating groups in the same nucleus.

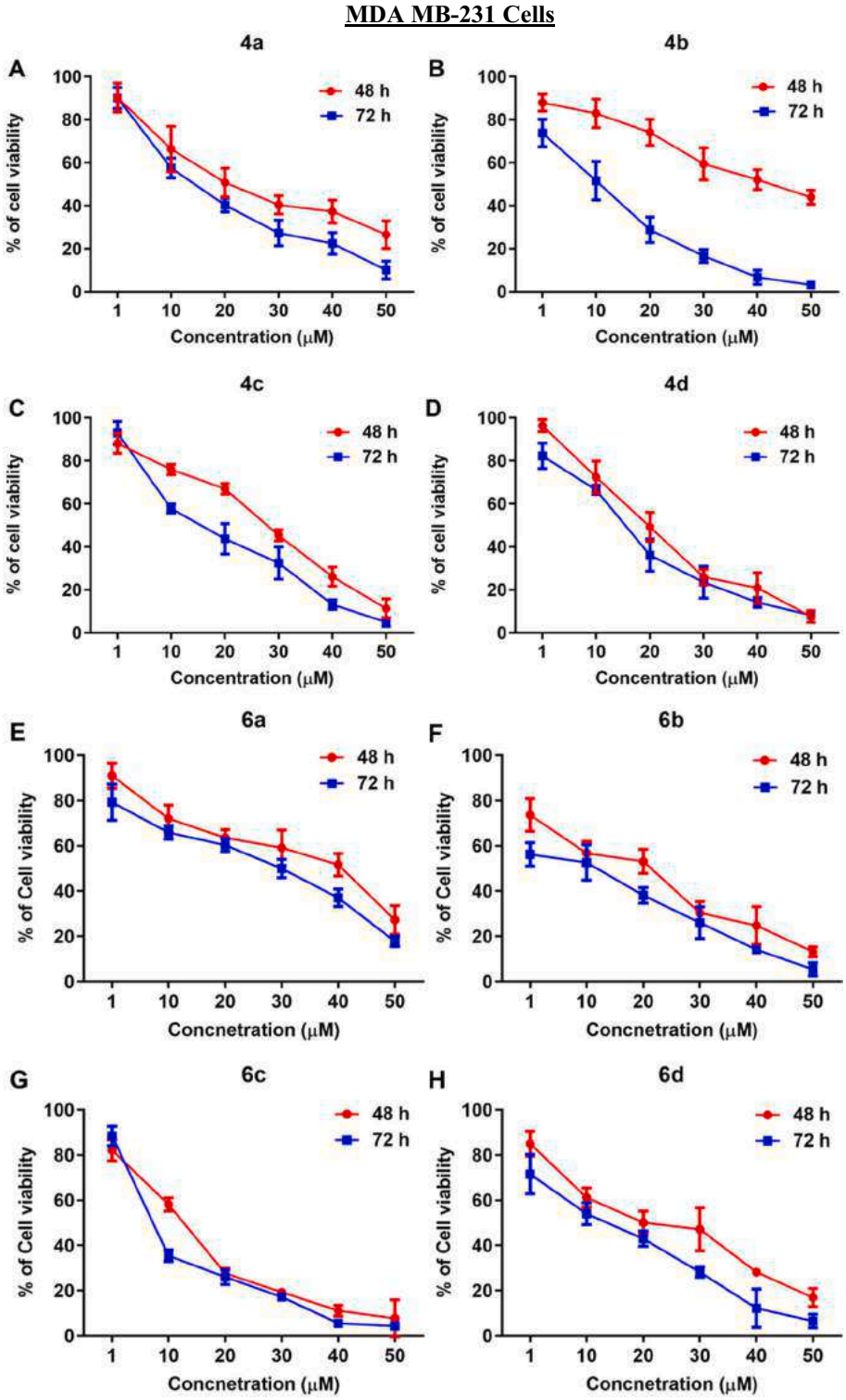

Fig. 9. *In vitro* cytotoxicity assay in MDA MB-231 cells. **A–H** Cells were treated with different concentrations (1–50 μM) of compounds (**4a–4d**) and (**6a–6d**) for 48 h and 72 h respectively; cell viability was assessed using the MTT assay (n = 6). Data represented as mean ± SD.

3.4. Antimicrobial activity

The *in-vitro* antimicrobial studies for the synthesized titled tri/tetra-substituted imidazole hybrids were screened for their antibacterial action against *S. aureus* (hswx88) and *E. coli* (MTCC 614), whereas the antifungal activity was evaluated against two pathogens *viz. C. albicans* (MTCC 3017), and *A. niger* (MTCC 9933). The results were expressed in terms of zone of inhibition (mm), and minimum inhibitory concentration (μg/mL) that was depicted in Table 5. Among all the compounds, the compounds containing bromo-substituted have outperformed for the antibacterial effect against the *S. aureus* topping the compounds **4b** (MIC 12.5 μg/mL; ZOI 22 mm) and **6d** (MIC 12.5 μg/mL; ZOI 24 mm), however, the *E. coli* strain found to be weighed on all the compounds. The compounds had shown a moderate zone of inhibition for both the fungal

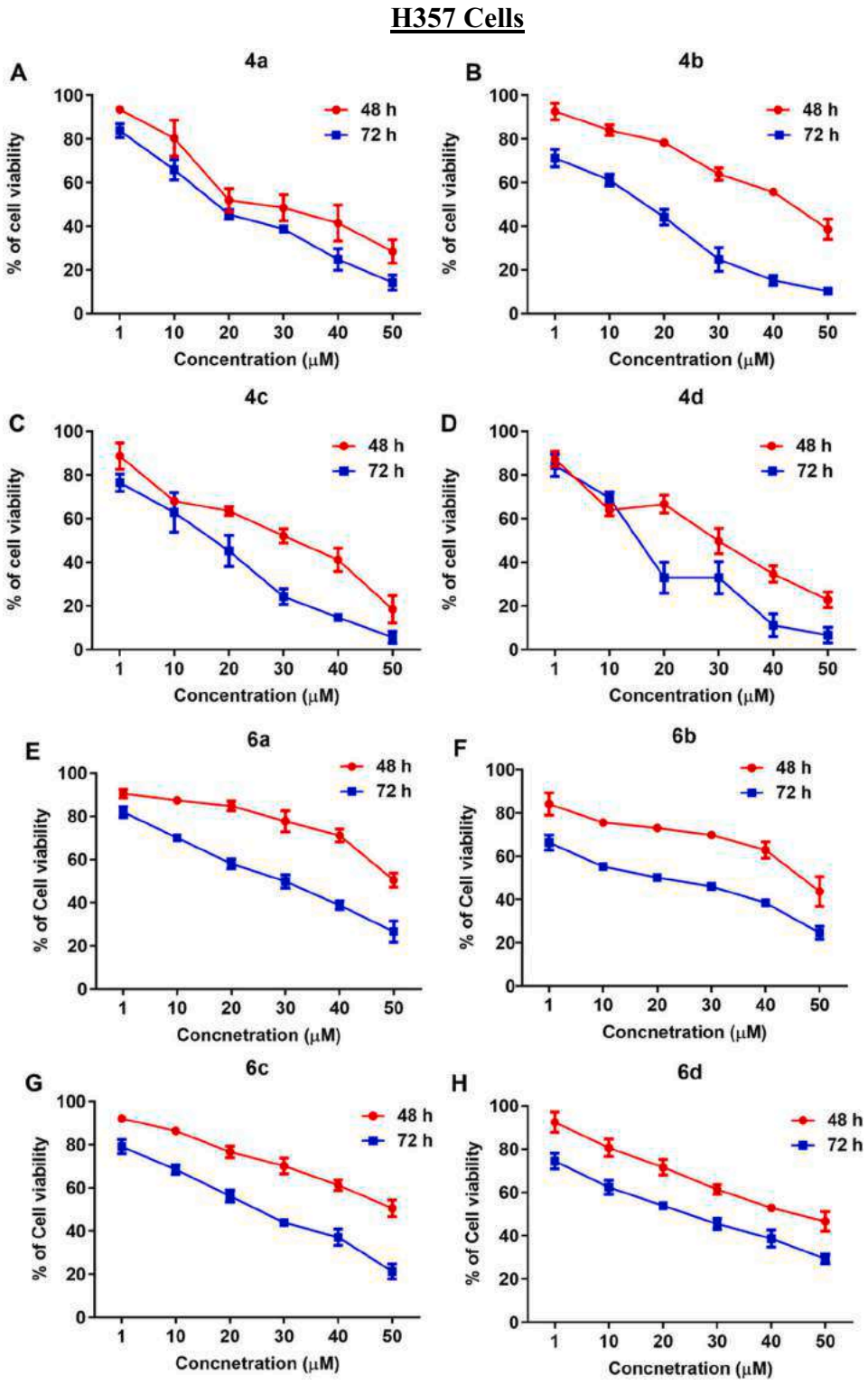

Fig. 10. *In vitro* cytotoxicity assay in H357 cells. **A–H** Cells were treated with different concentrations (1–50 μM) of compounds (**4a–4d**) and (**6a–6d**) for 48 h and 72 h respectively; cell viability was assessed using the MTT assay (n = 6). Data represented as mean ± SD.

strains, however, compound **4d** was found to inhibit the *T. rubrum* fairly with a MIC 12.5 μg/mL and a diameter of 21 mm for the zone of inhibition. Hence, the compounds containing bromo as a substituent could be carried forward for any subsequent antimicrobial studies.

The presence of two electron-donor substitutes, such as methoxy and hydroxy, at the C-2 phenyl position in compounds **4b** and **6d** of a particular molecule on the imidazole structural skeleton, may have broadened the range of antibacterial action against *S. aureus*, according to overall SARs addressing the antimicrobial activity. Contrarily, no such substances have any effect on *E. coli*. Compound **4d** has a bromo substitution at position 2 of the imidazole nucleus, which could be a reason for significant inhibition against *T. rubrum*.

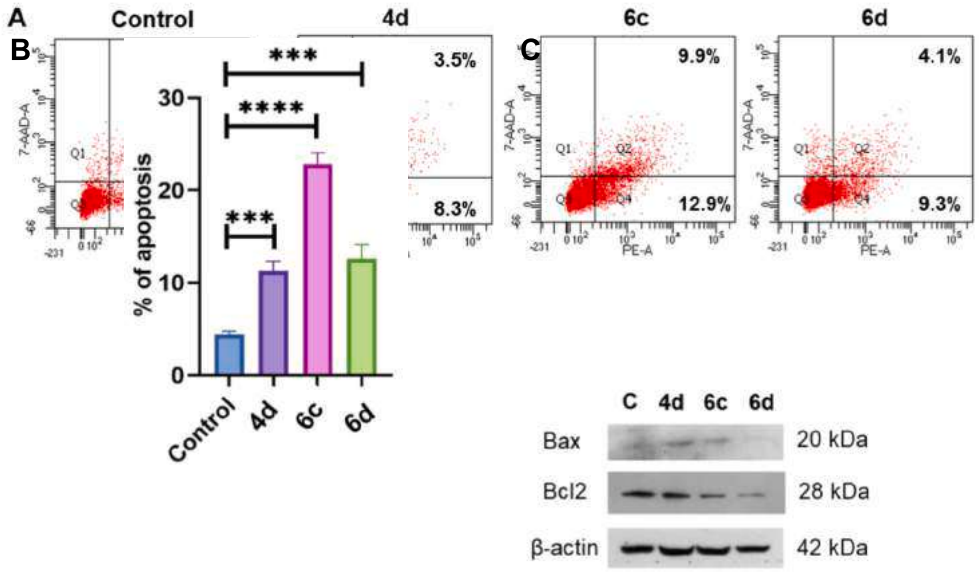

Fig. 11. **A–B** Representative images and bar graphs showing the percentage of apoptosis in MDA-MB-231 cells after treatment with **4d**, **6c**, and **6d** compounds (10 μM) for 48 h. Data represented as mean ± SD (n = 3), ***$p < 0.001$, ****$p < 0.0001$. **C** Representative Western blots demonstrating expression of pro-apoptotic marker (Bax) and anti-apoptotic markers (Bcl2) upon treatment with **4d**, **6c**, and **6d** compounds (10 μM) for 48 h.

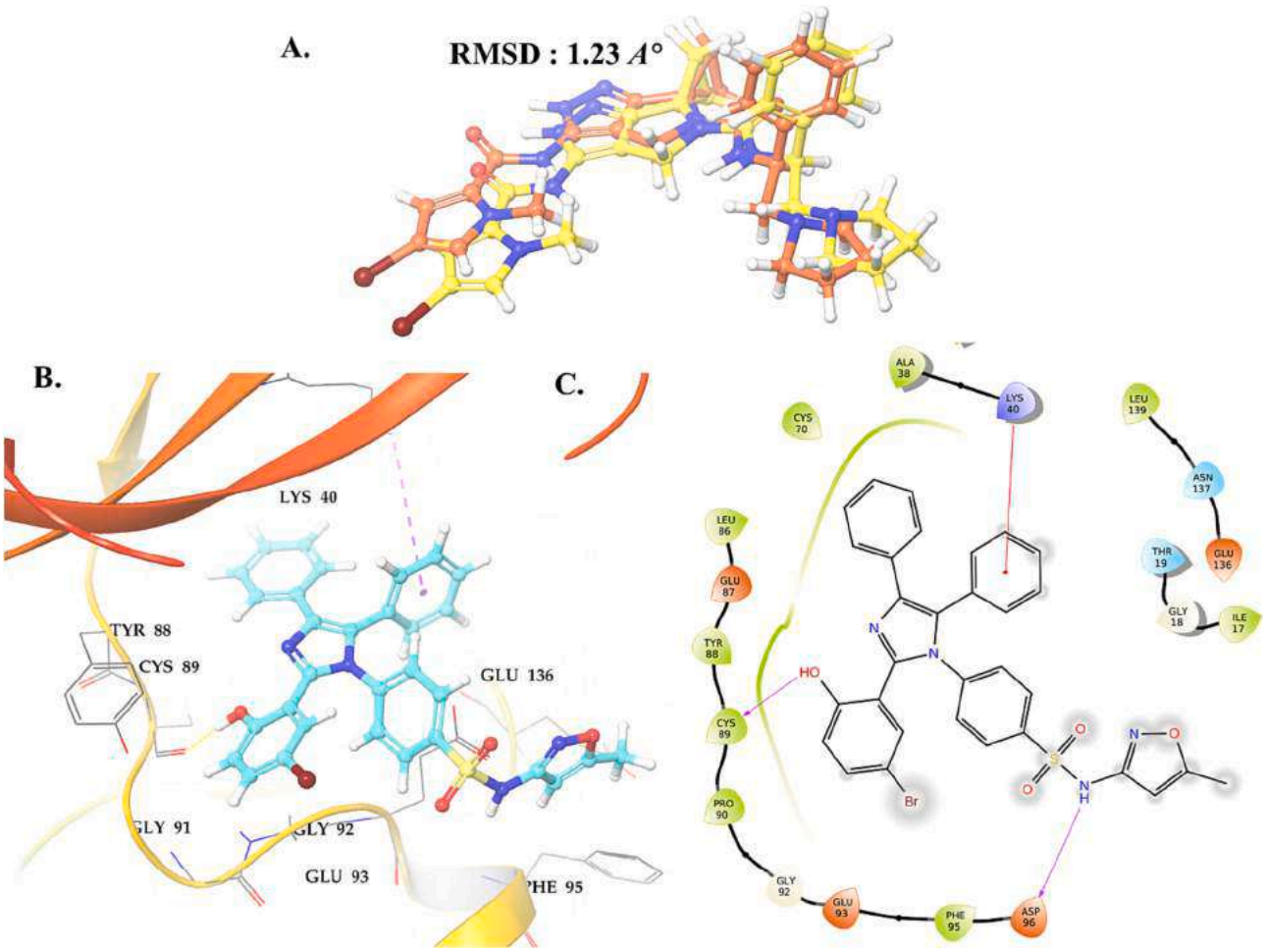

Fig. 12. **A**. Validation of the molecular docking protocol employed using the before docking (red) and after Glide SP docking (yellow) pose of co-crystallized ligand **B**. 2D and **C**. 3D interaction of Representative compound **6c** within the binding cavity of the receptor MELK.

3.5. Molecular docking analysis

To correlate the results of *in-silico* with *in-vitro* the molecular docking studies have been performed by using Schrodinger's glide. To validate the accuracy of the docking method, the co-crystallized ligand (pyrrolopyrazole inhibitor) was docked within the binding pocket of DNA gyrase. The resulting docked pose was then compared with the crystal structure pose by calculating the RMSD value, which was found to be 1.23 Å in this study. This value falls within the 2 Å threshold, confirming the reliability of the docking method. Fig. 12A illustrates that the docked pose aligns closely with the experimental orientation of DNA gyrase, indicating the validity of the docking method. The unphosphorylated protein has attracted the attention of the researchers due to its expression in several types of carcinoma cells. Hence, herein all the designed imidazole hybrids along with the synthesized compounds (**4a–4d)** and **(6a–6d)** were docked with the targeted protein Maternal embryonic Leucine zipper kinase (MELK), the unphosphorylated kinase which is a member of snf1/AMPK family belonging to the serine/threonine kinase group with a PDB ID: **4BKY**. Among all the docked ligands, compound **6c** bearing a hydroxyl group of salicylaldehyde residue in the desired tetra-substituted imidazole has shown a covalent hydrogen bonding with the amino group of cysteine residue (C89) of MELK in addition, another hydrogen bonding has been mediated with the nitrogen atom of sulphonamide and Aspartic acid (D96), displaying its affinity towards the kinase active site. It has been reported by Caneveri G. et al., 2013 a conformational change of residue Y88 when the *meta*-fluorophenyl group of co-crystal ligand - benzodipyrazole derivative as Cpd1 (co-crystal ligand) interacts with the active site of protein [50]. Also, there has been found to be detrimental claims towards the compounds efficacy when bulkier group faces or places itself in the hinge region or towards the face of "gatekeeper" residues (*viz.*, V25, L86, A38, I17), on this note the compound **6c** has been found to be free of any bulkier group towards the face region of the gatekeeper residues, neither there is any hinge region involvement for the compound in the kinase domain.

3.6. Molecular dynamics (MD) simulation

The dynamic nature and binding/conformational stability of the **6c**-MELK complex were explored through a long-range, up to 100 ns, MD simulation study. Several evaluating parameters, such as the root mean square deviation (RMSD) of protein Cα atoms, ligand atoms, protein root mean square fluctuation (RMSF), and protein-ligand contact mapping, were explored to investigate ligand-protein stability and dynamic behavior during the simulation time. The structural conformation of the protein Cα atoms during the MD simulation can be assessed through the RMDS of each frame obtained from the entire trajectory. The minimal deviation and steady variation of the RMSD throughout the simulation illustrate the stability of the protein–ligand complex [51–54]. The RMSD of Cα atoms in each frame was calculated and plotted against the simulation time and it is given in Fig. 13A, it was revealed that the RMSD of protein Cα atoms was substantially equilibrated after ligand binding, showing minute fluctuations from 1.50 to 2.25 Å. In addition to the RMSD of the protein Cα atoms, the RMSD of the ligand was calculated and found to be exceedingly low. The ligand RMSD was sustained at 2.5 Å after initial variation owing to equilibration. Slight fluctuations in RMSD were reported in the range of 1–3 Å, implying that the compound **6c** bound protein complex did not undergo any structural or conformational changes during the simulation run.

To investigate the impact of single amino acids on the stability of any protein–ligand interaction, the RMSF parameter is critical. It's the alteration in the orientation of each amino acid Cα atom during the simulation compared to the native state's initial orientation [55–58]. The RMSF values were computed to investigate the effect of compound **6c** on the flexibility of MELK Cα atoms. From Fig. 13B, it was observed that compound **6c** interacted with 19 amino acids of MELK protein during simulation which were Thr16 (0.658 Å), Ile17 (0.672 Å), Gly18 (0.815 Å), Thr19 (1.408 Å), Val25 (0.533 Å), Leu27 (0.507 Å), Ala38 (0.459 Å), Leu86 (0.45 Å), Tyr88 (0.539 Å), Cys89 (0.524 Å), Glu93 (0.576 Å), Phe95 (0.542 Å), Asp96 (0.659 Å), Ile99 (0.82 Å), Glu136 (0.57 Å), Asn137 (0.533 Å), Leu139 (0.448 Å), Ile149 (0.488 Å), and Asn268 (0.895 Å). All of these interacted residues were highlighted by a vertical green bar. The RMSF graph suggests that the fluctuation in the

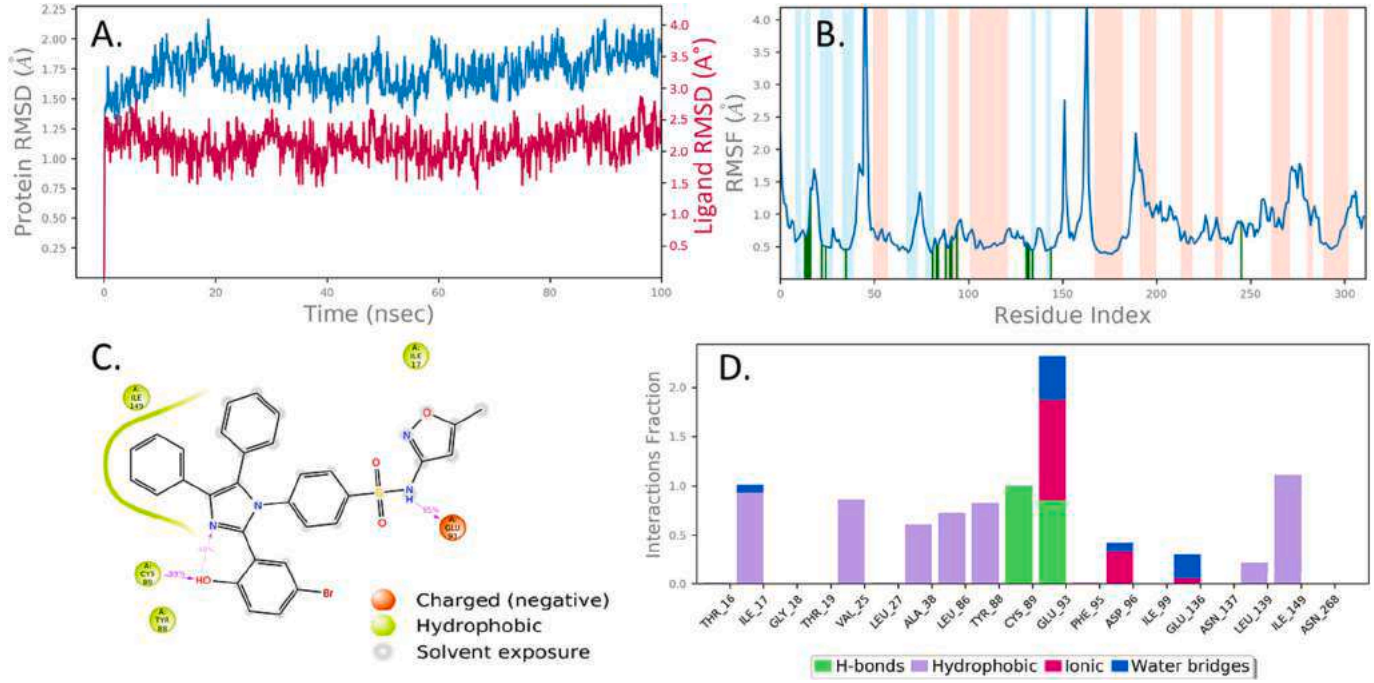

Fig. 13. MD simulation analysis of **6c** in complex with Maternal embryonic leucine zipper kinase (MELK) (PDB ID: 4BKY) **A**. RMSD (Protein RMSD is shown in grey while RMSD of compound **6c** are shown in red) **B**. Protein RMSF **C**. 2D Interaction diagram and **D**. Protein–ligand contact analysis of MD trajectory.

MELK protein Cα atoms is at minimum within the RMSF value of 1.0 Å when it binds with the compound **6c**. The fluctuation in some of the loop regions (white colour background) reaches 5.0 Å, but it is very low in the binding site region. The RMSF data presented above unquestionably indicated that the residues of MELK protein bound with compound **6c** stayed constant throughout the simulation. In a 2D ligand interaction diagram from the 100 ns simulation, the nitrogen atom of the sulphonamide moiety made hydrogen bond contact with the charged negative residue Glu93 at 85 % of the simulation duration, whereas residue Cys89 formed strong hydrogen bond interactions with the phenyl hydroxyl group at 99 % of the simulation trajectory Fig. 13D. During simulation, intramolecular hydrogen bonding was also observed with the hydroxyl group and nitrogen atom of tetra-substituted imidazole at 48 % of simulation time depicted in Fig. 13C. From the ligand interaction histogram, the compound **6c** was situated in the active pocket by forming hydrophobic interactions with the hinge region or the face of "gatekeeper" residues Thr16, Val25, Ala38, Leu86, Tyr88, Leu139, Ile149, and ionic interactions with Glu93, Asp96, and Glu136.

4. Physiochemical properties

The compounds containing tri/tetra -substituted imidazole (**4a–4d**) and (**6a–6d**) were noted to be in good agreement with all the parameters of Lipinski's Rule, however the compounds containing tetra-substituted have found to be in their higher limit for molecular weight and clogP value. The compounds violating the rule however have been found to have good agreement with toxicity prediction, therefore the hydrophilicity and hydrogen acceptor parameters of a required candidate could be modified by adding appropriate adjuvant or vehicle at the time of administration. The RO5 parameters have been calculated by the online available tools *viz*., Molinspiration (http://www.molinspiration.com/) and Molsoft (http://molsoft.com/mprop/) and rechecked through the ChemDraw software, which was well-illustrated in Table 1. The theoretical calculation of Absorption, Distribution, Metabolism, and Elimination of synthesized imidazole derivatives was performed using pre-ADMET https://preadmet.webservice.bmdrc.org/adme/including Blood-Brain Barrier (BBB), Caco-2 permeability (the Caco-2 cells for cell permeability into human intestinal cell barrier), Human Intestinal Absorption (produces permeability ration of Bioavailability and Absorption) and skin permeability, also the lethal dose LD_{50} for the novel imidazole derivatives have been predicted along with the toxicity class ranging from 150 to 1500 mg/Kg, determined by ProTox (http://tox.charite.de/tox/) documented in the Table 1. All the compounds displayed a safe profile while the compounds bearing sulphonamide attached to the imidazolyl core displayed the safest profile, which could be a defined approach for the compound **6c** which displayed early apoptosis to be a lead molecule for upcoming anticancer drug discovery voyage.

5. Conclusion

In conclusion, two series of 2, 4, 5-trisubstituted imidazole (**4a–4d**) and 1,2,4,5-tetrasubstituted imidazole (**6a–6d**) derivatives had been designed, and synthesized conventionally *via* one-step reaction, without using any catalyst. Further, they were investigated for their *in vitro* anticancer activity against MDA-MB-231, MIA Pa Ca-2 and H357 cancer cell lines after being validated through *in-silico* docking and MD simulation studies. The stability for the compound **6c** was found to produce no conformational changes to the binding region of protein and displaying good binding affinity towards the receptor MELK which has been known to modulate triple-negative breast cancer cells, and the *in-vitro* cytotoxicity study has been well supported by the *in-silico* study results. The *in-vitro* anticancer results indicated that the compound **6c** have inhibited the proliferation of all the tested cancer cell lines showing maximum inhibition to MDA MB 231 cells through the induction of apoptosis. Further, we have evaluated the anti-bacterial/anti-fungal activity of the synthesized imidazole derivatives and found that all of the above showing anti-microbial activity. Current work reflects the development of imidazole sulfonamide twining hybrids as potent chemotherapeutic agent for the pharmaceutical researchers in designing other imidazole derivatives in the field of cancer, in near future.

Single XRD crystallography

The data for CCDC's 2247503 can be available at Crystallographic Data Centre http://www.ccdc.cam.ac.uk/deposit@ccdc.cam.ac.uk.

Declaration of competing interest

The authors declare that they have no known competing financial interests or personal relationships that could have appeared to influence the work reported in this paper.

Acknowledgment

The authors are grateful to the Dean of SPS for their encouragement. This work was supported by the SOADU-Ph.D. fellowship (Registration No. 1981606006) to M. Mahapatra in Pharmacy. The NMR analysis work was carried out at the Central Research Facility, KIIT University, Bhubaneswar, Odisha, India.

Funding

We greatly appreciate the funding support for this research provided by the Indian Council of Medical Research, Government of India (ICMR-SRF to M Mahapatra Grant No. 3/2/2/2022-NCD-III)

Appendix A. Supplementary data

Supplementary data to this article can be found online at https://doi.org/10.1016/j.ijbiomac.2023.126084.

References

[1] F. Bray, B. Møller, Predicting the future burden of cancer, Nat. Rev. Cancer 6 (2006) 63–74, https://doi.org/10.1038/nrc1781.
[2] I. Ali, W.A. Wani, K. Saleem, Cancer scenario in India with future perspectives, Cancer Ther. 8 (2011) 56–70.
[3] U. GLOBOCAN, New Global Cancer Data, in, 2020.
[4] F. Bray, J. Ferlay, I. Soerjomataram, R.L. Siegel, L.A. Torre, A. Jemal, Global cancer statistics 2018: GLOBOCAN estimates of incidence and mortality worldwide for 36 cancers in 185 countries, CA Cancer J. Clin. 68 (2018) 394–424, https://doi.org/10.3322/caac.21492.
[5] G.V. Sharma, A. Ramesh, A. Singh, G. Srikanth, V. Jayaram, D. Duscharla, J.H. Jun, R. Ummanni, S.V. Malhotra, Imidazole derivatives show anticancer potential by inducing apoptosis and cellular senescence, MedChemComm. 5 (2014) 1751–1760, https://doi.org/10.1039/C4MD00277F.
[6] D. De Vita, A. Angeli, F. Pandolfi, M. Bortolami, R. Costi, R. Di Santo, E. Suffredini, M. Ceruso, S. Del Prete, C. Capasso, Inhibition of the α-carbonic anhydrase from vibrio cholerae with amides and sulfonamides incorporating imidazole moieties, J. Enzyme Inhib. Med. Chem. 32 (2017) 798–804, https://doi.org/10.1080/14756366.2017.1327522.
[7] S. Qiu, Z. Lin, Y. Zhou, D. Wang, L. Yuan, Y. Wei, T. Dai, L. Luo, G. Chen, Highly selective colorimetric bacteria sensing based on protein-capped nanoparticles, Analyst 140 (2015) 1149–1154, https://doi.org/10.1039/c4an02106a.
[8] P.N. Chopra, J.K. Sahu, Biological significance of imidazole-based analogues in new drug development, Curr. Drug Discov. Technol. 17 (2020) 574–584, https://doi.org/10.2174/1570163816666190320123340.
[9] B. Narasimhan, D. Sharma, P. Kumar, Biological importance of imidazole nucleus in the new millennium, Med. Chem. Res. 20 (2011) 1119–1140, https://doi.org/10.1007/s00044-010-9472-5.
[10] M.K. Kathiravan, A.B. Salake, A.S. Chothe, P.B. Dudhe, R.P. Watode, M.S. Mukta, S. Gadhwe, The biology and chemistry of antifungal agents: a review, Bioorg. Med. Chem. 20 (2012) 5678–5698, https://doi.org/10.1016/j.bmc.2012.04.045.
[11] D. Rajaraman, G. Sundararajan, N. Loganath, K. Krishnasamy, Synthesis, molecular structure, DFT studies and antimicrobial activities of some novel 3-(1-(3, 4-dimethoxyphenethyl)-4, 5-diphenyl-1H-imidazol-2-yl)-1H-indole derivatives and its molecular docking studies, J. Mol. Struct. 1127 (2017) 597–610, https://doi.org/10.1016/j.molstruc.2016.08.021.
[12] Y. Yang, A. Csakai, S. Jiang, C. Smith, H. Tanji, J. Huang, T. Jones, K. Sakaniwa, L. Broadwell, C. Shi, Tetrasubstituted imidazoles as incognito Toll-like receptor 8 a

(nta) gonists, Nat. Commun. 12 (2021) 4351, https://doi.org/10.1038/s41467-021-24536-4.
[13] T. Güngör, Microwave assisted, sequential two-step, one-pot synthesis of novel imidazo [1, 2-a] pyrimidine containing tri/tetrasubstituted imidazole derivatives, Turk. J. Chem. 45 (2021) 219–230, https://doi.org/10.3906/kim-2009-40.
[14] E.M. Ali, M.S. Abdel-Maksoud, U.M. Ammar, K.I. Mersal, K.H. Yoo, P. Jooryeong, C.-H. Oh, Design, synthesis, and biological evaluation of novel imidazole derivatives possessing terminal sulphonamides as potential BRAFV600E inhibitors, Bioorg. Chem. 106 (2021), 104508, https://doi.org/10.1016/j.bioorg.2020.104508.
[15] R. Guda, G. Kumar, R. Korra, S. Balaji, G. Dayakar, R. Palabindela, P. Myadaraveni, N.R. Yellu, M. Kasula, EGFR, HER2 target based molecular docking analysis, in vitro screening of 2, 4, 5-trisubstituted imidazole derivatives as potential anti-oxidant and cytotoxic agents, J. Photochem. Photobiol. B Biol. 176 (2017) 69–80, https://doi.org/10.1016/j.jphotobiol.2017.09.010.
[16] H. Mehrabi, F. Alizadeh-Bami, R. Ranjbar-Karimi, Catalyst-free synthesis of 1, 2, 4, 5-tetrasubstituted imidazoles from arylamins, benzonitriles, arylglyoxals, and Meldrum's acid, Tetrahedron Lett. 59 (2018) 1924–1927, https://doi.org/10.1016/j.tetlet.2018.03.093.
[17] A.P.G. Nikalje, M.S. Ghodke, F.A.K. Khan, J.N. Sangshetti, CAN catalyzed one-pot synthesis and docking study of some novel substituted imidazole coupled 1, 2, 4-triazole-5-carboxylic acids as antifungal agents, Chin. Chem. Lett. 26 (2015) 108–112, https://doi.org/10.1016/j.cclet.2014.10.020.
[18] B. Hu, Z. Wang, N. Ai, J. Zheng, X.-H. Liu, S. Shan, Z. Wang, Catalyst-free preparation of 1, 2, 4, 5-tetrasubstituted imidazoles from a novel unexpected domino reaction of 2-azido acrylates and nitrones, Org. Lett. 13 (2011) 6362–6365, https://doi.org/10.1021/ol202650z.
[19] N.N. Al-Mohammed, Y. Alias, Z. Abdullah, R.M. Shakir, E.M. Taha, A.A. Hamid, Synthesis and antibacterial evaluation of some novel imidazole and benzimidazole sulfonamides, Molecules 18 (2013) 11978–11995, https://doi.org/10.3390/molecules181011978.
[20] M. Mahapatra, S.K. Mekap, S. Mal, J. Sahoo, S.K. Sahoo, S.K. Paidesetty, Coumaryl-sulfonamide moiety: unraveling their synthetic strategy and specificity toward hCA IX/XII, facilitating anticancer drug development, Arch. Pharm. e2200508 (2023), https://doi.org/10.1002/ardp.202200508.
[21] C.R. Sahoo, J. Sahoo, M. Mahapatra, D. Lenka, P.K. Sahu, B. Dehury, R.N. Padhy, S. K. Paidesetty, Coumarin derivatives as promising antibacterial agent (s), Arab. J. Chem. 14 (2021), 102922, https://doi.org/10.1016/j.arabjc.2020.102922.
[22] M.M. Elbadawi, W.M. Eldehna, A. Nocentini, M.F. Abo-Ashour, E.B. Elkaeed, M. A. Abdelgawad, K.S. Alharbi, H.A. Abdel-Aziz, C.T. Supuran, P. Gratteri, Identification of N-phenyl-2-(phenylsulfonyl) acetamides/propanamides as new SLC-0111 analogues: synthesis and evaluation of the carbonic anhydrase inhibitory activities, Eur. J. Med. Chem. 218 (2021), 113360, https://doi.org/10.1016/j.ejmech.2021.113360.
[23] I.M. McDonald, L.M. Graves, Enigmatic MELK: the controversy surrounding its complex role in cancer, J. Biol. Chem. 295 (2020) 8195–8203, https://doi.org/10.1074/jbc.rev120.013433.
[24] H.L. Abdulrahman, A. Uzairu, S. Uba, In silico studies of some 2-anilinopyrimidine derivatives as anti-triple-negative breast cancer agents, Beni-Suef Univ, Aust. J. Basic Appl. Sci. 9 (2020) 1–12, https://doi.org/10.1186/s43088-020-00041-3.
[25] H. Patel, A. Ansari, R. Pawara, I. Ansari, H. Jadhav, S. Surana, Design and synthesis of novel 2, 4-disubstituted aminopyrimidines: reversible non-covalent T790M EGFR inhibitors, J. Recept. Signal Transduct. 38 (2018) 393–412, https://doi.org/10.1080/10799893.2018.1557207.
[26] N.C. Desai, A.S. Maheta, A.M. Jethawa, U.P. Pandit, I. Ahmad, H. Patel, Zeolite (Y-H)-based green synthesis, antimicrobial activity, and molecular docking studies of imidazole bearing oxydibenzene hybrid molecules, J. Heterocyclic Chem. 59 (2022) 879–889, https://doi.org/10.1002/jhet.4427.
[27] A. Malani, A. Makwana, J. Monapara, I. Ahmad, H. Patel, N. Desai, Synthesis, molecular docking, DFT study, and in vitro antimicrobial activity of some 4-(biphenyl-4-yl)-1, 4-dihydropyridine and 4-(biphenyl-4-yl) pyridine derivatives, J. Biochem. Mol. Toxicol. 35 (2021), e22903, https://doi.org/10.1002/jbt.22903.
[28] H. Patel, I. Ahmad, H. Jadhav, R. Pawara, D. Lokwani, S. Surana, Investigating the impact of different acrylamide (electrophilic warhead) on osimertinib's pharmacological spectrum by molecular mechanic and quantum mechanic approach, Comb. Chem. High Throughput Screen. 25 (2022) 149–166, https://doi.org/10.2174/1386207323666201204125524.
[29] R. Pawara, I. Ahmad, S. Surana, H. Patel, Computational identification of 2, 4-disubstituted amino-pyrimidines as L858R/T790M-EGFR double mutant inhibitors using pharmacophore mapping, molecular docking, binding free energy calculation, DFT study and molecular dynamic simulation, In Silico Pharmacol. 9 (2021) 1–22, https://doi.org/10.1007/s40203-021-00113-x.
[30] I. Ahmad, D. Kumar, H. Patel, Computational investigation of phytochemicals from *Withania somnifera* (Indian ginseng/ashwagandha) as plausible inhibitors of GluN2B-containing NMDA receptors, J. Biomol. Struct. Dyn. 40 (2022) 7991–8003, https://doi.org/10.1080/07391102.2021.1905553.
[31] H. Berendsen, B. Hess, E. Lindahl, D. Van Der Spoel, A. Mark, G. Groenhof, GROMACS: fast, flexible, and free, J. Comput. Chem. 26 (2005) 1701–1718, https://doi.org/10.1002/jcc.20291.
[32] R. Girase, I. Ahmad, R. Pawara, H. Patel, Optimizing cardio, hepato and phospholipidosis toxicity of the Bedaquiline by chemoinformatics and molecular modelling approach, SAR and QSAR, Environ. Res. 33 (2022) 215–235, https://doi.org/10.1080/1062936x.2022.2041724.
[33] G. Kalibaeva, M. Ferrario, G. Ciccotti, Constant pressure-constant temperature molecular dynamics: a correct constrained NPT ensemble using the molecular virial, Mol. Phys. 101 (2003) 765–778, https://doi.org/10.1080/0026897021000044025.
[34] G.J. Martyna, Remarks on "Constant-temperature molecular dynamics with momentum conservation", Phys. Rev. E 50 (1994) 3234, https://doi.org/10.1103/physreve.50.3234.
[35] D. Singh, P. Mohapatra, S. Kumar, S. Behera, A. Dixit, S.K. Sahoo, Nimbolide-encapsulated PLGA nanoparticles induces mesenchymal-to-epithelial transition by dual inhibition of AKT and mTOR in pancreatic cancer stem cells, Toxicol. in Vitro 79 (2022), 105293, https://doi.org/10.1016/j.tiv.2021.105293.
[36] M. Mahapatra, P. Mohapatra, S.K. Sahoo, A.K. Bishoyi, R.N. Padhy, S.K. Paidesetty, Design, synthesis, and in-silico study of chromen-sulfonamide congeners as potent anticancer and antimicrobial agents, J. Mol. Struct. 1283 (2023), 135190, https://doi.org/10.1016/j.molstruc.2023.135190.
[37] A.K. Bishoyi, M. Mahapatra, C.R. Sahoo, S.K. Paidesetty, R.N. Padhy, Design, molecular docking and antimicrobial assessment of newly synthesized p-cuminal-sulfonamide Schiff base derivatives, J. Mol. Struct. 1250 (2022), 131824, https://doi.org/10.1016/j.molstruc.2021.131824.
[38] A.K. Bishoyi, M. Mahapatra, S.K. Paidesetty, R.N. Padhy, Design, molecular docking, and antimicrobial assessment of newly synthesized phytochemical thymol Mannich base derivatives, J. Mol. Struct. 1244 (2021), 130908, https://doi.org/10.1016/j.molstruc.2021.130908.
[39] J. Sahoo, G. Parween, S. Sahoo, S.K. Mekap, S. Sahoo, S.K. Paidesetty, Synthesis, spectral characterization, in silico and in vitro antimicrobial investigations of some Schiff base metal complexes derived fromazo salicylaldehyde analogues, Indian J. Chem. 55B (2016) 1267–1276.
[40] J. Sahoo, S.K. Mekap, P.S. Kumar, Synthesis, spectral characterization of some new 3-heteroaryl azo 4-hydroxy coumarin derivatives and their antimicrobial evaluation, J. Taibah Univ. Sci. 9 (2015) 187–195, https://doi.org/10.1016/j.jtusci.2014.08.001.
[41] J. Sahoo, P.S. Kumar, Study of solvatochromic behavior and antimicrobial activities of some newly synthesized bis-azo-dapsone congeners, Indian J. Chem. 55B (2016) 724–733.
[42] S. Mal, T. Saha, A. Halder, S.K. Paidesetty, S. Das, W.T. Wui, U. Chatterji, P. Roy, EGF-conjugated bio-safe luteolin gold nanoparticles induce cellular toxicity and cell death mediated by site-specific rapid uptake in human triple negative breast cancer cells, J. Drug Deliv. Sci. Technol. 80 (2023), 104148, https://doi.org/10.1016/j.jddst.2022.104148.
[43] N. Özbek, H. Katırcıoğlu, N. Karacan, T. Baykal, Synthesis, characterization and antimicrobial activity of new aliphatic sulfonamide, Bioorg. Med. Chem. 15 (2007) 5105–5109, https://doi.org/10.1016/j.bmc.2007.05.037.
[44] J. Sahoo, P. Kshiroda, N. Sarangi, S. Rout, S. Paidesetty, In silico investigation and biological evaluation of synthesized sulfamethoxazole derivatives, Indian, J. Pharm. Sci. 82 (2020) 123–130, https://doi.org/10.36468/pharmaceutical-sciences.629.
[45] X. Wan, J. Hou, S. Liu, Y. Zhang, W. Li, Y. Zhang, Y. Ding, Estrogen receptor α mediates doxorubicin sensitivity in breast cancer cells by regulating E-cadherin, Front. Cell. Dev. Biol. 9 (2021), 583572, https://doi.org/10.3389/fcell.2021.583572.
[46] S.H. Wen, S.C. Su, B.H. Liou, C.H. Lin, K.R. Lee, Sulbactam-enhanced cytotoxicity of doxorubicin in breast cancer cells, Cancer Cell Int. 18 (2018) 1–18, https://doi.org/10.1186/s12935-018-0625-9.
[47] C. Skarbek, S. Serra, H. Maslah, E. Rascol, R. Labruère, Arylboronate prodrugs of doxorubicin as promising chemotherapy for pancreatic cancer, Bioorg. Chem. 91 (2019), 103158, https://doi.org/10.1016/j.bioorg.2019.103158.
[48] K. Brajša, I. Vujasinović, D. Jelić, M. Trzun, I. Zlatar, G. Karminski-Zamola, M. Hranjec, Antitumor activity of amidino-substituted benzimidazole and benzimidazo [1, 2-a] quinoline derivatives tested in 2D and 3D cell culture systems, J. Enzyme Inhib. Med. Chem. 31 (2016) 1139–1145, https://doi.org/10.3109/14756366.2015.1101093.
[49] X.H. Khoo, I.C. Paterson, B.H. Goh, W.L. Lee, Cisplatin-resistance in oral squamous cell carcinoma: regulation by tumor cell-derived extracellular vesicles, Cancers. 11 (2019) 1166, https://doi.org/10.3390/cancers11081166.
[50] G. Canevari, S. Re Depaolini, U. Cucchi, J.A. Bertrand, E. Casale, C. Perrera, B. Forte, P. Carpinelli, E.R. Felder, Structural insight into maternal embryonic leucine zipper kinase (MELK) conformation and inhibition toward structure-based drug design, Biochemistry 52 (2013) 6380–6387, https://doi.org/10.1021/bi4005864.
[51] R. Pawara, I. Ahmad, D. Nayak, S. Wagh, A. Wadkar, A. Ansari, S. Belamkar, S. Surana, C.N. Kundu, C. Patil, Novel, selective acrylamide linked quinazolines for the treatment of double mutant EGFR-L858R/T790M non-small-cell lung cancer (NSCLC), Bioorg. Chem. 115 (2021), 105234, https://doi.org/10.1016/j.bioorg.2021.105234.
[52] Y.O. Ayipo, I. Ahmad, Y.S. Najib, S.K. Sheu, H. Patel, M.N. Mordi, Molecular modelling and structure-activity relationship of a natural derivative of o-hydroxybenzoate as a potent inhibitor of dual NSP3 and NSP12 of SARS-CoV-2: in silico study, J. Biomol. Struct. Dyn. (2022) 1–19, https://doi.org/10.1080/07391102.2022.2026818.
[53] Y. Boulaamane, I. Ahmad, H. Patel, N. Das, M.R. Britel, A. Maurady, Structural exploration of selected C6 and C7-substituted coumarin isomers as selective MAO-B inhibitors, J. Biomol. Struct. Dyn. (2022) 1–15, https://doi.org/10.1080/07391102.2022.2033643.
[54] H.Y. Lee, D.Y. Cho, I. Ahmad, H.M. Patel, M.J. Kim, J.G. Jung, E.H. Jeong, M. A. Haque, K.M. Cho, Mining of a novel esterase (est3S) gene from a cow rumen metagenomic library with organosphosphorus insecticides degrading capability: catalytic insights by site directed mutations, docking, and molecular dynamic

simulations, Int. J. Biol. Macromol. 190 (2021) 441–455, https://doi.org/10.1016/j.ijbiomac.2021.08.224.
[55] R. Zrieq, I. Ahmad, M. Snoussi, E. Noumi, M. Iriti, F.D. Algahtani, H. Patel, M. Saeed, M. Tasleem, S. Sulaiman, Tomatidine and patchouli alcohol as inhibitors of SARS-CoV-2 enzymes (3CLpro, PLpro and NSP15) by molecular docking and molecular dynamics simulations, Int. J. Mol. Sci. 22 (2021) 10693, https://doi.org/10.3390/ijms221910693.
[56] S. Ghosh, S. Das, I. Ahmad, H. Patel, In silico validation of anti-viral drugs obtained from marine sources as a potential target against SARS-CoV-2 Mpro, J. Indian Chem. Soc. 98 (2021), 100272, https://doi.org/10.1016/j.jics.2021.100272.
[57] I. Ahmad, S.R. Akand, M. Shaikh, R. Pawara, S. Manjula, H. Patel, Synthesis, molecular modelling study of the methaqualone analogues as anti-convulsant agent with improved cognition activity and minimized neurotoxicity, J. Mol. Struct. 1251 (2022), 131972, https://doi.org/10.1016/j.molstruc.2021.131972.
[58] U. Acar Çevik, I. Celik, A. Işık, I. Ahmad, H. Patel, Y. Özkay, Z.A. Kaplancıklı, Design, synthesis, molecular modeling, DFT, ADME and biological evaluation studies of some new 1, 3, 4-oxadiazole linked benzimidazoles as anticancer agents and aromatase inhibitors, J. Biomol. Struct. Dyn. (2022) 1–15, https://doi.org/10.1080/07391102.2022.2025906.

Journal of Molecular Structure 1283 (2023) 135190

Contents lists available at ScienceDirect

Journal of Molecular Structure

journal homepage: www.elsevier.com/locate/molstr

Research article

Design, synthesis, and *in-silico* study of chromen-sulfonamide congeners as potent anticancer and antimicrobial agents

Monalisa Mahapatra[a], Priyanka Mohapatra[c], Sanjeeb Kumar Sahoo[c], Ajit Kumar Bishoyi[a,b], Rabindra Nath Padhy[b], Sudhir Kumar Paidesetty[a,*]

[a] *Department of Medicinal Chemistry, School of Pharmaceutical Sciences, Siksha 'O' Anusandhan Deemed to be University, Bhubaneswar, Odisha 751003 India*

[b] *Central Research Laboratory, Institute of Medical Sciences and SUM Hospital, Siksha 'O' Anusandhan Deemed to be University, Bhubaneswar, Odisha 751003, India*

[c] *Institute of Life Sciences, Bhubaneswar, Orissa 751 023, India*

ARTICLE INFO

Article history:
Received 4 July 2022
Revised 30 January 2023
Accepted 16 February 2023
Available online 23 February 2023

Keywords:
Coumarin
Schiffbase
Sulfonamide
Molecular docking
Antifungal activity
Cytotoxic activity

ABSTRACT

A series of *N-heteroaryl*-4-(1-(2-oxo-2*H*-chromen-3-yl) ethylideneamino) benzenesulfonamide (**5a-**5h) have been synthesized by the condensation reaction of appropriate *N*-heteroaryl- 4-amino benzenesulfonamide (**4a-4f**) with derivatives of 3-acetyl coumarin (**3a-3b**) in ethanol. The structures of these congeners were confirmed by $^{1}H/^{13}C$NMR, FTIR, HRMS, elemental analysis, and their powder characteristic was measured by XRD techniques. Further, the results of antimicrobial assay for compounds **5a, 5d,** and **5f** proved to be potent against the terbinafine resistant *Trichophyton rubrum* on the basis of an acceptable MIC value of 12.5 μg/ mL when compared to Ketoconazole. Moreover, compound **5f** had shown the highest zone of inhibition against *Staphylococcus aureus* as compared to Gentamicin. The designed hybrid molecules were previously screened and optimized through molecular docking using AutoDock4.2 and other concomitant parameters have also been validated. The docking results of the compounds **5d, 5e, 5f**, and 5h displaying binding energy in an ascending series, -9.28, -10.08, -11.88 and -12.4 Kcal/mol with the cancer causing protein further motivated for the assessment of *in vitro* anticancer activity. Therefore, the synthesized molecules were screened against different cancer cell lines (MDA-MB-231, MIA PaCa-2, and H357cells) and the results indicated that all the compounds inhibited the cell proliferation in a concentration-dependent manner at different time points.

1. Introduction

Cancer is a growing major health concern in the human race; in some years it has found its place at the top in the research field. Although, several treatments have been approved still chemotherapy remains to be the frontline treatment for almost all types of cancer. As reported by GLOBOCAN 2020, the mortality has been reached to 19.3 million worldwide [1]. According to global data by the International Agency of Research on Cancer (ICAR), out of every five people in a population, at least one is affected by cancer, of which, the incidence in female's remains higher. Demographic data reported that the cancers related to lungs, breast, and prostate to be the top four leading cancers by the year 2030. However, the pancreas, thyroid, and liver cancer will become a burden to society with unexpected cancer-related deaths [2]. The most aggressive breast cancer is often characterized as the heterogeneous group of cells carrying more than three subtypes, and each type can be targeted through molecular alterations as the receptors of estrogen, progesterone and the human epidermal growth factor receptor 2 (ErbB2) has been remained silent in most of the patients diagnosed with TNBC [3]. Though several therapies have been approved, still the clinical outcome went futile. Therefore, several new candidates with molecular-specific targets remain the call of the day. Pancreatic ductal adenocarcinoma (PDAC) cancer is the heterogeneous group of metastatic cell lines responsible for causing cancer with a dismal survival rate of 10% within 5 years of diagnosis report [4]. GLOBOCAN 2018, focused on the high lethality effect of the type of cancer reporting 432,242 deaths. Literature indicated that the MIA PaCa-2 cell line had been established from a Caucasian male of 65 years old carrying a tumor in the pancreas [5]. The cells mainly express differentiation in neuroendocrine cells and SSTR2 receptors, a subtype of somatostatin receptors. These differentiations were proved helpful for the detection and curative approach for the prognosis of adenocarcinomas

* Corresponding author.
E-mail address: sairampaidesetty@gmail.com (S.K. Paidesetty).

https://doi.org/10.1016/j.molstruc.2023.135190
0022-2860/

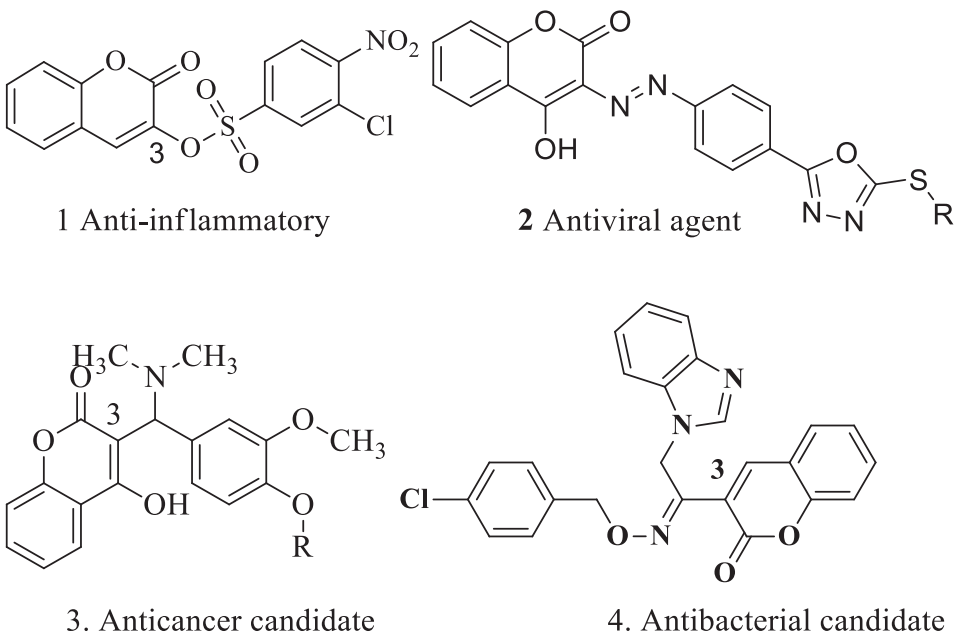

Fig. 1. Coumarin derivatives at C-3 position possess different biological properties.

[6]. Recently, synthesized coumaryl-sulfonamide candidates have been shown potent anticancer activity against human cell cancer lines, among which 7-dimethylamino-N-4-methoxyphenyl-coumar-3-yl sulfonamide has significantly inhibited the MDA-MD-231 cancer cell lines [7]. The prevalence of antibacterial resistance is more rapid, in microbes. The concept of conjugating phytochemicals with the synthetic pharmacophore has provided a potential opportunity for a safe and effective drug *viz*., the eminent commercial antibiotic Novobiocin, bearing coumarin-carboxamide moiety works by inhibiting bacterial DNA gyrase; employed for the treatment of severe urinary and respiratory tract infections [8–12].

Coumarins are the most abundant naturally occurring secondary metabolite and a part of the structure of the flavonoid; chemically-containing fused Benz [α] pyrone ring system. Among all the phyto-candidates, the derivatives of C3 position of coumarins have been well known for their medicinal properties including inhibition of platelet aggregation, steroid 5α-reductase, and also being diversified in biological fields' viz., anti-inflammatory [13], antiviral [14], anticancer [15], and antibacterial action [16] Fig. 1.

These azomethine groups is a versatile synthetic precursor and have been exploited for the preparation of various saturated heterocyclic compounds by cyclization process, some marketed drugs viz., Nitrofurantoin, fumoxicillin and furazolidinone have been in demand by inhibiting the DNA replication by inducing cross linkage between the strands [17]. (Fig. 2). For the development of a newer antibacterial agent, the coumarin moiety has been proved as a potent pharmacophore [18].

Sulphonamide group of antibacterial drugs are the structural analog of pABA as well as a competitive inhibitor of bacterial *Dihydroptereate synthetase i.e*., an essential enzyme for the biosynthesis of bacterial folic acid, the adjunct of trimethoprim with Sulfamethaoxazole (SMZ) was used in the treatment of pneumonia caused by the fungus *Pneumocystis carinii* in immunocompromised HIV patients [19]. Since, the sulfonamide causes resistance as a single component SMZ in several bacterial infections. Thus, we have attempted to enhance its activity by the conjugation of obsolete sulfur drugs with several other pharmacophore groups [20,21] which was already explored by our earlier research work; when a diazenyl sulfonamide group was introduced either into the 4-hydroxycoumarin congeners at their C-3 position or in the suitable position of phytochemicals (viz., thymol, p-cuminal, vanillin) [22–24].

The aim of our work was to synthesize new candidates with promising anticancer activity for the reported earlier anticancer activity of the core compound coumarin and the age old existing sulfa drug as antimicrobial agent. Further, the hybridization approach has resulted to possess excellent antimicrobial and anticancer activity of the compounds. The advent of molecular hybridization techniques for the drug design has unlocked many pathways to develop new molecules possessing a broad range of biological activity. This hybridization process requires a connector

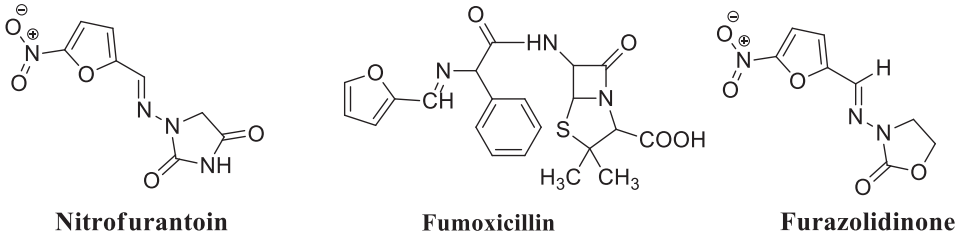

Fig. 2. Schiffbase derived anti-infective drugs.

link between two pharmacophore moieties which is achieved by the principles of medicinal chemistry approach.

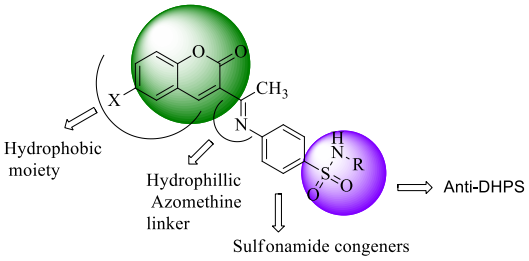

Designed Coumaryl- sulfonamide Pharmacophore model for antimicrobial and Anticancer activity

Rationality of newly developed Coumaryl-Sulfonamide Congeners

2. Materials and methods

2.1. Materials

All the necessary chemicals were used as AR grade and procured from Sigma-Aldrich and were used without purification. The λ_{max} for the desired synthesized compounds was noted by the instrument UV-Visible spectrometer (JASCO V-630 spectrophotometer). The functional group was analyzed by JASCO FT/IR 4600 spectrophotometer. The $^{1}H/^{13}C$NMR spectral data on a Bruker analyzer spectrometer with (DMSO-d_6 or $CDCl_3$) as solvent and Tetramethylsilane (TMS) as internal standard and chemical shift are reported in term of ppm, δ values. LC-MS (Shimadzu-Mass spectrophotometer) and elemental analysis (C, H, N) was performed on Perkins Elmer - 2400 CHNS analyzer. The reaction mixture was monitored by Thin-layer chromatography (TLC) using appropriate solvents ethyl acetate and n-Hexane in 1:1. An X-ray diffraction (XRD) pattern of silica was obtained with Cu Ka X-ray source including- a step of 0.02 (2θ) and run 2θ = 6–80 ºC at room temperature.

2.2. Synthesis of substituted 3-acetyl-coumarin (3a-3b)

The substituted 3-acetyl coumarin have been synthesized by the equimolar concentration of the alcoholic solution (20 mL) of corresponding salicylaldehyde derivative **1a-1b** (0.01 mL) and ethyl acetoacetate **2** (0.01 mL) with the addition of few drops of piperidine in the mixture and refluxed for 2 h. Then the reaction mixture was poured in ice-cold water and kept overnight in the refrigerator. The obtained precipitate was filtered and recrystallized from ethanol [25].

2.3. Synthesis of N-heteroaryl-4-(1-(2-oxo-2H-chromen-3-yl) ethylideneamino) benzene sulfonamide (5a-5h)

The substituted Schiff base 3-acetyl coumarin has been synthesized by refluxing the reaction mixture of the equimolar concentration of an alcoholic solution (20 ml) of corresponding substituted 3-acetyl coumarin (0.01 mL) and individual sulfur drug (0.01 mL) with the addition of few drops of glacial acetic acid about 1 h. Then, the reaction solutions poured in crushed ice and kept it overnight in the refrigerator. Finally, the obtained precipitate was filtered, washed with cold ethanol, and recrystallized from ethanol [26].

2.4. Spectral characterisation of Coumarin-sulfonamide hybrids 5a-5h

4-((1-(2-oxo-2*H*-chromen-3-yl) ethylidene) amino)-*N*-(pyridin-2-yl) benzenesulfonamide (5a)

Yield: 78%; white powder; Uv-Visible (λ_{max}, DMSO): 290, 346 nm; IR (ATR, γ,cm^{-1}): 3413, 3242 (NHstr.), 2787(CH2str.), (ArCHstr.), 1738(C=Ostr.), 1674(C=Nstr.), 1635(C=Cstr.), 1581(CHAr), 1364,1159 (SO_2str.), 997(S-Nstr.), 823,755(1,4-disubt.Ar);^{1}HNMR (DMSO-$d_6$$\delta$ppm, 400 MHz); 7.69–7.90 (*d*, 4H, PhenylH), 6.60 (*d*,1H, pyridyl H-3), 7.49 (*m*,1H, pyridyl H-4), 6.57 (*m*,1H, pyridyl H-5), 8.62 (*d*,1H, pyridyl H-6), 7.49 (*s*,1H,Coumarinyl H-4), 7.93 (*d*, 1H, Coumarinyl H-5, J = 1.6 Hz), 7.44 (*t*, 1H Coumarinyl H-6J = 8.14 Hz), 7.75 (*t*, 1H, Coumarinyl H-7, J = 8.85 Hz), 7.39 (*d*,1H,Coumarinyl H-8, J = 10 Hz), 10.90 (*s*,1H, NH), 3.36 (*s*, 3H, $C\underline{H}_3$); ^{13}C NMR (400 MHz, DMSO-D_6); 173.27, 156.49, 144.61, 132.67, 128.63, 127.34, 126.11, 119.40, 114.54, 22.58; Analysis for $C_{22}H_{17}N_3O_4S$; Calcd %: C, 63.00; H, 4.09; N, 10.02; S, 7.64; Found %: C, 62.84; H, 3.92; N, 10.56.S, 7.55; ESI-HRMS (m/z): Anal. Calcd. for $C_{22}H_{17}N_3O_4S$ [M + H]+ 419.09; found: 420.05(M+1).

4-((1-(2-oxo-2*H*-chromen-3-yl) ethylidene) amino)-*N*-(pyrimidin-2yl)benzenesulfonamide (5b).

Yield: 77%; white powder; Uv-Visible (λ_{max}, DMSO): 296 nm; IR (ATR, γ,cm^{-1}): 3418, 3299 (NHstr.), 3072, 3039 (ArCHstr.), 2868 (CH_2str.), 1709(C=Ostr.), 1667(C=Nstr.), 1603(C=Cstr.), 1577 (CHAr bend), 1321, 1132 (SO_2str.), 968 (S-Nstr.), 818,767(1,4-disubt.Ar); ^{1}HNMR (DMSO-$d_6$$\delta$ppm, 400 MHz); 7.58-7.86 (*d*, 4H, PhenylH), 8.45 (*d*,1H, pyrimidinyl H-4), 6.50 (*m*,1H, pyrimidinyl H-5), 8.44 (*d*,1H, pyrimidinyl H-6), 7.40 (*s*,1H,Coumarinyl H-4), 7.42 (*d*, 1H Coumarinyl H-5, J = 8.12 Hz), 6.96 (*t*, 1H, Coumarinyl H-6, J = 8.14 Hz), 7.58 (*t*, 1H, Coumarinyl H-7, J = 8.12 Hz), 6.53 (*d*, 1H Coumarinyl H-8, J = 4.01 Hz), 8.57 (*s*,1H, NH), 3.27 (*s*, 3H, $C\underline{H}_3$); ^{13}C NMR (400 MHz, DMSO-D_6); δ 195.04, 158.29, 157.76, 153.66, 153.08, 145.70, 141.22, 136.63, 132.58, 129.87, 125.44, 124.86, 120.11, 118.45, 116.40, 115.56, 112.17, 30.09.; Analysis for $C_{21}H_{16}N_4O_4S$; Calcd%: C, 59.99; H, 3.83; N, 13.22; S, 7.63; Found%: C, 59.84; H, 3.92; N, 13.56.S, 7.55; ESI-HRMS (m/z): Anal. Calcd. for $C_{21}H_{16}N_3O_5S$ [M + H]+ 421.38; found: 421.55 (M+1).

N-carbamimidoyl-4-((1-(2-oxo-2*H*-chromen-3-yl) ethylidene) amino)benzenesulfonamide (5c).

Yield: 72%; white powder; Uv-Visible (λ_{max}, DMSO): 288, 345 nm; IR (ATR, γ,cm^{-1}): 3337(NHstr.),3095 (CHAr str.),2981 (CH_2str.),1731 (C=O str.), 1672 (C=Nstr.),1606 (C=CArstr.), 1354, 1134 (SO_2str.) 1069 (S-Nstr.)767 (CHAr bend.);^{1}HNMR (DMSO-$d_6$$\delta$ppm, 400 MHz); δ 8.63 (*s*,1H,NH), 7.73-7.93 (*d*, 4H, PhenylH), 7.69 (*s*,1H,Coumarinyl H-4), 7.73 (*d*, 1H, Coumarinyl H-5, J = 4.10 Hz), 7.45 (*t*, 1H, Coumarinyl H-6, J = 8.12 Hz), 7.44(*t*, 1H, Coumarinyl H-7, J = 8.12 Hz),7.44 (*d*, 1H, Coumarinyl H-8, J = 4.10 Hz), 3.34 (*s*,3H,CH_3). ^{13}C NMR (400 MHz, DMSO-D_6); δ 195.67, 159.00, 158.28, 155.14, 151.92, 147.61, 135.04, 131.32, 127.80, 125.43, 124.96, 118.70, 116.65, 112.85, 30.60; Analysis for $C_{18}H_{16}N_4O_4S$; Calcd %: C, 59.64; H, 4.12; N, 8.18; S, 9.37; Found %: C, 59.84; H, 3.88; N, 8.56.S, 9.57;ESI-HRMS (m/z): Anal. Calcd. for $C_{18}H_{16}N_4O_4S$ [M + H]+ 385.38; found: 385.45 (M+1).

N-((4-((1-(2-oxo-2*H*-chromen-3-yl)ethylidene) amino)phenyl)sulfonyl)acetamide (5d).

Yield: 75%; white powder; Uv-Visible (λ_{max}, DMSO): 291, 349 nm, IR (ATR, γ,cm^{-1}): 3340(CHArstr.), 1730(C=Ostr.), 1673(C=Nstr.), 1611(C=CAr str.), 1354,1177 (SO_2str.) 1007(S-Nstr.), 820 (CHAr bend.);^{1}HNMR (DMSO-d_6 δ ppm, 400 MHz); δ 8.67(s,1H,NH), 7.75–7.97 (*d*, 4H, ArH), 7.53(s,1H,Coumarinyl H-4), 7.73 (*d*,1H, Coumarinyl H-5, J = 3.14 Hz), 7.44 (*t*,1H, Coumarinyl H-6, J = 7.61 Hz), 7.46 (*t*, 1H, Coumarinyl H-7, J = 7.89 Hz),7.42 (*d*, 1H, Coumarinyl H-8, J = 3.27 Hz),3.33 (s,6H,2$C\underline{H}_3$). ^{13}C NMR (400 MHz, DMSO-D_6); δ 195.63, 168.85, 158.90, 155.13, 154.16, 147.39, 135.02, 131.31, 130.29, 125.46, 124.93, 124.31, 118.69, 116.64, 112.27, 30.59; Analysis for$C_{19}H_{16}N_2O_5S$ Calcd %: C, 56.24; H, 4.20; N, 14.57; S, 8.34; Found %: C, 56.15; H, 3.92; N, 14.56.S, 8.57;ESI-HRMS (m/z): Anal. Calcd. for $C_{19}H_{16}N_2O_5S$ [M + H]+ 385.28; found: 385.55 (M+1).

4-((1-(2-oxo-2*H*-chromen-3-yl)ethylidene)amino) benzenesulfonamide (5e)

Yield: 72%; white powder; Uv-Visible (λ_{max}, DMSO): 293, 339 nm; IR (ATR, γ,cm^{-1}): 3375, 3295 (NHstr.), 3028, (ArCH-str.), 2933(CH_2str.), (ArCHstr.),1729(C=Ostr.), 1673(C=Nstr.), 1611(C=Cstr.), 1352,1156(SO_2str.), 972(S-Nstr.), 829 (1,4-disubt.Ar); ^{1}HNMR (DMSO-$d_6$$\delta$ppm, 400 MHz); 7.75–7.97 (*d*, 4H, PhenylH), 7.73 (*s*,1H,Coumarinyl H-4), 7.48(*d*,1H, Coumarinyl H-5, *J* = 4.50 Hz),7.40 (*t*, 1H, Coumarinyl H-6, *J* = 7.25 Hz), 7.46 (*t*, 1H,Coumarinyl H-7, *J* = 7.45 Hz), 7.42 (*d*,1H,Coumarinyl H-8, *J* = 4.12 Hz),8.67 (s,1H, NH), 3.34 (s, 3H, C$\underline{H}_3$); ^{13}C NMR (400 MHz, DMSO-D_6); δ 195.63, 159.98, 155.03, 147.60, 135.02, 130.02, 125.47, 124.94, 118.09, 116.64, 30.60; Analysis for $C_{17}H_{14}N_2O_4S$; Calcd %: C, 59.37; H, 4.19; N, 7.29; S, 8.34; Found %: C, 59.23; H, 4.28; N, 7.45.S, 8.57;ESI-HRMS (m/z): Anal. Calcd. for $C_{17}H_{14}N_2O_4S$ [M + H]+ 342.38; found: 342.87 (M+1).

N-(5-methylisoxazol-3-yl)−4-((1-(2-oxo-2*H*-chromen-3yl) ethylidene) amino) benzenesulfonamide (5f).

Yield: 72%; white powder; Uv-Visible (λ_{max}, DMSO): 264 nm; IR (ATR, γ,cm^{-1}): 3483, 3261 (NHstr.), 2873(CH2str.), 1710(C=Ostr.), 1672(C=Nstr.), 1605(C=Cstr.), 1579(CHAr), 1381,1186(SO_2str.), 970(S-Nstr.), 824,754 (1,4-disubt.Ar);^{1}HNMR (DMSO-$d_6$$\delta$ppm, 400 MHz); 7.60-7.89 (*d*, 4H, phenyl H), 5.98 (s,1H, isoxazolyl H-4), 7.59 (s,1H,Coumarinyl H-4), 7.86 (*d*, 1H, Coumarinyl H-5, *J* = 4.76 Hz), 7.42 (*t*, 1H Coumarinyl H-6, *J* = 7.12 Hz), 7.63 (*t*, 1H, Coumarinyl H-7, *J* = 7.62 Hz), 7.45 (*d*,1H,Coumarinyl H-8, *J* = 3.12 Hz), 11.23 (s,1H, NH), 3.32 (s, 6H, C$\underline{H}_3$); ^{13}C NMR (400 MHz, DMSO-D_6); 173.45, 156.37, 144.59, 134.99, 132.62, 129.89, 129.02, 128.61, 127.81, 126.13, 119.33, 114.53, 110.52, 30.58; Analysis for $C_{21}H_{17}N_3O_5S$; Calcd %: C, 59.57; H, 4.05; N, 9.92;S; 7.57 Found %: C, 59.84; H, 9.80; N, 10.56; S, 7.47; ESI-HRMS (m/z): Anal. Calcd. for $C_{21}H_{17}N_3O_5S$ [M + H]+ 423.28; found: 423.85 (M+1)

4-((1-(7-bromo-2-oxo-2*H*-chromen-3-yl)ethylidene) amino)-*N*-(pyridin-2-yl)benzenesulfonamide (5g).

Yield: 75%; white powder; Uv-Visible (λ_{max}, DMSO): 279 nm; IR (ATR, γ,cm^{-1}): 3413, 3242 (NHstr.), 2925(CH_2str.), (ArCHstr.),1731(C=Ostr.), 1687(C=Nstr.), 1634(C=Cstr.), 1580(CHAr), 1354,1128(SO_2str.), 1258(C-Ostr.), 997(S-Nstr.), 833,767(1,4-disubt.Ar); ^{1}HNMR (DMSO-$d_6$$\delta$ppm, 400 MHz); 7.50-7.95 (*d*, 4H, ArH), 6.55 (*d*,1H, pyridyl H-3), 7.46 (*m*,1H, pyridyl H-4), 6.14 (*m*,1H, pyridyl H-5), 8.67 (*d*,1H, pyridyl H-6), 7.50 (s,1H,Coumarinyl H-4), 7.73 (*d*, 1H Coumarinyl H-5, *J* = 7.92 Hz), 7.53 (*t*, 1H, Coumarinyl H-6, *J* = 6.23 Hz), 7.40 (*d*, 1H, Coumarinyl H-8, *J* = 7.12 Hz), 8.61 (s,1H, NH), 3.33 (*s*, 3H, C$\underline{H}_3$); ^{13}C NMR (400 MHz, DMSO-D_6); 175.82, 159.5, 155.29, 153.87, 153.25, 148.85, 140.09, 128.804, 128.90, 127.60, 127.82, 126.60, 123.35, 123.20, 118.90, 117.85, 116.80, 113.80, 20.13; Analysis for $C_{22}H_{16}BrN_3O_4S$; Calcd%: C, 53.02; H, 3.24; N, 8.43; S, 6.43; Found%: C, 52.84; H, 3.52; N, 8.56.S, 6.55;ESI-HRMS (m/z): Anal. Calcd. for $C_{22}H_{16}BrN_3O_4S$ [M + H]+ 498.28; found: 498.85 (M+1).

4-((1-(7-bromo-2-oxo-2*H*-chromen-3-yl) ethylidene) amino)-*N*-(5-methylisoxazol-3-yl)benzenesulfonamide (5h).

Yield: 79%; white powder; Uv-Visible (λ_{max}, DMSO): 288, 345 nm; IR (ATR, γ,cm^{-1}): 3384, 3259 (NHstr.), 3073, (ArCH-str.), 2982(CH_2str.), 1734(C=Ostr.), 1673(C=Nstr.), 1603(C=Cstr.), 1593(CHAr), 1354,1187(SO_2str.), 980(S-Nstr.), 831,768(1,4-disubt.Ar);^{1}HNMR (DMSO-$d_6$$\delta$ppm, 400 MHz); 7.43–7.90 (*d*, 4H, PhenylH), 6.88 (*s*,1H, isoxazolyl H-4), 7.43 (*s*,1H,Coumarinyl H-4), 7.92 (*d*,1H, Coumarinyl H-5, *J*= 4.54 Hz), 7.47 (*t*, 1H Coumarinyl H-6, *J* = 6.92 Hz), 7.41 (*d*,1H,Coumarinyl H-8, *J* = 6.90 Hz), 8.61 (*s*,1H, NH), 2.35 (s, 3H, C$\underline{H}_3$); ^{13}C NMR (400 MHz, DMSO-D_6); 158.54, 154.05, 145.99, 137.02, 132.17, 125.38, 119.69, 118.40, 117.50, 30.92, 30.53; Analysis for $C_{21}H_{16}BrN_3O_5S$; Calcd %: C, 50.21; H, 3.21; N, 8.36; S, 6.38; Found %: C, 49.75; H, 3.42; N, 9.56.S, 6.55;ESI-HRMS (m/z): Anal. Calcd. for $C_{21}H_{16}BrN_3O_5S$ [M + H]+ 503.28; found: 503.85 (M+1).

2.5. Antimicrobial assay

The antimicrobial sensitivity testing of the twelve **(5a-**5h**)** synthesized compounds were assayed using the agar well diffusion method against selected pathogenic strains viz., *S. aureus* (NCTC 6571), and *E. coli* (NCTC 10418) the two uropathogenic bacterial strains, while *C. tropicalis* (MCC 1559), and *T.rubrum* (MCC 1598) the two dermatopathogenic strains. Before the screening, these individual bacterial strains were inoculated in nutrient broth (NB) and Sabouraud dextrose broth (SDB), for fungus culture and incubated for about 24–48 h at 37 ºC. The antibacterial and antifungal activity protocol commences by inoculating the test organism onto the sterilized petri-plates filled upto 25 mL with Muller-Hinton Agar (MHA) and Sabouraud dextrose agar (SDA), respectively. Then, aseptic wells were bored as per the availability of samples, and each well was loaded with 80 μL of test samples, previously dissolved in DMSO at a concentration of 100 µg/ mL. Gentamicin and Ketoconazole were used as standard (positive control) for the antibacterial and antifungal screening respectively whereas DMSO solvent was introduced as a negative control. Then each plate of the bacterial isolate was incubated for 24 h at 37 ºC±2 and for the fungal isolate, the incubator was maintained at 30ºC±2, 72 h. After incubation, the zone of inhibition outstretched by the tested samples as well as by the controls was reported on the mm scale [27].

2.6. Determination of MIC (Bacteria and fungus)

Minimum inhibitory concentration (MIC) of newly synthesized coumarin congeners was determined by the microdilution method using 96 microwell plates (Flat Bottom; Polystyrene, Eppendorf). The antibacterial and antifungal activity was evaluated for the selected conjugates following the zone of inhibition data against two bacterial strains *Staphylococcus aureus* and *Escherichia coli* and a fungal strain *Trichophyton rubrum*, respectively. Each well of microtiter was filled with 100 µL of Muller-Hinton broth and Sabaraoud Dextrose Broth for antibacterial and antifungal activity respectively. The serial dilution experiment begins by pouring 100 µL aliquot of the test sample from its stock solution (mg/L in 10% DMSO) to the first well making it's the highest concentration of the sample and subsequently, the other ten wells were serially diluted by pouring and withdrawing until the last well is filled with the lowest concentration of the sample.Another well in 96 well titer plate does not contain a tested sample that acts as a negative control. This procedure utilizes only 20 µL of inoculum (10^7 CFU/ mL) and 5 µL of indicator (2, 3, 5-triphenyl tetrazolium chloride, 0.5%) for each well and incubation temperature was maintained at 30 ºC for 24–48 h (bacterial strains) and 48–72 h (fungal strains). The synthesized compounds were serially diluted with different concentrations of 400, 200, 100, 50, 25, 12.5, 6.25, 3.125, 1.56, 0.78, 0.39 µg/ mL in 10% DMSO. The MIC of the test samples was noted by observing the color change in the wells that occurred due to the inhibition of bacterial growth [28].

2.7. Cell line and culture condition

Human breast cancer cell line MDA-MB-231 cells, pancreatic cancer cell line MIA PaCa-2 cells and oral cancer cell line H357 cells were purchased from American Type Culture Collection (ATCC) (Manassas, VA, USA). MDA-MB-231cells and MIA PaCa-2 cells were routinely maintained in DMEM media supplemented with 10% fetal bovine serum (PAN-Biotech GmbH, Germany) and 1% penicillin-streptomycin (Sigma-Aldrich,St. Louis,USA) at 37 °C in

a humidified atmosphere of 5% CO_2 (Hera Cell, Thermo Scientific, USA). H357 cells were cultured in DMEM/F12 media (PAN-Biotech GmbH, Germany) supplemented with 10% fetal bovine serum (Gibco, USA), hydrocortisone (Sigma-Aldrich,St. Louis,USA) and 1% penicillin-streptomycin (Sigma-Aldrich,St. Louis,USA) at 37 °C in a humidified atmosphere of 5% CO_2 (Hera Cell, Thermo Scientific, USA) [29].

2.8. MTT cell proliferation assay

MDA MB-231, MIA PaCa-2 and H357cells were seeded at a density of 2×10^3 cells per well in a 96-well plate. After 24 h of seeding, cells were treated with different concentration (1, 10, 20, 30, 40 and 50 µM) of compounds (**5d, 5e, 5f**, and 5 h) for 48 h and 72 h. Cell viability was assessed by MTT based colorimetric assay. The inhibitory concentration causing 50% of cell death (IC_{50}) was calculated by nonlinear regression analysis through OriginPro8.5 software [30].

2.9. Western blotting

6×10^5 cells of MDA-MB-231 cells were grown overnight at 37 °C in 60 mm petri dish (Corning). The cells were then treated with 10 μM of drug (**5d, 5e, 5f**, and 5h) and incubated for 48 h at 37 °C.Following drug treatment, the cells were collected, washed with PBS, and whole-cell lysate was procured from them using radioimmunoprecipitation assay (RIPA) buffer supplemented with protease inhibitor cocktail, phenylmethylsulfonyl fluoride (PMSF; 1 mM), and Na3VO4 (2 mM). Protein concentration was estimated by BCA kit (Pierce). Separation of protein lysates was done on sodium dodecyl sulfate−polyacrylamide gel electrophoresis (SDS-PAGE) gel and transferred on poly (vinylidene difluoride) (PVDF) membrane of size 0.45 μm (GE Healthcare). Thereafter, the membranes were blocked in 7.5% skimmed milk for 1 h. Subsequently, the membranes were washed with PBS/PBST to remove excess skimmed milk and incubated with primary antibody β-actin (Santa Cruz Biotechnology, Inc., CA), Bax and Bcl-2 (Cell Signalling Technology, Inc., MA) (dilution 1:1000) for overnight at 4 °C. Next day, the membranes were washed and incubated with horseradish peroxidase (HRP)-conjugated secondary antibody with dilution 1:5000 (Novus Biologicals, MO) prior to the development of blots by enhanced chemiluminescence system. The band intensity of western blots was determined using ImageJ software [31].

2.10. Ligand and target protein preparation

The structures of compounds, **5a-**5h were sketched and selected as ligand by using virtual library that involves simple condensations of substituted coumarin with an individual sulfanilamide derivative *viz*., sulfapyridine (SP), sulfadiazine (SD), sulfaguanidine (SG), sulfacetamide (SA), sulfamethoxazole (SMZ) by ChemDraw Ultra tool (ChemBioOffice 12.0 suite),and further, were optimized with ACD Labs freeware 2015. The docking study has been performed to obtain optimized conformation with plausible binding cavities by minimizing energy against the macromolecular targets **1N8Z** (HER2 receptor of Human complexing with Herceptin in the paratope region of the receptor), **5V5Z** (CYP51 enzyme of *C.albicans*), **1AJ0** (*E.coli* DHPS), and **1AD1** (*S.aureus* DHPS), through AutoDockVina. AutoDock is widely employed due to its high reproducibility of conformers, precision, and accuracy for predicting the binding mode through docking scores [32]. The standard docking protocol was followed, where the retrieved protein from RCSB Protein Data Bank https://www.rcsb.org/,was prepared by removing water molecules and other heteroatoms using ACD Labs, further the (.) pdb was converted to (.) pdbqt by assigning Kohlman charges and polar hydrogens to the protein. All the optimized ligand was saved in mol files which were converted to (.) pdb files using an open babel command prompt in Ubuntu20.04. Now, these pdb files individually prepared by AutoDock making necessary changes like all rotatable bonds, degrees of freedom (torsional), atomic partial charges, and non-polar hydrogen. To end the protocol, a final command was typed through the AutoDockVina command prompt. The protein-ligand interaction of the docked candidates was visualized through Biovia Discovery Studio [33].

3. Result and discussion

3.1. Chemistry

A series of coumarin compounds bearing sulfonamide group (**5a-**5h) were synthesized and characterized by different spectral studies. Initially, the compounds have been prepared by a two-step reaction; it involves the condensation of corresponding 2-hydroxy benzaldehyde (**1a-1b)** with ethylacetoacetate **2** in presence of piperidine gave an intermediate substituted 3-acetyl coumarin **3a-3b**,which was further reacted individually with different *N*'-heteroaryl-4-amino benzene sulfonamide **4a-4f** drugs to obtained desired Schiff base **5a-**5h products (Scheme 1). The reactions primarily involves the Pechmann's condensation of β-ketoester with substituted salicylaldehyde gave cyclized products which subsequently undergoes nucleophilic addition reaction in between desired amines and 3-acetyl coumarin generating azomethine derivative of coumarin **5a-**5h. All the new synthesized compounds were confirmed by ^{1}HNMR, ^{13}CNMR, and FTIR, and elemental analysis.

The frequency of carbonyl stretching for both coumarin ring and acetyl group of the intermediate product has appeared at 1703 and 1665 cm^{-1} in FTIR spectral data. In addition to that ^{1}HNMR spectral data of these intermediate products, **3a-3b** had shown five-four aromatic multiplets with one singlet peak for chromene H and methyl respectively. Further, these compounds were converted into respective Schiff base by treatment with individual sulfanilamide derivative in ethanol, FTIR spectra of these desired congeners suggested that the frequency of carbonyl stretching (C=O str.) of ketone disappeared due to the occurring of the desired reaction and appeared at ∼1634 $cm^{-1}$for azomethine (-C=N-), and additionally peaks at 1376–1339, 1175–1155 cm^{-1} and 980–975 cm^{-1}contributes to sulfonamide (SO_2NH-) group in all the structures. All the synthetic molecules have been exhibited a C=N peak between γ 1677 and 1673 cm^{-1}; in ^{13}CNMR of all the congeners has been shown at nearly equal to δ 195 ppm that attribute to the presence of the C=N group whereas carbonyl of pyrone system has appeared at more or less equal to δ 159 ppm [34]. Moreover, all the synthesized molecules have not yet been reported earlier. All the necessary spectral data of the synthesized molecules were depicted in Suppl Figs. 1–32.

X-ray diffraction pattern of compound **5a** shows ten reflections, between 2θ ranges from 10 to 35◦with maximum at 25.884º corresponding to inter-planar distance d = 3.25 Å and compound 5g shows eleven reflections, between 2θ ranges from 10 to 32º with maximum at 18.623º (d = 4.69 Å) (Suppl. Figs. 31 and 32). Main peaks have been indexed by trial and error method [35].

3.2. Antibacterial activity

A series of synthesized titled coumarin congeners were performed for antibacterial action against *S. aureus* (NCTC 6571), and *E. coli* (NCTC10418), and the antifungal activity was evaluated against two pathogens viz. *C. tropicalis* (MCC 1559), *T. rubrum* (MCC 1598). Antimicrobial action results were expressed in terms of zone of inhibition (mm), minimum inhibitory concentration (μg/ mL) that was depicted in Table 3. An interpretation of antimicrobial

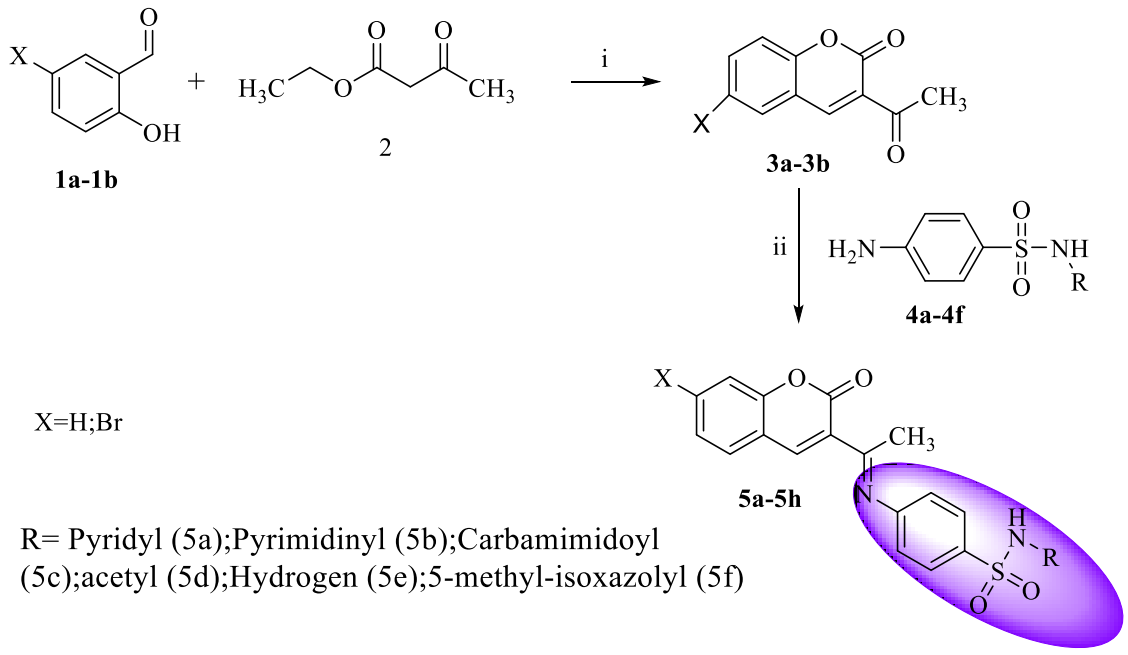

Scheme 1. Synthesis of chromene-sulfonamide congeners.

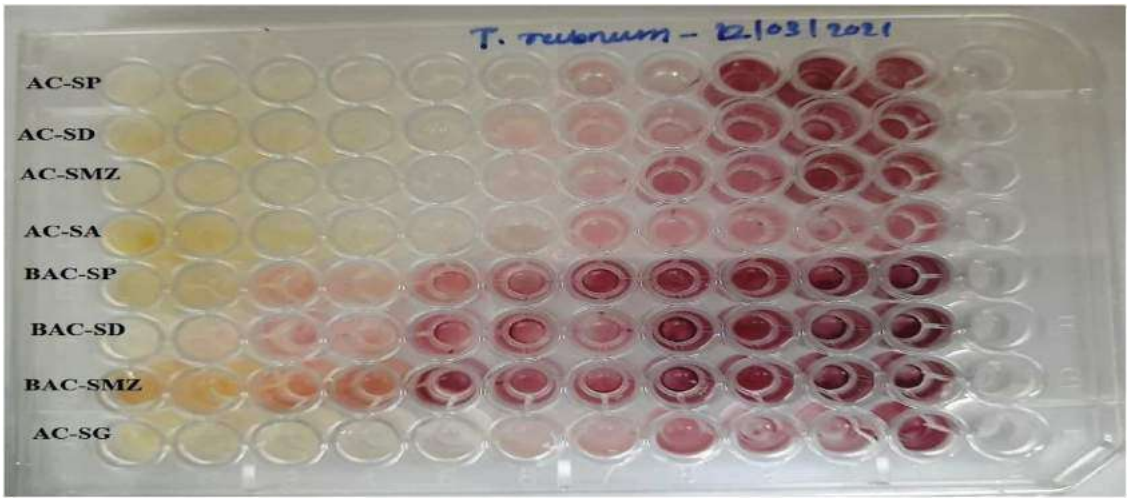

Fig. 3. Antifungal activity (MIC plate) with *T.rubrum* of Coumaryl-Sulfonamide based congeners.

activity results is illustrated in (Figs. 3 and 4) [36]. The results of antibacterial activity of newly derived coumarin-sulphonamide congeners indicate that the compounds **5a and 5f** have been exhibited a good zone of inhibition at **25 & 28 mm** with the gram-positive bacteria *S. aureus* compared to standard Gentamicin but moderate inhibition was found against *E. coli*. The zone of inhibition of the above compounds was expressed in Suppl Figs. 37 and 38. Among these three congeners, the compound *N*-(5-methyl–isoxazole-3-yl)-4-{(*E*)-[1-(2-oxo-2*H*-1-benzopyran-3-yl) ethylidene] amino} benzene-1-sulfonamide **5f** had been shown significant inhibition at **28 mm** (comparatively larger zone than the standard), and 18 mm against *S. aureus* and *E. coli* respectively. However, all the compounds were found to be effective against *S. aureus* except **5b** which also found to inhibit the *E. coli* moderately.

Metabolite of plant-derived coumarin derivative with the phenolic system has been explored with profound pharmacological activities. Therefore, several literature studies have been emphasized on coumarin nucleus as a lead molecule to design a new structure-based drug. The compounds **5a** and **5f** has been the lead candidate among all the synthesized compounds for antimicrobial action against *S.aureus* and *T. rubrum*. The structure activity relationship suggests; that the corresponding compounds chemically containing electron donating moieties viz., pyridyl (**5a**) or isoxazolyl (**5f**) substituted sulfonamide in attachment with acetyl coumarin ring at C-3 position through a azomethine linker could may have enhance the antimicrobial activity whereas, other compounds bearing either attachment of guanyl or acetyl to sulfonamide could be less potent due to low electron density influenced on sulfonamide. Literature reveals that compounds having 4-imino sulfamoyl moiety on the phenyl ring at para position increase the lipophilicity of the compound [36]. The lipophilic property is directly favored by antimicrobial activity; as it facilitates a molecule to cross through the

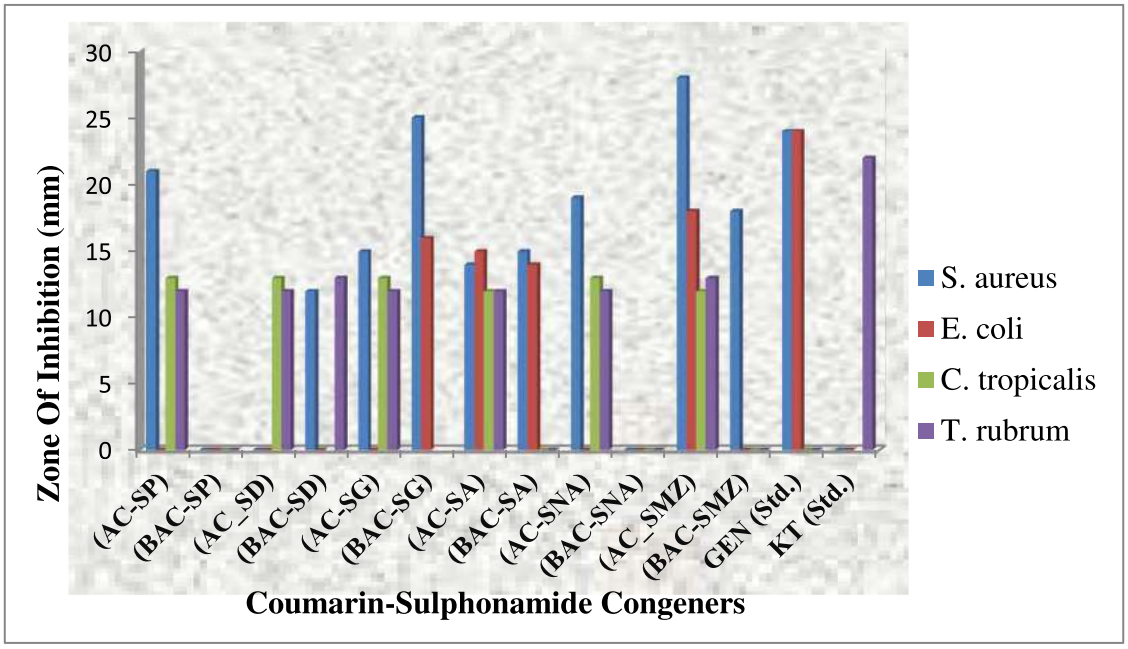

Fig. 4. Graphical interpretation of coumarin hybrids with bacterial and fungal strains.

cell membranes and reach its bacterial target sites. The log P value of 3.52 also assists the antimicrobial data for all the compounds however; the isoxazolyl ring has been proved to be potent against both fungus and bacteria. The bacteriostatic sulfonamides could be modified to bactericidal after conjugating with the coumarin nucleus due to the active site binding of the coumarin ring to the DHPS enzyme [37].

Table 2 Antimicrobial activity of Coumarin congeners in terms of zone of inhibition and MIC values (5a-5h)

3.3. Antifungal activity

The antifungal activity results indicated that the compounds4-{(*E*)-[1-(2-oxo-2*H*-1-benzopyran-3-yl)ethylidene]amino}-*N*-(pyridin-2-yl)benzene-1-sulfonamide **5a**, *N*-{4-(*E*)-[(1-(2-oxo-2*H*-1-benzopyran-3-yl)ethylidene)amino]benzene-1-sulfonyl}acetamide **5d,** and *N*-(5-methyl-1,2-oxazol-3-yl)−4-{(*E*)-[1-(2-oxo-2*H*-1-benzopyran-3-yl)ethylidene]amino}benzene-1-sulfonamide **5f** had been found to exhibit good inhibition at a same inhibition zone diameter of 17 mm against *T. rubrum* (Suppl Fig. 25), when compared to standard Ketoconazole. Among all the compounds, **5f** was only found to exhibit good activity against *C. tropicalis* at 18 mm. Sulfamethoxazole conjugated acetylcoumarin was more effective than Bromo-substituted acetylcoumarin-SMZ against *T. rubrum* whereas the Schiffs Base of Bromo-substituted coumarin sulfa-drugs like SG /SA/SNA/SMZ has no antifungal activity. The compounds **5a, 5d**, and **5f** have been exhibited significant inhibition against *T. rubrum* at MIC 12.5 µg/ mL whereas the compound **5b** and **5c** had shown moderate antifungal action with *T. rubrum*, no such compounds are active against *C. tropicalis.*

3.4. Anticancer activity

The cytotoxic effect of compounds (**5d, 5e, 5f** and 5h) on MDA MB-231, MIA Pa Ca-2 and H357 cells were evaluated by MTT assay. Results illustrated the above compounds have shown cytotoxic effect at different time points in a concentration dependent manner (1, 10, 20, 30, 40 and 50 µM) (Fig. 5) (Table 4). The IC_{50} (Concentration at which 50% of cell death) values of compounds (5d, 5e, 5f, and 5h) evaluated for the above study are shown in Table 4. It was found that all compounds induce similar type of cytotoxicity at 48 h treatment; however, among all compounds 5g have shown higher cytotoxicity in all the cell line at 72 h of treatment. It is known that cancer cells escape from apoptosis by the down regulation of pro-apoptotic proteins and constitutive activation of anti-apoptotic proteins. In this regards, expression of these proteins were evaluated following 48 h treatment with compounds (**5d, 5e, 5f**, and 5 h) (10 µM). Results suggest that pro-apoptotic protein marker Bax was upregulated and anti-apoptotic protein marker Bcl2 was downregulated in all the treatment groups as compared to control, thereby delineating that the above compounds induced apoptosis in MDA-MB-231 cells (Fig. 6).

Table 2. Inhibitory concentration (IC_{50}) values of different compounds (5d, 5e, 5f, and 5 h) in MIA PaCa-2, MDA MB 231 and H357 cell lines after 48 h and 72 h of treatment as observed by cell cytotoxicity assay. Data represented as mean ± SEM, (n=3).

3.5. Molecular docking analysis

Fungal targeted class of synthetic drugs viz., azoles (widely used and accepted class for both superficial and invasive fungal

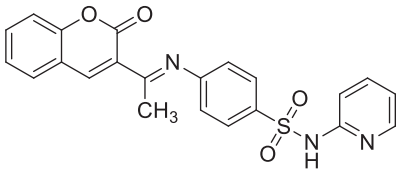

5a antifungal action with T.rubrum
MIC=12.5µg/mL

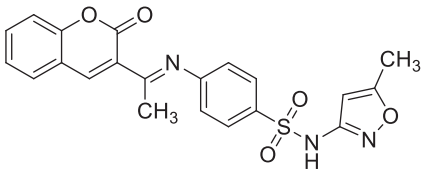

5f antifungal action with T.rubrum
MIC=12.5µg/mL

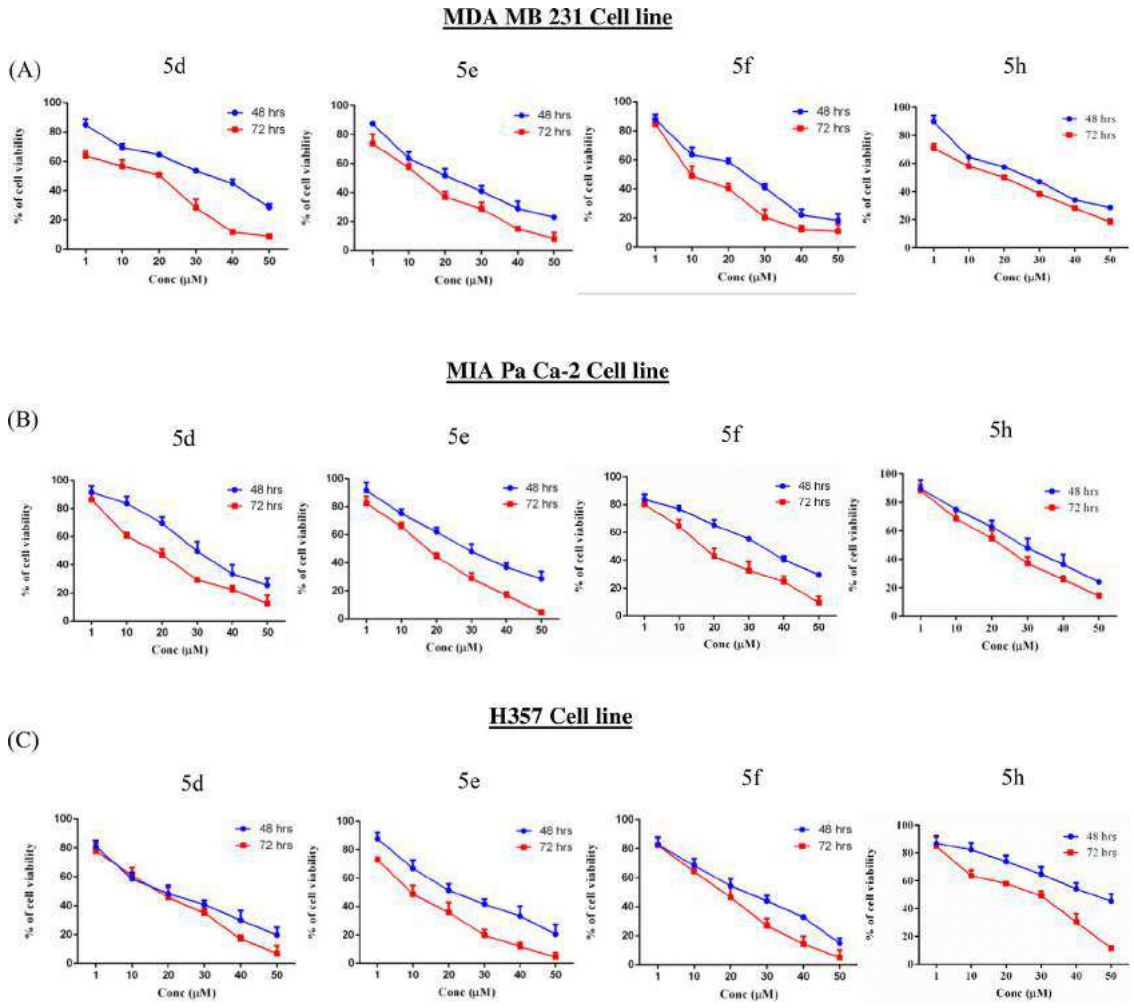

Fig. 5. *In vitro* cytotoxicity assay. (A) MDA MB-231 cells (B) MIA Pa Ca-2 cells (C) H357 cells were treated with different concentration of 5d, 5e, 5f and 5h drugs (1–50 µM) for 48 h and 72 h, respectively; cell viability was assessed using the MTT assay (n=6).

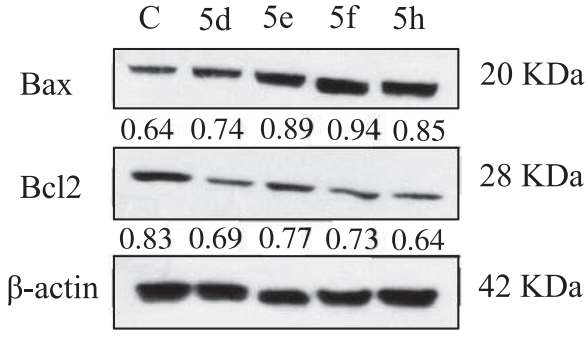

Fig. 6. Compounds (5d, 5e, 5f, and 5h) induce apoptosis. Representative western blots demonstrating expression of pro-apoptotic marker (Bax) and anti-apoptotic markers (Bcl2) following treatment with 5d, 5e, 5f and 5 h drugs (10 µM) for 48 h in MDA-MB –231 cells.

diseases), polyenes (a certain type of macrolide antibiotics obtained naturally from *Streptomyces species* of Actinomycetes class), and echinocandins (semi-synthetically derived, targeting the β-1,3-glucan synthase fungus) desire to inhibit the fungus by attacking the cell wall synthesis either azole being specific to the enzyme lanosterol 14α-demethylase or polyene degrading the cell wall by sequestering the ergosterol into the fungal cell wall. The fungal metabolism initiates from squalene; as a precursor for the biosynthesis of ergosterol. Lanosterol C14α-demethylase is a unique enzyme that catalyzes the conversion of lanosterol to ergosterol *via* fungal Cytochrome- P450; hence the target LDM of *Candida species* was selected for molecular docking [38].

Similarly, Dihydropteratesynthetase (DHPS) was selected as the bacterial target which is an essential enzyme for the biosynthesis of folic acid in bacteria. As folic acid is an essential cofactor in most of the prokaryotes and eukaryotes for the synthesis of bacterial proteins; tetrahydrofolates cannot get utilized directly by the prokaryotes, therefore, they require a substrate known as pABA (para-aminobenzoic acid) which helps them to synthesize folic acid through *de novo* pathway. This *de novo* pathway involves an enzyme DHPS, as it catalyzes the condensation reaction between the substrate pABA and DHPPP (7, 8- dihydropterin pyrophosphate, a highly conserved sequence found in almost all prokaryotes). Thus, the bacterial DHPS was the selected target for performing the molecular docking of the coumarin derivatives [39,40].

A preliminary investigation for all probable binding affinity with targeted enzymes and their interactions of the synthesized congeners for the prediction of their theoretical biological data of twelve coumarin-congeners **5a-h** was performed for molecular docking studies with human epidermal growth factor receptor2 (HER2) of PDB ID: 1N8Z bacterial target dihydropteroate synthetase (DHPS) enzyme of PDB ID: 1AD1, 1AJ0, and PDB ID: 5V5Z for the fungal target. The probable biological data of these derivatives were predicted by the PASS prediction tool which was de-

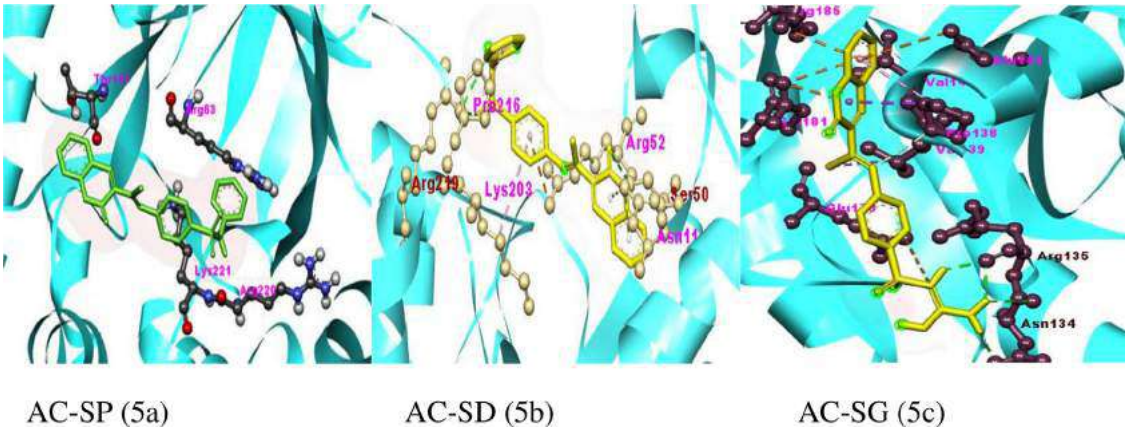

Fig. 7. Binding Affinity with *Staphylococcus* aureus PDB ID: 1AD1.

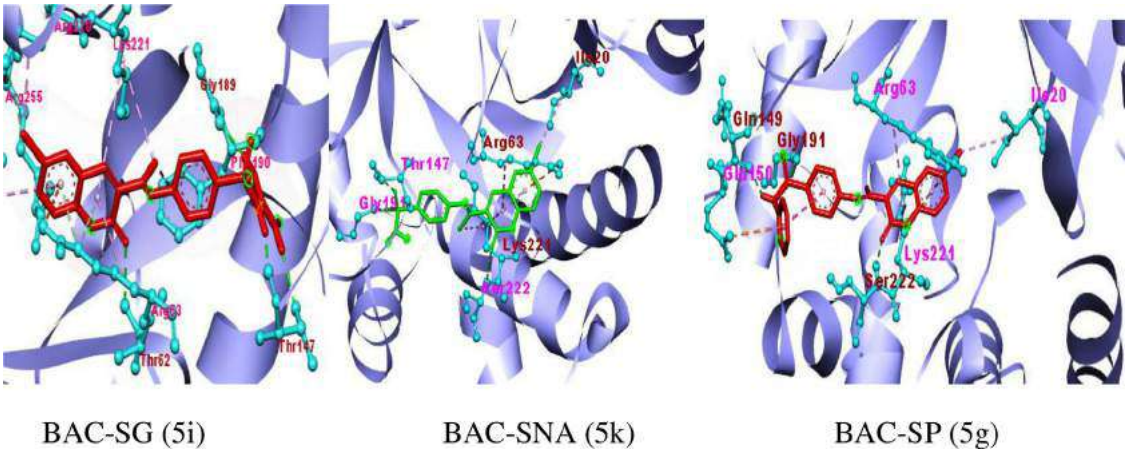

Fig. 8. Binding Affinity with Eischerecia coli Dihydroptereate Synthase PDB ID: 1AJ0.

picted in Table 5. As the PASS prediction results have been predicted for activities viz., Anti-infective, Dihydropteroate synthase Inhibitor, and Aspergillopepsin II inhibitor, therefore, the molecular docking have been proceeded using targets HER2 (Extracellular region), DHPS and lanosterol 14α-demethylase. The ligand-protein interaction of some potent candidates for the coumarin hybrids was also visualized. As the docking study is considered as a hypothetically approved protein-ligand interaction prediction, hence, the analysis of all the eight synthesized compounds against the target lanosterol 14α-demethylase were in the effective decreasing order of the compounds 5g, **5f, 5b** & **5a, 5c, 5d**, 5h, & **5e** as **−10.8 > −10.7 > −10.6 > −10.3 > −10.1 > −9.7 > −9.0 > −8.9 > −8.8** Kcal/mol respectively. Similarly, the docking score against two bacterial targets (DHPS) was documented in Table 5; moreover the targeted breast cancer receptor HER2 has shown docking scores out of the blue viz., **−11.88, −10.08 and −12.4** Kcal/mol of compounds **5f,** 5g**,** and 5h respectively and the ligplot of those have been provided in Suppl Figs. 33–35. The highest-ranked docking pose of all the complex compounds suggests that the molecules mediate the hydrogen bonding with residues in the binding sites of the target. As the sulfamethoxazole **(SMZ)** bearing 3-acetyl-6-substituted coumarin **5f** and 5h congener had shown excellent docking scores with all the targets as well as performed satisfactory activity against all the microbial species and also cancer cell lines, thus for better understanding a comparative docking score of the sulfa drug (SMZ) alone has been displayed in Table 5, and an enhancement of activity could be expected after the introduction of coumarin moiety with a Schiff base which is evident from the docking score [41].

The minimum docking score of **BAC-SP** 5 g suggests its affinity towards the fungal enzyme however it has shown a moderate score with the two bacterial targets. The docking results with the fungal target (5V5Z) of all the compounds suggested that compound 5 g had been shown the minimum binding energy with the highest docking score −10.8 Kcal/mol interacting with H377 of the target by hydrogen bonding while the hydrophobic interactions involve L376, P230 amino acid residues. The compound-complex 5 g makes two hydrogen-bonding interactions; it mediates between the oxygen of sulfonyl group of sulphonamide with the amino acid side chain of H377 (Fig. 9). Moreover, the same complex with docking score −7.3 Kcal/mol and −8.0 Kcal/mol with the bacterial targets 1AD1 and 1AJ0 respectively, makes three hydrogen bonding interaction mediated between amino of sulphonamide with Q149; oxygen of sulfonyl radicle of sulphonamide with G191, and oxygen of carbonyl group with S222 for the target 1AJ0 (Fig. 8). Similarly, for the target 1AD1 the compound 5 g interacts with the oxygen of sulfonyl radicle of sulphonamide with R263 by hydrogen bonding whereas K251 (σ- π interaction between phenyl ring and the side chain of lysine).

Compound **AC-SD 5b** carrying sulphonamide -pyrimidinyl in the structure has displayed the second-highest binding affinity with the fungal target −10.6 Kcal/mol while the same compound had shown binding affinity at −7.6, −6.9 Kcal/mol for the bacterial targets 1AD1 and 1AJ0 respectively. Herein, the two hydrogen bond

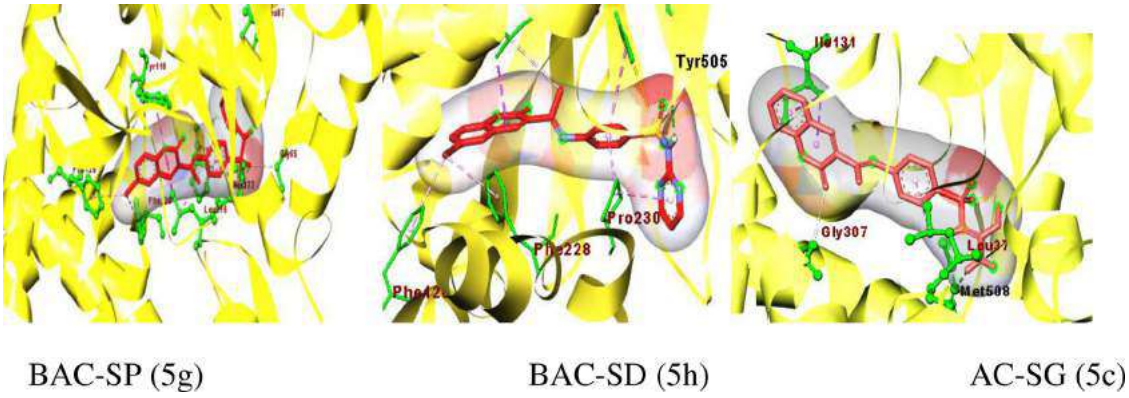

Fig. 9. Binding Affinity with Fungal Lanosterol C14α- Demethylase PDB ID: 5V5Z.

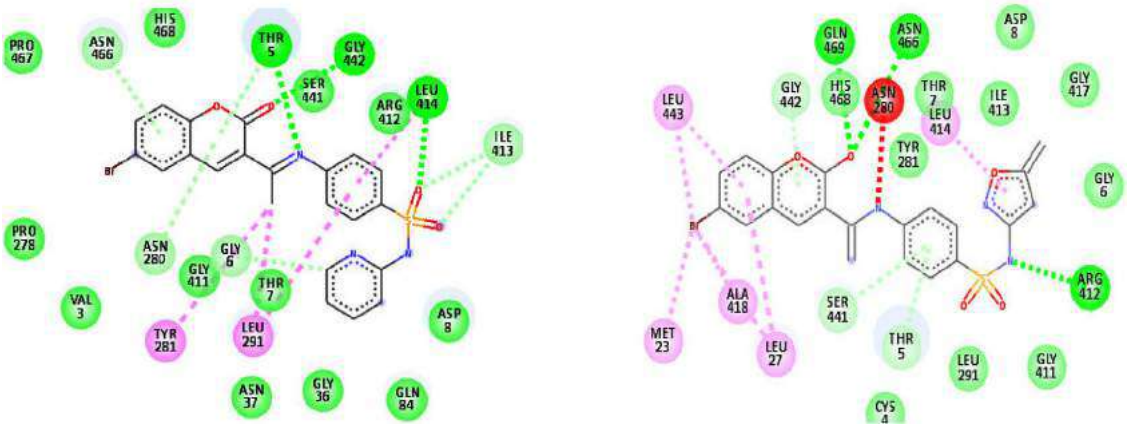

Fig. 10. Ligplot of compounds 5g and 5l with PDB ID 1N8Z.

interaction has been mediated in between oxygen of sulphonamide radicle with the amino group of S50 and the other, R219 showed created H-bond with the oxygen of sulphonamide as well as with N-atom of the pyrimidine ring. Some other hydrophobic interactions were also visualized viz., π-π alkyl at K203 with phenyl ring of sulphonamide, and the residue P216 interacts with the pyrimidinyl ring for the target 1AD1 (Fig. 7). Similarly, the same complex with bacterial target 1AJ0; showed two hydrogen bond interactions in between oxygen of sulfonyl radicle of sulphonamide with the side chain of D258 & R220; the hydrophobic interactions involve π-π alkyl with residues M47, V259, K260, and π-σ interaction was shown with the residue L46.

Compound **AC-SMZ 5f** containing sulfonamide-isoxazolyl in coumarin that has displayed a good binding affinity with the specific fungal target −10.7 Kcal/mol whereas the same compound showed their docking energy at −8.1 and −7.4 Kcal/mol for bacterial targets 1AD1 and 1AJ0 respectively**.** Herein, the carbonyl oxygen of coumarin and nitrogen of isoxazole ring interacts with the side chains of R52 and R204 with the fungal target by hydrogen bond whereas the other interactions were also mediated *viz.*, π-π alkyl, π-σ, and few hydrophobic interactions at I9, H241, and K203. Similarly, for bacteria; target 1AJ0, the compound **5f** made hydrogen bond interaction with the amino acid residue Q226; other interactions viz., π-π alkyl (side chains of A151 and K221 interacted with isoxazolyl and phenyl ring of coumarin), π-σ (side chain of R63 with phenyl ring of coumarin) (Suppl. Figs. 33–36). Similarly, for the fungal target 5V5Z, the carbonyl oxygen of the compound **5f** interacts with the side chain of Y64 by an H-bond; whereas the other interaction of π-π alkyl is mediated between Y132, P230, M508, L88, and L87 with methyl of isoxazolyl, phenyl ring of sulphonamide, phenyl rings of coumarin moiety respectively.

Compound **BAC-SMZ** 5h containing Bromo group in the 7th position of coumarin-sulphonamide - pyrimidinyl in the structure has shown docking scores as −7.4, −7.6, and −10.6 Kcal/mol with 1N8Z, 1AD1, 1AJ0, and 5V5Z, respectively. Herein, interaction with the bacterial target 1AD1 displayed with the side chain of S16 making H-bond with the pyrimidinyl ring; other interactions involve π-π alkyl (R202 and R204 with the amine group of sulphonamide and the Bromo group involve respectively). Likewise,the interaction of 1AJ0 involving two conventional hydrogen bonding (R63 with the carbonyl group and R235 with the oxygen of sulfonyl radicle of sulphonamide), three π-π alkyls (M139, I117, and K221 with the 7-Bromo, phenyl of coumarin, and phenyl of sulphonamide group). The interactions of fungal target 5V5Z include one conventional H-bond between amine of sulphonamide and side chain of Y505, three π-π alkyls (F126, F228, and P230 with the Bromo group and the pyrimidinyl ring), and also a π-σ interaction between the side chain of L376 and the coumarinyl ring (Figs. 9 and 10).

4. Physiochemical properties

All the compounds were in good agreement and obeyed the RO5 rule which indicates that these compounds have been shown 'druggable property' and no such candidate had violated the RO5 parameters calculated by the tools ChemDraw, other online tools were also used viz., Molinspiration (http://www.molinspiration.com/) and Molsoft (http://molsoft.com/mprop/) which well-illustrated in Table 1. The theoretical calculation of Absorption, Distribution, Metabolism, and Elimination of synthesized coumarin derivatives was carried out and compared with the RO5 parameters. The pre-ADMET profile includes Blood-Brain Barrier

Table 1
Molecular properties of newly synthesized coumarin analogues (RO5).

Compounds	Chemical structure and chemical name	Lipinski rule of five (RO5)				
		MW	HA	HB	cLogP	tPSA
AC-SP (5a)	4-{(*E*)-[1-(2-oxo-2*H*-1-benzopyran-3-yl)ethylidene]amino}-*N*-(pyridin-2-yl)benzene-1-sulfonamide	419	7	1	3.79	101.64
AC-SD (5b)	4-{(E)-[1-(2-oxo-2H-1-benzopyran-3-yl)ethylidene]amino}-N-(pyrimidin-2-yl)benzene-1-sulfonamide	420	8	1	2.86	114.53
AC-SA (5c)	*N*-carbamimidoyl-4-{(*E*)-[1-(2-oxo-2*H*-1-benzopyran-3-yl)ethylidene]amino}benzene-1-sulfonamide	384	8	4	2.07	138.62
AC-SA (5d)	*N*-(4-{(*E*)-[1-(2-oxo-2*H*-1-benzopyran-3-yl)ethylidene]amino}benzene-1-sulfonyl)acetamide	423	7	1	2.35	105.81
AC-SNA (5e)	4-{(*E*)-[1-(2-oxo-2*H*-1-benzopyran-3-yl)ethylidene]amino}benzene-1-sulfonamide	342	6	2	2.62	102.74
AC-SMZ (5e)	*N*-(5-methyl-1,2-oxazol-3-yl)−4-{(*E*)-[1-(2-oxo-2*H*-1-benzopyran-3-yl)ethylidene]amino}benzene-1-sulfonamide	423	8	1	3.52	114.78
BAC-SP (5 g)	4-{(*E*)-[1-(6-bromo-2-oxo-2*H*-1-benzopyran-3-yl)ethylidene]amino}-*N*-(pyridin-2-yl)benzene-1-sulfonamide	498	7	1	4.57	101.64
BAC-SMZ (5 h)	4-{(*E*)-[1-(6-bromo-2-oxo-2*H*-1-benzopyran-3-yl)ethylidene]amino}-*N*-(pyrimidin-2-yl)benzene-1-sulfonamide	499	8	1	3.65	114.53

Table 2
Predicted Antiinfective, Dihydropteroate synthase inhibitor, and Aspergillopepsin II inhibitor activities (Pa >Pi) activities of synthesized coumarin-sulfonamide conjugates using PASS Programme.

Compounds	Pre-ADMET Scores Of Newly Synthesized Coumarin Congeners				Toxicity	
	Blood-Brain Barrier (BBB)	Caco-2 Permeability	Human intestinal absorption(HIA, %)	Skin_Permeability (logKp,cm/hour)	LD50 mg/kg	Class
5a	0.0128	16.35	96.37	−2.383	83	3
5b	0.133	20.98	99.13	−2.137	1030	4
5c	0.062	0.393	80.20	−2.728	1030	4
5d	0.093	4.28	98.88	−2.19	1030	4
5e	0.014	0.498	97.69	−2.07	25000	6
5f	0.030	5.96	97.63	−2.41	3471	5
5g	0.0981	11.03	97.66	−1.819	1500	4
5h	0.028	0.867	96.96	−2.41	10000	6

Table 3
Antimicrobial activity of Coumain congeners in terms of zone of inhibition and MIC values (5a-5h).

Coumarin congeners (5a-l)	*S. aureus* (NCTC 6571)		*E. coli* (NCTC 10418)		*C. tropicalis* (MCC 1559)	*T. rubrum* (MCC 1598)	
	ZOI (mm)	MIC (μg ml^{-1})	ZOI (mm)	MIC (μg ml^{-1})		ZOI (mm)	MIC (μg ml^{-1})
AC-SP (5a)	**21**	100	NA	100	13	17	**12.5**
AC_SD (5b)	ND	NA	NA	50	13	12	25
AC-SG (5c)	15	50	NA	100	13	12	25
AC-SA (5d)	14	NA	15	50	12	17	**12.5**
AC-SNA (5e)	19	NA	ND	NA	13	12	NA
AC_SMZ (5f)	**28**	25	18	50	18	17	**12.5**
BAC-SP (5g)	20	100	NA	200	NA	10	200
BAC-SMZ (5h)	12	100	NA	400	NA	13	200
GEN (Std.)	24		24		−−−−-	−−−−	−−-
KT (Std.)	−−	−−−−-	−−−	−−−−		22	1.56

Table 4
Inhibitory concentration (IC_{50}) values of different compounds (5d, 5e, 5f, and 5 h) in MIA PaCa-2, MDA MB 231 and H357 cell lines after 48 h and 72 h of treatment as observed by cell cytotoxicity assay. Data represented as mean ± SEM, (n=3).

IC_{50}(μM)						
Drug	MIA PaCa-2		MDA MB 231		H357	
	48 h	72 h	48 h	72 h	48 h	72 h
5d	30.29±0.24	17.99±2.35	26.36±2.95	18.37±1.99	22.21±3.13	17.22±0.96
5e	27.48±1.27	17.94±0.42	23.04±2.29	7.78±3.78	22.01 ±0.10	8.68±1.10
5f	26.29± 2.57	16.83±1.23	26.98±2.72	14.15±1.49	24.52±1.50	15.91±1.19
5 h	29.71±0.79	17.40±4.45	24.17±1.32	20.22±0.32	35.35±2.38	22.59±3.72

(BBB), Caco-2 permeability (the Caco-2 cells for the prediction of oral drug absorption method), Human Intestinal Absorption (Sum of Bioavailability and Absorption), skin permeability was statistically calculated for generating sufficient evidence for the newly synthesized coumarin analogs and the lethal dose LD_{50} alongwiththe probable toxicity class ranging from 150 to 1500 mg/Kg for coumarin congeners were determined by the online tool, ProTox (http://tox. charite.de/tox/) documented in the Table 2; all the compounds except **5a**, all other newly synthesized coumarin derivatives could be included under safe drugs as per their toxicity profile, thus can be further investigated as a lead molecule for performing various biological activities.

Table 5
Molecular docking score and the ligand-protein interaction for the newly synthesized Coumaryl-Sulfonamide Congeners.

Compounds	Docking Score (Kcal/mol) and Ligand Interaction							
	PDB ID 5V5Z	Ligand Interaction	PDB ID 1AD1	Ligand Interaction	PDB ID 1AJ0	Ligand Interaction	PDB ID 1N8Z	Ligand Interaction
SMZ	**−7.4**		**−6.4**		**−6.4**		**−8.4**	
AC-SP (5a)	−10.3	131I, 118Y, 230P, 376 L	−7.6	128 M, 199A, 202R, 219R, 241H, 239R	−8.0	63R, 220R, 221K	−8.94	281Y, 413I, 291 L, 414L
AC_SD (5b)	−10.6	131I, 118Y, 230P, 307 G, 380F, 508 M	−7.6	50S, 52R, 203 K, 216P, 219R,	−6.9	20I, 46 L, 47 M, 50A, 220R, 258D, 259 V, 260 K	−9.28	5T, 281Y, 412R, 291 L, 414L
AC-SG (5c)	−9.7	131I, 376 L, 508 M	−7.6	134 N, 135R, 139R, 141E, 178E, 181E, 185R,	−8.6	63R, 219S	−8.34	5T, 414 L, 442 G, 278P, 281T
AC-SA (5d)	−9.7	87 L, 118Y, 230P, 233F, 376L	−7.7	2T, 3 K, 39E, 248 K, 251K	−8.0	147T, 149Q, 190F, 191 G, 221 K, 255R	−8.81	5T, 281Y, 412R, 291 L, 414L
AC-SNA (5e)	−8.8	131I, 376 L, 378S	−7.4	106 W, 109 L, 132 N, 142E	−7.9	20I, 63R, 220R, 221 K, 258D	**−10.88**	8D, 5T, 281Y, 291 L, 414L
AC_SMZ (5f)	−10.7	64T, 87 L, 132Y, 118Y, 230P, 233F, 508 M	−8.1	9I, 52R, 84D, 204R, 239R	−7.4	63R,151A, 221 K, 226Q	**−11.88**	5T, 412R, 414 L, 278P, 281Y, 291 L,
BAC-SP (5g)	**−10.8**	87 L, 88 L, 118Y, 126F, 228F, 337H, 376L	−7.3	3 K, 180A, 251 K, 263R	−8.0	20I, 63R, 149Q, 150E, 191 G, 221 K, 222S	−8.45	5T, 414 L, 442 G, 281Y, 291 L
BAC-SMZ (5 h)	−10.6	126F, 228F, 230P, 376 L, 377H, 505Y	−7.4	16S, 17F, 202R, 204R	−7.6	63R, 117I, 221 K, 139 M, 235R, 255R	**−12.4**	5T, 414 L, 442 G, 278P,281Y,291 L

5. Conclusion

This piece of research work concludes that the newly synthesized coumarin congeners have been successfully synthesized, interpreted, and gave satisfactory yield. The antimicrobial screening of the compounds was evaluated that the compound bearing Schiff base of coumarin-sulfamethoxazole **5f** and coumarin-sulfapyridine **5a** had shown good antimicrobial and antifungal activity compared to standard Gentamicin and Ketoconazole respectively. The structural features have also been suggested the presence of azomethine, heteroaryl-sulfamoyl in the coumarin nucleus could be responsible for increasing antimicrobial action and also reducing terbinafine resistant dermatophytes fungal strain. By studying the anti-cancer activity in different cancer cell lines *in vitro*, it was found that the compounds **5d, 5e, 5f**, and 5h have shown anti-cancer activity by inducing apoptosis. The compounds bearing 6-bromo substitution found to be efficacious than the non-substituted compounds.

Declaration of Competing Interest

The authors declare that they have no known competing financial interests or personal relationships that could have appeared to influence the work reported in this paper.

CRediT authorship contribution statement

Monalisa Mahapatra: Investigation, Software, Methodology, Writing – review & editing. **Priyanka Mohapatra:** Investigation, Methodology. **Sanjeeb Kumar Sahoo:** Data curation, Investigation, Methodology. **Ajit Kumar Bishoyi:** Methodology. **Rabindra Nath Padhy:** Supervision. **Sudhir Kumar Paidesetty:** Conceptualization, Data curation, Writing – original draft.

Data availability

No data was used for the research described in the article.

Acknowledgments

Authors are grateful to Deans SPS and IMS & Sum Hospital for encouragements. This work was supported by the SOADU PhD fellowship to M. Mahapatra (Registration No. 1981606006) in Pharmaceutical Chemistry. The NMR analysis work was carried out at Sophisticated Analytical Instrument Facility, CSIR-Central Drug Research Institute, Lucknow. The cancer activity was done by the Institute of Life Science, Bhubaneswar India.

Supplementary materials

Supplementary material associated with this article can be found, in the online version, at doi:10.1016/j.molstruc.2023.135190.

References

[1] H. Sung, J. Ferlay, R.L. Siegel, M. Laversanne, I. Soerjomataram, A. Jemal, B.F DMV, "Global Cancer Statistics 2020: GLOBOCAN estimates of incidence and mortality worldwide for 36 cancers in 185 countries", CA Cancer J. Clin. 71 (3) (2021) 209–249, doi:10.3322/caac.21660.
[2] F. Bray, M. Laversanne, E. Weiderpass, I. Soerjomataram, "The ever-increasing importance of cancer as a leading cause of premature death worldwide", Cancer 127 (16) (2021) 3029–3030, doi:10.1002/cncr.33587.
[3] L. Rahib, B.D. Smith, R. Aizenberg, A.B. Rosenzweig, J.M. Fleshman, L.M. Matrisian, "Projecting cancer incidence and deaths to 2030: the unexpected burden of thyroid, liver, and pancreas cancers in the United States", Cancer Res. 74 (2014) 2913–2921, doi:10.1158/0008-5472.CAN-14-0155.
[4] A. Yunis, G.K. Arimura, D.J. Russin, "Human pancreatic carcinoma (MIA PaCa-2) in continuous culture: sensitivity to asparaginase", Int. J. Cancer 19 (1977) 128–135, doi:10.1002/ijc.2910190118.
[5] R.L. Siegel, K.D. Miller, A. Jemal, "Cancer statistics", CA Cancer J. Clin. 66 (2016) 7–30, doi:10.3322/caac.21332.
[6] G. Weckbecker, I. Lewis, R. Albert, H.A. Schmid, D. Hoyer, C. Bruns, "Opportunities in somatostatin research: biological, chemical and therapeutic aspects", Nat. Rev. Drug Discov. 2 (2003) 999–1017.
[7] J. Zhang, Y. Tan, G.L. Chen, M. Nie, Z. Wang, H. Ji, "Coumarin sulfonamides and amides derivatives: design, synthesis, and antitumor activity *in vitro*", Molecules 26 (2021) 786, doi:10.3390/molecules26040786.
[8] M.A. Ghannoum, L.B. Rice, "Antifungal agents: mode of action, mechanisms of resistance, and correlation of these mechanisms with bacterial resistance", Clin. Microbiol. Rev. 12 (1999) 501–517.
[9] C. Jia, J. Zhang, L. Yu, C. Wang, Y. Yang, X. Rong, K. Xu, M. Chu, "Antifungal activity of coumarin against Candida albicans is related to apoptosis", Front. Cell. Infect. Microbiol. 8 (2019), doi:10.3389/fcimb.2018.00445.
[10] L.R. Singh, S.R. Avula, S. Raj, A. Srivastava, G.R. Palnati, C.K.M. Tripathi, M. Pasupuleti, K.V. Sashidhara, "Coumarin–benzimidazole hybrids as a potent antimicrobial agent: synthesis and biological elevation", J. Antibiot. (2017) 1–8, doi:10.1038/ja.2017.70.
[11] D. James, "The discovery and development of amphotericin B", Dis. Chest 54 (1968).
[12] V.R. Cerrato, G. Prado, L. Huelves, P. Naves, V. Ruiz, E. Garcíaa, C. Ponte, F. Soriano, "Comparative efficacy of novobiocin and amoxicillin in experimental sepsis caused by β-lactam-susceptible and highly resistant pneumococci", Int. J. Antimicrob. Agents. 35 (2010) 544–549.
[13] N. Vukovic, S. Sukdolak, S. Solujic, N. Niciforovic, "Substituted imino and amino derivatives of 4-hydroxycoumarins as novel antioxidant, antibacterial and antifungal agents: synthesis and *in vitro* assessments", Food Chem. (2010), doi:10.1016/j.foodchem.2009.11.040.

[14] S. Prakash, R. Ramasubburayan, V.S. Ramkumar, E. Kannapiran, A. Palavesam, G. Immanuel, "*In vitro*-scientific evaluation on antimicrobial, antioxidant, cytotoxic properties and phytochemical constituents of traditional coastal medicinal plants", Biomed. Pharmacother. 83 (2016) 648–657, doi:10.1016/j.biopha.2016.07.019.
[15] L. Scorzoni, E. de Paula, A.C. Silva, C.M. Marcos, P.A. Assato, W.C. de Melo, H.C. de Oliveira, C.B. Costa-Orlandi, M.J. Mendes-Giannini, A.M Fusco-Almeida, "Antifungal therapy: new advances in the understanding and treatment of mycosis", Front. Microbiol. 8 (2017) 36, doi:10.3389/fmicb.2017.00036.
[16] S. Mishra, A. Pandey, S. Manvati, "Coumarin: an emerging antiviral agent", Heliyon 6 (2020), doi:10.1016/j.heliyon.2020.e03217.
[17] A.A. Shanty, J.E. Philip, E.J. Sneha, M.R.P. Kurup, S. Balachandran, P.V. Mohanan, "Synthesis, characterization and biological studies of Schiff bases derived from heterocyclic moiety", Bioorg. Chem. 70 (2017) 67–73, doi:10.1016/j.bioorg.2016.11.009.
[18] C.R. Sahoo, J. Sahoo, M. Mahapatra, D. Lenka, P.K. Sahu, B. Dehury, R.N. Padhy, S.K Paidesetty, "Coumarin derivatives as promising antibacterial agent(s)", Arab. J. Chem. 14 (2021) 102922, doi:10.1016/j.arabjc.2020.102922.
[19] S.S. Swain, S.K. Paidesetty, R.N. Padhy, T. Hussain, "Isoniazid–phytochemical conjugation: a new approach for potent and less toxic anti-TB drug development", Chem. Biol. Drug Des. 96 (2) (2020) 714–730.
[20] A.K. Bishoyi, M. Mahapatra, S.K. Paidesetty, R.N. Padhy, "Design, molecular docking, and antimicrobial assessment of newly synthesized phytochemical thymol Mannich base derivatives", J. Mol. Struct. 130908 (2021), doi:10.1016/j.molstruc.2021.130908.
[21] A.K. Bishoyi, M. Mahapatra, S.K. Paidesetty, R.N. Padhy, "Design, molecular docking and antimicrobial assessment of newly S.K. synthesized p-cuminal-sulfonamide Schiff base derivatives", J. Mol. Struct. (2020) 1250:131824, doi:10.1016/j.molstruc.2021.131824.
[22] C.R. Sahoo, S.K. Paidesetty, S. Sarathbabu, B. Dehury, N. Senthil Kumar, Molecular dynamics simulation, synthesis and topoisomerase inhibitory actions of vanillin derivatives: a systematic computational structural integument", J. Biomol. Struct. Dyn. (2021) 1–11, doi:10.1080/07391102.2021.1961867.
[23] S.S. Swain, S.K. Paidesetty, R.N Padhy, "Synthesis of novel thymol derivatives against MRSA and ESBL producing pathogenic bacteria", Nat. Prod. Res. (2018) DOI, doi:10.1080/14786419.2018.1474465.
[24] S.S. Swain, S.K. Paidesetty, B. Dehury, M. Das, S.C. Vedithi, R.N. Padhy, "Computer-aided synthesis of dapsone-phytochemical conjugates against dapsone-resistant Mycobacterium leprae", Sci. Rep. (2020) 10, doi:10.1038/s41598-020-63913-9.
[25] P.M. Ronad, M.N. Noolvi, S. Sapkal, S. Dharbhamulla, V.S. Maddi, "Synthesis and antimicrobial activity of 7-(2-substituted phenylthiazolidinyl)-benzopyran-2-one derivatives", Eur. J. Med. Chem. 45 (2010) 85–89, doi:10.1016/j.ejmech.2009.09.028.
[26] S.S. Garg, J. Gupta, S. Sharma, D. Sahu, "An insight into the therapeutic applications of coumarin compounds and their mechanisms of action", Eur. J. Pharm. Sci. 152 (2020), doi:10.1016/j.ejps.2020.105424.
[27] A. Achari, D.O. Somers, J.N. Champness, P.K. Bryant, J. Rosemond, D.K. Stammers, "Crystal structure of the anti-bacterial sulphonamide drug target dihydropteroate synthase", Nat. Struct. Biol. 4 (1997).
[28] R.A. Proctor, "Role of folate antagonists in the treatment of methicillin-resistant Staphylococcus aureus infection", Clin. Infect. Dis. 46 (2008) 584–593.
[29] N.C. Desai, N. Bhatt, H. Somani, A. Trivedi, "Synthesis, antimicrobial and cytotoxic activities of some novel thiazole clubbed 1, 3, 4-oxadiazoles", Eur. J. Med. Chem. 67 (2013) 54–59, doi:10.1016/j.ejmech.2013.06.029.
[30] D. Singh, P. Singh, A. Pradhan, R. Srivastava, S.K. Sahoo, "Reprogramming cancer stem-like cells with nanoforskolin enhances the efficacy of paclitaxel in targeting breast cancer", ACS Appl. Bio Mater. 4 (2021) 3670–3685.
[31] A. Singh, J.V. Singh, A. Rana, K. Bhagat, H.K. Gulati, R. Kumar, R. Salwan, K. Bhagat, G. Kaur, N. Singh, R. Kumar, H. Singh, S. Sharma, P.M.S. Bedi, "Monocarbonyl curcumin-based molecular hybrids as potent antibacterial agents", ACS Omega 4 (2019) 11673–11684, doi:10.1021/acsomega.9b01109.
[32] Z.C. Wang, Y.J. Qin, P.F. Wang, Y.A. Yang, Q. Wen, X. Zhang, H.Y. Qiu, Y.T. Duan, Y.T. Wang, Y.L. Sang, H.L. Zhu, "Sulfonamides containing coumarin moieties selectively and potently inhibit carbonic anhydrases II and IX: design, synthesis, inhibitory activity and 3D-QSAR analysis", Eur. J. Med. Chem. 66 (2013) 1–11, doi:10.1016/j.ejmech.2013.04.035.
[33] M. Das, W. Duan, S.K. Sahoo, "Multifunctional nanoparticle–EpCAM aptamer bioconjugates: a paradigm for targeted drug delivery and imaging in cancer therapy", Nanomed. Nanotechnol. Biol. Med. 11 (2015) 379–389.
[34] J. Sahoo, S.K. Mekap, S.K. Paidesetty, "Synthesis, spectral characterization of some new 3-heteroaryl azo4-hydroxy coumarin derivatives and their antimicrobial evaluation", J. Taibah Univ. Sci. 9 (2015) 187–195.
[35] B.D. Cullity, in: "Elements of X-ray Diffractions", Wesley publishing Co., England, 1959, pp. 85–88.
[36] S.A. Ali Shah Tirmazi, M.A. Qadir, M. Ahmed, M. Imran, R. Hussain, M. Sharif, M. Yousaf, M Muddassar, "Levofloxacin and sulfa drugs linked *via* Schiff bases: exploring their urease inhibition, enzyme kinetics and *in silico* studies", J. Mol. Struct. (2021) 130226, doi:10.1016/j.molstruc.2021.130226.
[37] E.H. Avdović, D.S. Dimić, J.M.D. Marković, N. Vuković, M.Đ. Radulović, M.N. Živanović, N.D. Filipović, J.R. Đorović, S.R. Trifunović, Z.S. Marković, "Spectroscopic and theoretical investigation of the potential anti-tumor and antimicrobial agent, 3-(1-((2-hydroxyphenyl) amino) ethylidene) chroman-2, 4-dione", Spectrochim. Acta A Mol. Biomol. Spectrosc. Spectrochim Acta A. 206 (2019) 421–429, doi:10.1016/j.saa.2018.08.034.
[38] A. Hamad, M.A. Khan, I. Ahmad, A. Imran, R. Khalil, T.A. Adhami, K.M. Rahman, N.Z. Quratulain, Z. Shafq, "Probing sulphamethazine and sulphamethoxazole based Schiff bases as urease inhibitors; synthesis, characterization, molecular docking and ADME evaluation", Bioorg. Chem. 125 (2020) 104–336, doi:10.1016/j.bioorg.2020.104336.
[39] J. Ramakrishnan, S.S. Rathore, T. Raman, "Review on Fungal enzyme inhibitors-Potential drug targets to manage human fungal infections", RSC Adv. (2016) DOI, doi:10.1039/C6RA01577H.
[40] M.F. Chellat, L. Raguz, R. Riedl, "Targeting antibiotic resistance", Angew. Chem. Int. Ed. 55 (2016) 6600–6626 DOI, doi:10.1002/anie.201506818.
[41] M. Mahapatra, S.K. Mekap, S. Mal, J. Sahoo, S.K. Sahoo, S.K Paidesetty, "Coumaryl-sulfonamide moiety: unraveling their synthetic strategy and specificity toward hCA IX/XII, facilitating anticancer drug development", Arch. Pharm. (2020), doi:10.1002/ardp.202200508.